

Thesis presented to the Instituto Tecnológico de Aeronáutica, in partial fulfillment of the requirements for the degree of Doctor of Science in the Graduate Program of Physics, Field of Plasma Physics

Armando José Pinto

**EFFECTS OF A FUEL-RICH GLIDING ARC DISCHARGE IN
PLASMA-ASSISTED FUEL-LEAN COMBUSTION**

Thesis approved in its final version by signatories below:



Prof. Dr. Pedro Teixeira Lacava
Advisor



Prof. Dr. Julio César Sagás
Co-advisor



Prof. Dr. Pedro Teixeira Lacava
Pro-Rector of Graduate Courses

Campo Montenegro
São José dos Campos, SP – Brazil
2019

Cataloging-in-Publication Data
Documentation and Information Division

Pinto, Armando José

Effects of a fuel-rich gliding arc discharge in plasma-assisted fuel-lean combustion

/ Armando José Pinto.

São José dos Campos, 2019.

119f.

Thesis of Doctor of Science – Course of Physics. Area of Plasma Physics – Instituto Tecnológico de Aeronáutica, 2019. Advisor: Prof. Dr. Pedro Teixeira Lacava. Co-advisor: Prof. Dr. Julio César Sagás.

1. Combustão. 2. Descargas elétricas a arco. 3. Física de plasmas. 4. Controle de poluição. 5. Física. I. Instituto Tecnológico de Aeronáutica. II. Effects of a fuel-rich gliding arc discharge in plasma-assisted fuel-lean combustion.

BIBLIOGRAPHIC REFERENCE

PINTO, Armando José. **Effects of a fuel-rich gliding arc discharge in plasma-assisted fuel-lean combustion.** 2019. 119 f. Thesis of Doctor of Science – Instituto Tecnológico de Aeronáutica, São José dos Campos.

CESSION OF RIGHTS

AUTHOR'S NAME: Armando José Pinto

PUBLICATION TITLE: Effects of a fuel-rich gliding arc discharge in plasma-assisted fuel-lean combustion.

PUBLICATION KIND/YEAR: Thesis / 2019

It is granted to Instituto Tecnológico de Aeronáutica permission to reproduce copies of this thesis and to only loan or to sell copies for academic and scientific purposes. The author reserves other publication rights and no part of this thesis can be reproduced without the authorization of the author.

Armando José Pinto

Av. Dr. Néilson D'Ávila, 1178.

CEP: 12245-031 – São José dos Campos - SP

EFFECTS OF A FUEL-RICH GLIDING ARC DISCHARGE IN PLASMA-ASSISTED FUEL-LEAN COMBUSTION

Armando José Pinto

Thesis Committee Composition:

Prof. Dr. Rodrigo Sávio Pessoa	Chairperson	- ITA
Prof. Dr. Pedro Teixeira Lacava	Advisor	- ITA
Prof. Dr. Julio César Sagás	Co-advisor	- UDESC
Prof. Dr. Homero Santiago Maciel	Internal Member	- ITA
Prof. Dr. Fernando Souza Costa	External Member	- INPE
Prof. Dr. Mario Ueda	External Member	- INPE

ITA

To my family, my girlfriend, and friends.

Acknowledgments

To all my family for the unconditional encouragement and emotional support.

To my girlfriend Sâmea Cristina Alves for all the encouragement, companionship and love.

To my advisors for scientific support, priceless discussions and to be excellent professional examples.

To all my lab friends (from the Laboratory of Combustion, Propulsion and Energy – LCPE, and from the Plasma and Process Lab - LPP). In particular to Maycon Ferreira Silva, for the fun, celebrations, brilliant discussion moments and always had the disposition to help me in the moments of need.

To Dr. Maria Esther Sbampato for assistance in the chemical analysis part of this study.

To Dr. Marcelo Pêgo Gomes for providing me his singular view about physics and education.

To Ronaldo Vieira Lobato and Emanuel Vicente Chimanski for the companionship along our academic journey over the last six years.

To the Brazilian Coordination for the Improvement of Higher Education Personnel (CAPES) for financial support.

*"I gotta stop somewhere,
I'll leave you something to imagine!"*

– Richard P. Feynman

Resumo

Processos de combustão são um fator importante no progresso humano. Entretanto, os gases de exaustão resultantes podem conter espécies de risco, seja pela sua toxicidade para as espécies vivas ou por contribuírem para a degradação ambiental. Dentre as diferentes técnicas usadas para o controle de emissão de poluentes advindos da combustão, pode se destacar o uso de plasmas fora do equilíbrio termodinâmico devido à sua ação como fonte de espécies quimicamente ativas, tais como radicais e espécies ionizadas, além de elétrons livres que promovem a ionização e dissociação de moléculas no gás presente. Nesse estudo, uma descarga de arco deslizante gerada em uma pré-mistura rica em combustível foi aplicada a uma chama pobre em combustível, estabilizada por *swirl*, ambos gerados em mistura de ar e gás natural. O diagnóstico elétrico da descarga foi realizado com o intuito de verificar a influência da vazão de gás e da composição da mistura na frequência de repetição da descarga e mostrou que tanto o aumento da vazão de gás quanto da quantidade de combustível na mistura eleva a frequência de repetição da descarga. A análise química dos produtos da combustão assistida a plasma mostrou que a descarga age como uma fonte de espécies oxigenadas e hidrogenadas (O, H, H₂, OH), que aceleram a oxidação dos hidrocarbonetos e diminuem os níveis de monóxido de carbono, aprimorando o processo de combustão.

Abstract

Combustion processes have been an important factor in human progress. However, the exhaust gases can contain high-risk species, either by its toxicity to living beings or for contributing to environmental degradation. Among different techniques used for combustion pollutant control, it can be highlighted the use of non-equilibrium plasmas. This kind of plasma is a source of chemically active species such as radicals, ionized and metastable species, and also free electrons which promote the ionization and dissociation of the background gas molecules. In this study, a gliding arc discharge generated in a fuel-rich premixed mixture was applied to a swirl global fuel-lean flame, both of them generated in a mixture of air and natural gas. The discharge electrical diagnostic was performed to verify the influence of the gas flow rate and the mixture composition on the discharge repetition frequency. Both the increase of the total gas mass flow rate and of the fuel amount in the mixture increase the discharge repetition frequency. The chemical analysis of the plasma-assisted combustion exhaust gas showed that the discharge acts as a source of oxygen and hydrogen species (O, H, H₂, OH). It accelerates the hydrocarbon oxidation and lowers the levels of carbon monoxide, improving the combustion process.

List of Figures

Figure 2.1 - Illustration of the microwave plasma burner used by Wu et al	20
Figure 2.2 – Argon plasma-assisted flames of premixed and non-premixed methane-air mixtures in different equivalence ratios	21
Figure 2.3 – Diffusion flame of propane and air response to the increase of the applied voltage in the presence of plasma.....	23
Figure 2.4 – Schematic drawing of the burner used by Gao et al.....	25
Figure 2.5 – Stoichiometric flames of methane and air assisted by the gliding arc discharge.....	25
Figure 2.6 – Schematic of the experimental setup used by Kong et al	26
Figure 2.7 - Image of (a) the flame, (b) and (c) GA with flame and (d) GA without flame	27
Figure 2.8 - Example of the development of a gliding arc discharge in 2D geometry.....	42
Figure 2.9 – CH ₄ and H ₂ concentrations as functions of the input power for different equivalence ratios	44
Figure 3.1 - Schematics of the burner and the plasma reactor	47
Figure 3.2 - Schematics of the recirculation structure generated by a swirl flow (top) and an example of the flame generated by the present burner without plasma	48
Figure 3.3 – Flame swirl number (S') as a function of the plasma reactor equivalence ratio Φ_{reactor}	49
Figure 3.4 - Fuel injection modes of the burner	50
Figure 3.5 - Combustion chamber (on top) and the gas sample probe (bottom).....	51
Figure 3.6 - Schematics of the combustion chamber and the burner with respective dimensions	52

Figure 3.7 – Raw data concentration of the main compounds as a function of the sample probe position.....	55
Figure 4.1 - Typical voltage waveform of the GA.....	58
Figure 4.2 – Typical current waveform of the GA..	59
Figure 4.3 - Discharge mean voltage (a) and mean current (b) as functions of the reactor equivalence ratio for the two tested fuel mass flow rates.....	60
Figure 4.4 - Voltage waveforms (a,c) and respective FFTs (b,d) for two different conditions with $\Phi_{\text{reactor}} = (3.0 \pm 0.1)$	61
Figure 4.5 - Voltage waveforms and respective FFTs (in blue) for two conditions with a total mass flow rate of 1.85 g/s.....	62
Figure 4.6 – Discharge repetition frequency as a function of the reactor equivalence ratio (a) and total mass flow rate (b).....	63
Figure 4.7 - Mean voltage (a), mean current (b) and discharge frequency (c) of the gliding arc discharge in the presence of the flame as function of the swirler air mass flow rate ($\dot{m}_{\text{Air(Swirler)}}$) for two plasma equivalence.....	65
Figure 5.1 - Concentrations of O ₂ , and CO ₂ as functions of the reactor equivalence ratio (Φ_{reactor}) for $\Phi_{\text{global}} = 0.21$	68
Figure 5.2 - THC and CO behaviors as a function of the reactor equivalence ratio (Φ_{reactor}) for $\Phi_{\text{global}} = 0.21$	69
Figure 5.3 - NO _x concentration as function of the reactor equivalence ratio (Φ_{reactor}) for $\Phi_{\text{global}} = 0.21$	71
Figure 5.4 - CH ₄ concentration as function of the reactor equivalence ratio (Φ_{reactor}) for $\Phi_{\text{global}} = 0.21$	72
Figure 5.5 - Ethane concentration as function of the reactor equivalence ratio (Φ_{reactor}) for $\Phi_{\text{global}} = 0.21$	73

Figure 5.6 - Propane concentration as function of the reactor equivalence ratio (Φ_{reactor}) for $\Phi_{\text{global}} = 0.21$.	74
Figure 5.7 - Acetylene and ethylene concentrations as function of the reactor equivalence ratio (Φ_{reactor}) for $\Phi_{\text{global}} = 0.21$.	75
Figure 5.8 - Formaldehyde and methanol concentrations as a function of the reactor equivalence ratio (Φ_{reactor}) for $\Phi_{\text{global}} = 0.21$.	76
Figure 5.9 - Scheme of the plasma action over the flame exhaust gas.	78

List of Abbreviations and Acronyms

AC	Alternating Current
CONAMA	Brazilian National Environment Council
DBD	Dielectric Barrier Discharge
DC	Direct Current
FFT	Fast Fourier Transform
FTIR	Fourier-Transform Infrared
FVF	Forward Vortex Flow
GA	Gliding Arc
LTE	Local Thermodynamic Equilibrium
OES	Optical Emission Spectroscopy
PAC	Plasma-assisted Combustion
PLIF	Planar Laser-Induced Fluorescence
PTFE	Polytetrafluorethylene
RQL	Rich-Quench-Lean
RVF	Reverse Vortex Flow
TALIF	Two Photon Absorption Laser-Induced Fluorescence
THC	Total Hydrocarbon Content
UNFCCC	United Nations Framework Convention on Climate Change

List of Symbols

Φ	Equivalence ratio
Φ_{global}	Global equivalence ratio
Φ_{reactor}	Reactor equivalence ratio
I	Discharge current
I_m	Mean discharge current
\dot{m}_{Air}	Air mass flow rate
$\dot{m}_{\text{Air(Swirl)}}$	Swirler air mass flow rate
\dot{m}_{F}	Fuel mass flow rate
\dot{m}_{TOTAL}	Total mass flow rate
NG	Natural Gas
P'	Representative quantity of the discharge electrical power
R_{ex}	Fuel-air ratio in the experimental conditions
R_{st}	Fuel-air ratio in the stoichiometric conditions
U	Discharge voltage
U_m	Mean discharge voltage

Contents

1	INTRODUCTION	15
1.1	Motivation	15
1.2	Objectives	16
1.3	Outline of the Thesis.....	17
2	PLASMA-ASSISTED COMBUSTION.....	18
2.1	Introduction	18
2.2	Non-equilibrium plasmas applied to combustion.....	19
2.3	Pollutants generated by combustion processes.....	28
2.4	A brief description of the PAC chemical kinetics.....	32
2.5	Gliding arc discharges.....	42
2.6	Gliding arc applied to PAC	43
3	EXPERIMENTAL SETUP.....	46
3.1	System description.....	46
3.2	Discharge characterization methodology	53
3.3	Gas analysis methodology	54
4	GLIDING ARC DISCHARGE IN FUEL-RICH CONDITIONS.....	58
5	PLASMA-ASSISTED COMBUSTION RESULTS.....	67
5.1	O ₂ , H ₂ O and CO ₂	68
5.2	THC and CO	69
5.3	NO _x	71
5.4	Hydrocarbons	72
6	CONCLUSIONS AND SUGGESTIONS FOR FUTURE STUDIES	81
6.1	Conclusions	81
6.2	Recommendations for future studies	83
	BIBLIOGRAPHY.....	84
	APPENDIX A – MATHEMATICAL CALCULATION OF THE SWIRL NUMBER ...	91
	APPENDIX B – CONCENTRATION GRAPHS OF THE EXHAUST GAS COMPONENTS	98
	APPENDIX C – TABLES REFERENT TO THE VARIATIONS ON THE CONCENTRATION OF THE EXHAUST GAS COMPOSITION	110

1 Introduction

1.1 Motivation

Combustion processes are strongly linked to the humankind advance since its early age. The control of the fire by early humans provided them a source of warmth, protection against predators, improved their ability of occupation of new areas, and also enlarged their diet due to an improvement on hunting and cooking (JAMES et al., 1989; WEINER et al., 1998). Nowadays, combustion is more linked to transportation, power generation and industrial applications, and its control and improvement still remain an essential topic.

Great concern about the combustion is its pollutant emissions such as nitrogen and sulfur oxides (NO_x and SO_x), carbon monoxide (CO), unburned hydrocarbons and particulates. Most of these emissions are highly toxic and contributes to global warming also. Although CO_2 also contributes to the greenhouse effect, it is an inherent product of the combustion. Therefore, as CO_2 is a desirable compound on the combustion exhaust gas, it preferable to treat it after the combustion process.

Since the adoption of the United Nations Framework Convention on Climate Change (UNFCCC) in 1992 (UNITED NATIONS, 1992), many actions have been proposed to reduce the pollutant emissions from industrial processes such as Kyoto Protocol (UNITED NATIONS, 1998), the Paris Agreement (UNITED NATIONS, 2015) and local actions as the European Union Emissions Trading System (EUROPEAN COMMISSION CLIMATE ACTION, 2016). This last set to the European Union a periodically reducing cap on the total amount of certain greenhouse gases that can be emitted by installations.

In accordance with Kyoto Protocol, Brazil developed its own guidelines and objectives on the reduction of combustion emission levels, mainly by means of the National Policy on Climate Changes (PRESIDENCY OF THE REPUBLIC OF BRAZIL, 2009) and the resolutions from the National Environment Council (CONAMA) (NATIONAL ENVIRONMENT COUNCIL - CONAMA, 2012).

Among various technologies to reduce pollutant emissions from combustion, the possibility of application of non-equilibrium plasmas in atmospheric pressure has increased due to its action as heat and radical-pool source, promoting changes in the chemical routes, which can decrease the production of undesirable compounds. Moreover, this kind of plasma

can also improve combustion by enlarging the flammability limits (SAGÁS; MACIEL; LACAVA, 2016; VARELLA; SAGÁS; MARTINS, 2016) and increasing flame stability (WU et al., 2015).

In this context, the present study is concerned with an experimental investigation about the plasma-assisted combustion in a global-lean swirling flame. The lean combustion is one of the strategies used in gas turbine systems to prevent NO_x emissions. However, due to the low temperature in the flame zone, the kinetic mechanism is slower and part of the oxidation reactions can be quenched, increasing the emission of unburned hydrocarbons and CO.

In the present study, the use of a gliding arc (GA) plasma is proposed and investigated as a tool to minimize this situation. The plasma application aims to accelerate the combustion kinetics of a global fuel-lean flame feeding it with the species generated by a fuel-rich GA, in order to diminish the concentrations of the total hydrocarbon content (THC) and carbon monoxide (CO) in the exhaust gas, keeping the nitrogen oxides (NO_x) levels acceptable. The results of the present research can give valuable information to future applications such as gas turbines and systems that operates in fuel-lean conditions.

The GA plasma was chosen for this application due to its high versatility, low production cost and because its use does not require considerable geometric modifications in the combustion system. Besides that, the present study represents a continuation of the research in GA applied to plasma-assisted combustion developed by the Laboratory of Combustion, Propulsion and Energy (LCPE) at the Technological Institute of Aeronautics (SAGÁS, 2009, 2013; SAGÁS et al., 2011; VARELLA, 2015).

Plasma-assisted combustion (PAC) literature is short of studies comparing the combustion exhaust gas composition with and without the plasma application in the same conditions. Given that, the present study analyzes the influence of the gliding arc discharge on the exhaust gas composition by performing this direct comparison. This methodology allows verifying what compounds the plasma application impacts, and what effects are due to the flame dynamics and which are due to the presence of the plasma.

1.2 Objectives

The main goal of this study was to verify the gliding arc plasma effect on emissions of

a global fuel-lean swirl flame by directly comparing the conditions with and without plasma in the same system.

To accomplish this goal, some secondary objectives are outlined:

- i. the electrical characterization of the discharge was performed to verify how the mass flow rate and the concentration of the feed gas mixture influence the discharge characteristics such as the mean current and voltage, and repetition frequency.
- ii. a set of tests was performed to verify the effect of the flame in the gliding arc electrical properties, to guarantee that it was possible to isolate the effect of the discharge on the direct comparison between flame conditions with and without plasma application.
- iii. The analysis of the combustion exhaust gas with and without plasma application allowed verifying the role of the plasma in the combustion process. Especially the effect of the plasma on the CO and hydrocarbons oxidation as well as in the NO_x formation.

1.3 Outline of the Thesis

In chapter 2, an introduction to the subject of plasma, GA and a discussion of the plasma-assisted combustion is presented, exposing the advantages of using plasma in combustion processes with an overview of the state of the art in plasma-assisted combustion. A brief discussion about the PAC chemical kinetics and a description of the basic phenomenology of the gliding arc are also provided in this chapter.

In chapter 3, a detailed description of the experimental setup is presented. It also includes a discussion about the methodology used to perform the discharge electrical characterization and the exhaust gas composition analysis.

In chapter 4 the electrical characterization of the discharge in fuel-rich conditions is presented and the effects of the mass flow rate and concentration of the feed gas mixture are discussed. It is important to notice that in this chapter, only the discharge was studied, not overall aspects of the plasma-assisted combustion process.

In chapter 5, the effects of the discharge on the composition of the burner exhaust gas is discussed. In this analysis, the effect of the global equivalence ratio and the plasma reactor

equivalence ratio were taken into account. Correlation between the results and the main chemical pathways given in the literature is also presented.

Finally, in chapter 6, the main conclusions and recommendations for future studies are discussed.

2 Plasma-assisted combustion

2.1 Introduction

Plasma is an ionized gas that is electrically neutral in a macroscopic view, i.e., the negative charge particle density is balanced by the positive ions. Although it occurs sparsely in nature, plasmas can be artificially generated quite easily by an electrical discharge in a gaseous media, which promotes the gas breakdown and turns it into plasma. The artificially generated plasmas make it possible to open up vast application opportunities, from biomedical to electronics and metallurgical industry. In chemical applications, plasmas offer temperatures and energy densities that much exceed those of the conventional chemical technologies. They also can produce very high concentrations of chemically active species such as electrons, ions, atoms, radicals, excited species and photons. Some radicals and excited species produced by plasmas can be very difficult to obtain in conventional chemical technologies. In plasmas that are far from thermodynamic equilibrium, those chemical active species density can be very high, keeping the gas temperature as low as the room temperature (FRIDMAN, 2008). These plasma features allow a significant improvement in chemical processes by promoting new chemical pathways that cannot be achieved by conventional chemistry.

Given that, in plasmas composed by different species, each one can present a different temperature. Therefore, plasmas can be classified in thermal and non-thermal plasmas (FRIDMAN, 2008). The first one is in local thermodynamical equilibrium, so electrons and heavy species (ions and neutrals) have the same temperature. In non-thermal plasmas (also called non-equilibrium plasmas) electron temperature is far higher than that of the heavy species and, thereby the plasma presents itself far from the thermodynamic equilibrium (GOMEZ et al., 2009).

Some examples of thermal plasmas are arc plasma torches and some radio-frequency inductively coupled discharges. Thermal plasmas present vast application in fields that require

a huge heat transfer (given that thermal plasmas can reach temperatures up to 20000 °C) such as waste treatment (GOMEZ et al., 2009), metallurgy industry and also some coating processes (BOULOS, 1996). In thermal plasmas, the electron energy is from the order of 1 eV and the electron density is high, more than 10^{20} m^{-3} (GLEIZES, ALAIN AND GONZALEZ, JEAN-JACQUES AND FRETON, 2005).

Since thermal plasma species have the same temperature, such plasmas have low chemical selectivity i.e., the capacity of the system to transfer energy mainly to chemical reactions. Then, the energy transfer is mostly via translational degrees of freedom of the gas molecules. Therefore, this kind of plasma is not indicated to be used for low-temperature chemistry applications (GOMEZ et al., 2009).

However, in non-equilibrium plasmas, as the electron temperature is much higher than that of the heavy particles, the ionization and chemical processes are determined by the electron temperature and then, less sensitive to the gas temperature (FRIDMAN, 2008). Therefore, the chemical activity of non-equilibrium plasma relies on the production of active radicals and excited species through electron impact (STARIKOVSKII et al., 2006).

In this way, although the equilibrium plasmas show a high neutral temperature and high electron number density, they consume a large amount of energy and cannot prioritize the active species production in comparison with the non-equilibrium plasmas (JU; SUN, 2015). Therefore, thermal plasmas contribution to combustion process is mainly via heat transfer and present poor chemical selectivity.

Among several ways to generate non-equilibrium plasmas, it can be included the dielectric barrier discharge (DBD), corona discharge, microwave plasmas, nanosecond pulsed discharges and the gliding arc discharge.

2.2 Non-equilibrium plasmas applied to combustion

The advantage in using non-equilibrium plasma in plasma-assisted combustion (PAC) is that they have high electron temperatures (1-10 eV) and are more kinetically active (compared with thermal plasmas) due to its fast production of radicals and excited species. This kind of plasma transfers energy mainly through electron impact dissociation and excitation (HICKS et al., 2005; SUN et al., 2013).

In the PAC of hydrocarbons, the production of species such as H_2 , atomic O and H, O_3 , radicals such as OH, as well as ionized and excited species; modify the fuel oxidation routes and can be a great way to improve the combustion ignition (KOSAREV et al., 2016; ZHAO et al., 2016), flame stabilization (WU et al., 2015) and emission control (LEE et al., 2013; SONG et al., 2013; VARELLA; SAGÁS; MARTINS, 2016). Although these plasmas are attractive due to their chemical action on the system, their possible contribution as a source of heat and to modify the transport process (JU; SUN, 2015) cannot be neglected.

There is a good number of studies using non-thermal plasmas to enhance combustion, reduce emissions (LEE et al., 2013; SONG et al., 2013; VARELLA; SAGÁS; MARTINS, 2016; WANG et al., 2017a), and improve fuel reforming (TU; WHITEHEAD, 2014; XIA et al., 2017), using numerous techniques of generation of plasma such as microwave, DBD (CHA et al., 2005), nanosecond-pulsed discharges (NSPD) (CHENG et al., 2018) and gliding arc (JU; SUN, 2015; XIA et al., 2017).

Microwave plasma, typically using 2.45 GHz frequency (MEDEIROS, 2016) is a kind of plasma usually generated by feeding a transversal gas flow through a waveguide. The electromagnetic energy of the microwaves can be transferred to the gas flow and thus initiate and sustain a discharge (FRIDMAN; KENNEDY, 2004). Some advantages of using microwave plasma are the large generated plasma volume as well as the absence of the high-temperature electrode, which increases the system lifetime.

In the experiments of Wu et al. (WU; FUH; WANG, 2015), a microwave plasma with 120 W was generated in argon crossing a counter-flow arrangement of methane and air, as can be seen in figure 2.1.

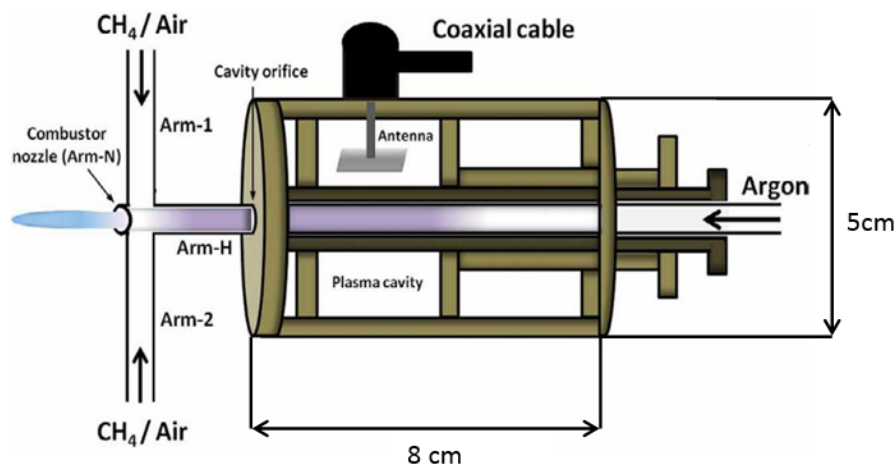


Figure 2.1 – Illustration of the microwave plasma burner used by Wu et al. Adapted from (WU; FUH; WANG, 2015). The cross-shaped quartz tube arms Arm-1, Arm-2 and Arm-H have inner diameter of 4 mm and outer diameter of 6 mm.

The authors showed that the plasma extends the flammability limits of both premixed and non-premixed flames to a global-lean equivalence ratio (Φ) of 0.2. The plasma also changes the flame color and shape to a deep blue tongue-like in the non-premixed case, as can be seen in figure 2.2:

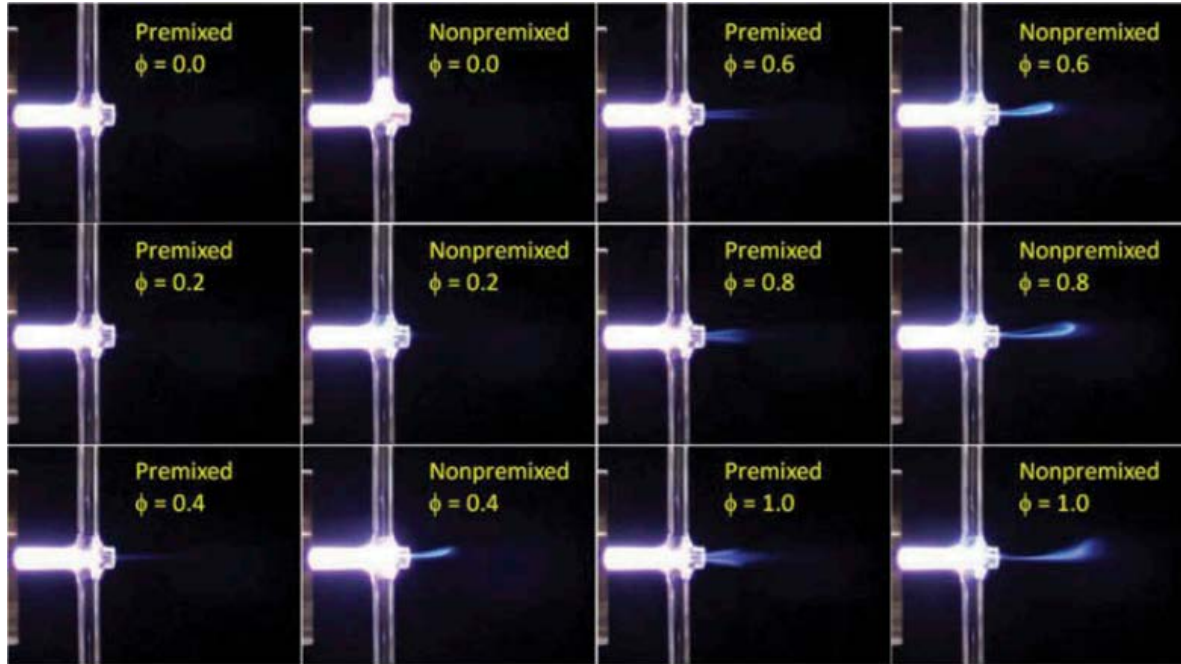


Figure 2.2 – Argon plasma-assisted flames of premixed and non-premixed methane-air mixtures in different equivalence ratios (WU; FUH; WANG, 2015). Φ ranging from 0 to 1.0. Plasma power equals to 120 W. Argon flow rate (horizontal) was kept at 0.84 slm, while methane-air flow rate (vertical) was kept at 2.0 slm.

The equivalence ratio (Φ) is used to define the gas mixture condition:

$$\Phi = \frac{R_{ex}}{R_{st}} \quad (E1)$$

where R_{ex} is the fuel-air mass ratio in experimental conditions and R_{st} the fuel-air mass ratio in the stoichiometric condition (complete fuel oxidation). Therefore, $\Phi < 1$ indicates a fuel-lean mixture, $\Phi = 1$ a stoichiometric mixture and $\Phi > 1$ a fuel-rich mixture.

By optical emission spectroscopy (OES), the authors found out that the non-premixed PAC flame spectrum presents lines referent to the C_2 and CH in the hybrid and flame zones, while in the spectrum of premixed PAC flame these species lines were not observed. These

results suggest different reaction pathways in the two cases, which was corroborated by the very distinct number density profiles of the OH radical in the premixed and non-premixed PAC flames.

The dielectric barrier discharge (DBD) is generated when at least one electrode is covered by a dielectric material. It is a discharge that occurs in a big number of micro-discharges that cover the whole inter-electrode area and presents filamentary structures (BRANDENBURG, 2017; STARIKOVSKAIA, 2006). The atmospheric pressure DBD typically uses alternating or pulsed high voltage power supplies and the reactor is made in planar or coaxial geometries (BRANDENBURG, 2017). Moreover, the dielectric barrier limits the current and so, it can prevent arc formation (STARIKOVSKAIA, 2006). The DBD can also generate a plasma that covers all the inter-electrode area for a low energy cost.

Cha et al. (CHA et al., 2005) used a DBD in a co-flow jet of propane and air diffusion flame for soot suppression. They used a wire-cylinder type reactor with a 400 Hz AC power supply. The central electrode was a stainless steel rod with a diameter of 1 mm and the cylindrical electrode was a woven stainless mesh (1x1 mm). The woven mesh had a width of 10 mm and surrounded the outer quartz tube that served as a dielectric barrier and that was located 10 mm upstream from the fuel nozzle exit. The electrical power of the plasma remained lower than 25 W in all conditions.

The authors found that increasing the applied voltage, there is a decrease in the flame length and a change of the flame shape, as shown in figure 2.3. When operating in the electrostatic regime (without gas breakdown), the decrease in the flame length reduces its yellow luminosity, indicating less soot formation. However, in the plasma regime, the authors report that the yellow luminosity disappears and only a blue flame was observed.

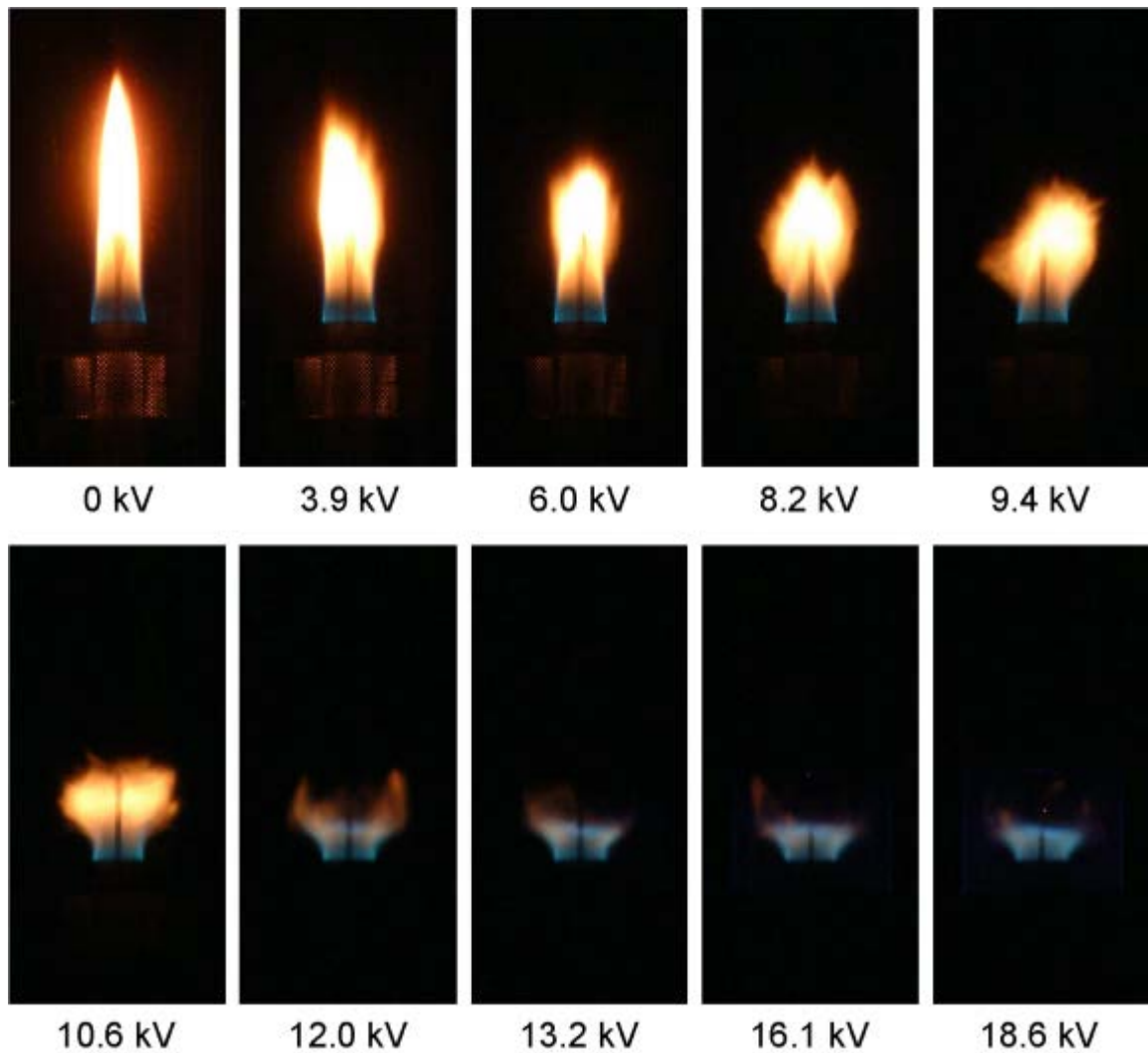


Figure 2.3 – Diffusion flame of propane and air response to the increase of the applied voltage in the presence of plasma (CHA et al., 2005). Flame length without applied voltage is 45 mm. At 13.2 kV, the flame length is about 7 mm.

Moreover, with the use of laser-induced fluorescence (LIF) diagnostic, no soot formation was detected when operating in the plasma regime. It is pointed out that in the electrostatic regime, the lowering of soot was linked to the transport effect of ionic wind on the fuel-oxidizer mixing, while in the plasma regime it is possibly linked to the well-known produced species such as O, O₃, OH, and H.

In the case of nanosecond pulsed discharges (NSPD), the plasma is generated by using a nanosecond pulsed high voltage generator. This kind of discharge is operated at high frequencies up to tens of kHz. If a short duration pulse (from units to ten ns) would be used, it will generate a streamer discharge. On the other hand, if the pulse presents a longer duration (tens to hundreds of ns), the discharge will gain spatial uniformity, in a DBD-like way

(STARIKOVSKAIA, 2006). Among the advantages of using a nanosecond pulse discharge is the fact that it is uniform at low and moderate gas density, and naturally synchronized in time in the case of multi-streamer configuration (STARIKOVSKAIA, 2014).

Pilla et al. (PILLA et al., 2006) used an atmospheric pressure NSPD generated in air, sustained by an electrical pulse with 10 kV and 10 ns of duration at a repetitive frequency of 30 kHz, to stabilize and improve the efficiency of a fuel-lean turbulent premixed flame of propane and air. The plasma power was 75 W and at low pulse voltages, the discharge is a diffuse glow. The discharge was located at the recirculation zone of the flame. At higher pulse voltages the discharge becomes filamentary with great luminosity. The authors only achieve enhancement of the lean flammability limit and the stabilization of the flame with the use of the filamentary mode. The glow OES spectrum also did not present OH, O or H emissions, indicating that this discharge mode has no noticeable effect on the flame kinetics.

In addition, they found that the plasma extended the region of flame stabilization, allowing to achieve flame in low equivalence ratios that it would not exist without plasma. By means of OES, the authors showed that the discharge in filamentary mode is a source of H and O atoms, as well as OH radicals, which accelerate the propane combustion.

Gliding arc (GA) discharges are generated between two divergent electrodes and dragged out by a transversal gas flow (FRIDMAN, 2008; OMBRELLO et al., 2006; SUN et al., 2013). The plasma generated by the GA typically presents moderate gas temperature (1000 - 3000 K), but high electron temperature (above 1 eV) and high plasma density (on the order of 10^{20} to 10^{24} m⁻³) (KOLEV; BOGAERTS, 2018; TU; WHITEHEAD, 2014). The gliding arc also presents a high versatility: it can be constructed in various geometries from 2D configuration to coaxial and in vortex flow geometries, it can operate with AC or DC power supplies, and it can be generated in high currents (units of A) to reach a regime of thermal equilibrium, or in low currents (tens to hundreds of mA) to operate in non-equilibrium regime.

Gao et al. (GAO et al., 2018) used high-speed imaging, electrical measurements, and planar laser-induced fluorescence (PLIF) to verify the effects of a 35 kHz AC GA applied to a highly turbulent non-premixed methane-air burner. The schematic drawing of the burner is shown in figure 2.4.

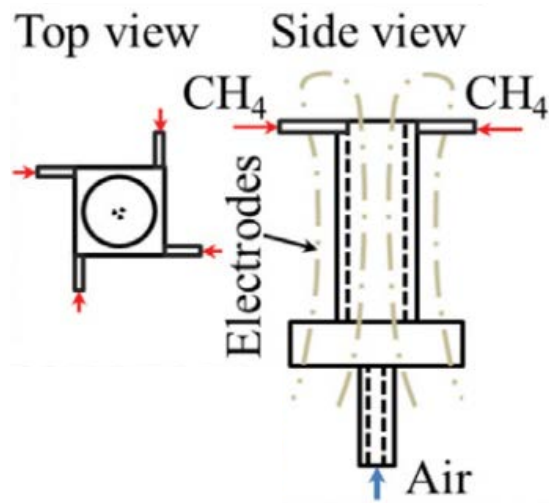


Figure 2.4 – Schematic drawing of the burner used by Gao et al. Adapted from (GAO et al., 2018). Burner walls are made in ceramic material. Air flow duct has 3.8 inner diameter. Electrodes are internally water-cooled.

The authors showed that under high flow conditions, the flame cannot be sustained without plasma for periods higher than tens of milliseconds. In the presence of the discharge, the flame stabilizes close to the discharge column, as can be seen in figure 2.5.

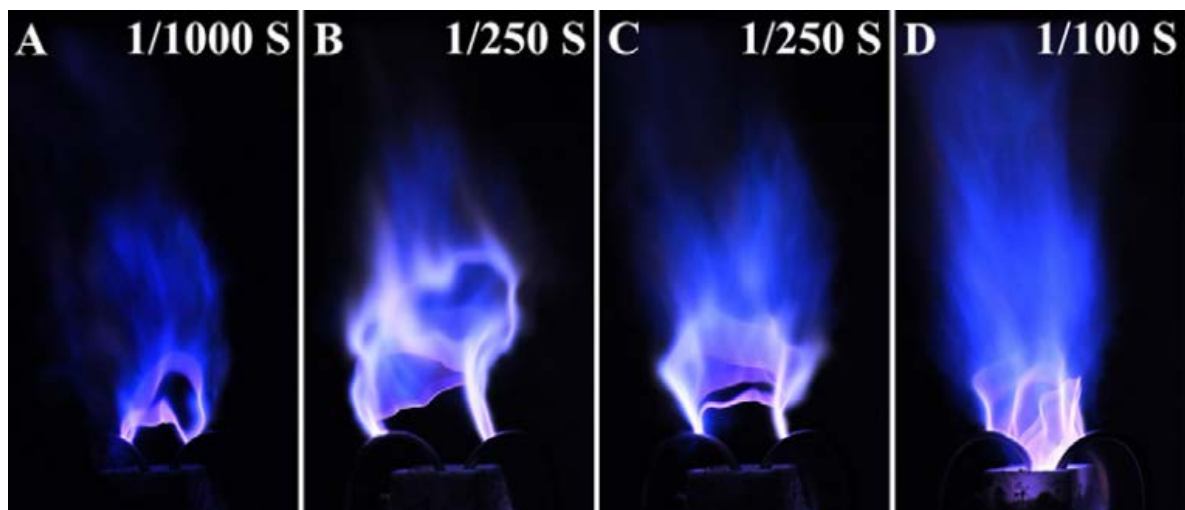


Figure 2.5 – Stoichiometric flames of methane and air assisted by the gliding arc discharge. Exposure times used for different images is marked out (GAO et al., 2018).

As showed by the CH₂O PLIF, the flame front is located 3-5 mm away from the discharge channel. They also point out that the concentration of OH increases around eight times in the presence of the discharge. Although the OH PLIF intensity is much higher for CH₄-air mixtures than for pure air, this signal keeps almost constant when the equivalence ratio increases from 0.4 to 1.

Most studies in PAC verify the influence of the plasma on flames. However, there is a lack of information about the influence of the flame in the discharges characteristics. Therefore, Kong et al. (KONG et al., 2018) studied the influence of a premixed flame on a planar AC gliding arc discharge. The schematic of the experimental setup reactor is shown in figure 2.6.

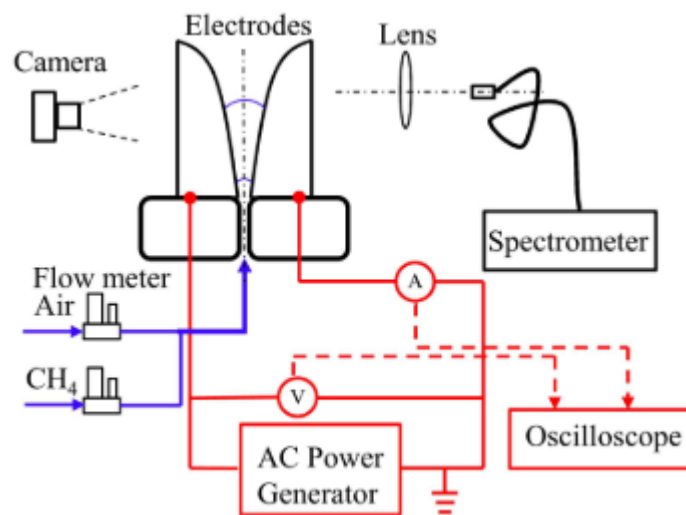


Fig. 2.6 – Schematic of the experimental setup used by Kong et al (KONG et al., 2018). The gap between the electrodes was 2.6 mm.

The discharge was generated in a premixed methane and air mixture and the flame was generated between the electrodes, as shown in figure 2.7.

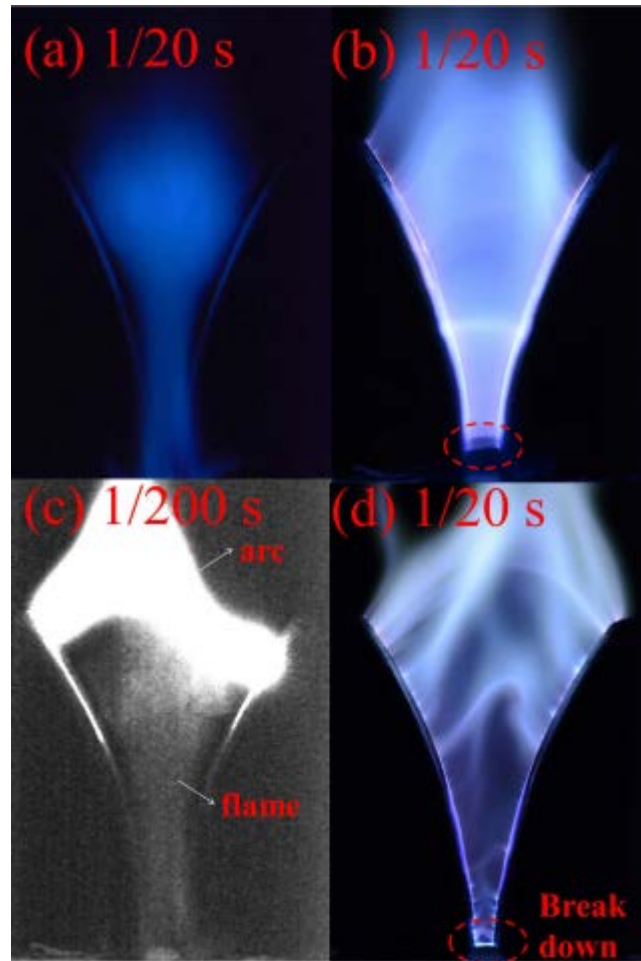


Fig. 2.7 - Image of (a) the flame, (b) and (c) GA with flame and (d) GA without flame. Exposure time for imaging has been marked on each image (KONG et al., 2018). Methane flow rate was 6 SLPM and air flow rate was 0.97 SLPM. Power input for the discharge was 100 W. Panel (b) recorded all the trajectories of the GA. In panel (c), which exposure time was reduced when compared with (b), the weak flame emission can be distinguished from the plasma emission.

The authors observed that the plasma channel in pure air is rather twisted, while the plasma in the presence of a flame moves stably and smoothly along the electrodes and no bright spark appears in the bottom inter-electrode gap in this case.

In the case of the electrical characteristics, it was shown that the discharge repetition frequency is much higher when there is flame, which was corroborated by reduction in the breakdown voltage and increase of the current peak value. Above the stoichiometric condition, the increase in the equivalence ratio also increases the breakdown voltage until $\Phi = 1.5$. After that, the breakdown voltage becomes nearly constant. The current has opposite behavior: it drops when the flame is ignited and as the equivalence ratio increases, the current

remains almost constant, close to 2.4 A. The authors argue that the presence of the flame increases the temperature and so, the gas viscosity and velocity. Thus, the flow becomes less turbulent. Moreover, the increase of the local temperature of the breakdown spot reduces the number density of molecules and consequently, the voltage necessary to generate the plasma.

Lin et al. (LIN et al., 2019) developed an AC gliding arc plasma fuel injector operating with kerosene and air to study the interaction of gliding arc plasma and the kerosene spray. Their focus was to improve the ignition and extinction performance in fuel-lean conditions. The GA characteristics were obtained by optical emission spectroscopy (OES), measurements of voltage and current and recording of the discharge development by a high-speed camera. Particle/Droplet image analysis (PDIA) was used to diagnose the plasma effect on the pulverization of the fuel. The exhaust gas composition was analyzed using a gas chromatograph.

It was observed that the plasma column has a string-like shape that glides along the Venturi nozzle. The GA starts in a glow-type discharge and during its development it becomes a spark-type discharge, evidenced by the current peaks observed in the current waveforms.

In this paper it is shown that the plasma expands the lean flame blowout limit up to 48%. The use of GA also decreases the droplet size of kerosene spray. The authors attribute this decrease to the heat release from oxygen and nitrogen molecules to the medium that increases the gas temperature. This heat release allied to the high-frequency change of the discharge position decrease the fuel viscosity and the deformation and oscillation of the fuel column. These effects result in an acceleration of the droplet detachment from the fuel column (LIN et al., 2019). The authors also point out that instabilities produced by the gliding arc also increase the secondary droplet formation. These effects produce a spray with smaller droplets, which extend the ignition limits.

In the gas analysis, it was observed that light hydrocarbons such as CH_4 , C_2H_4 , and C_2H_2 were generated in GA.

2.3 Pollutants generated by combustion processes

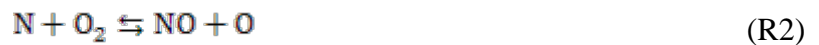
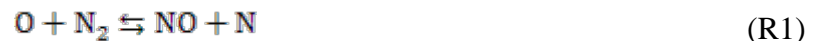
Before describing the plasma chemical action on the combustion, it is important to highlight the main processes involving the combustion generated pollutants. The main

pollutant compounds found in natural gas combustion are unburned hydrocarbons, CO and nitrogen oxides (NO_x).

Unburned hydrocarbons result from the fuel incomplete combustion. Their presence is commonly associated with a low temperature, which reduces the oxidation rates of CO and hydrocarbons (DEREK DUNN-RANKIN PETER THERKELSEN, 2016).

In fuel-air combustion, most of the NO_x corresponds to NO. For fuels that do not present nitrogen in its composition, nitrogen oxide (NO) can be formed through four mechanisms: Zeldovich mechanism (or thermal), the N₂O mechanism, prompt mechanism (or the Fenimore mechanism) and the NNH mechanism. The discussion here follows the one presented by Turns (TURNS, 2013).

The thermal mechanism (also known as the Zeldovich mechanism) consists of the following two reactions:



In fuel-rich conditions the O₂ concentration is low, so reaction (R2) plays a minor role and reaction of atomic nitrogen (N) and the hydroxyl radical (OH) become important.



The temperature dependence of this mechanism is evidenced by the high activation energy of reaction (R1), close to 319050 J/mol (TURNS, 2013). Thus, the Zeldovich mechanism is the main process of NO generation in temperatures above 1800 K. As the formation of NO by the thermal mechanism is slow compared to the fuel oxidation time scale, it is considered that the Zeldovich mechanism takes place in the post-flame zone.

The N₂O mechanism plays an important role in fuel-lean conditions at low temperature. This mechanism consists of three reactions:



In this mechanism, a third molecule M promotes the formation of nitrous oxide (N₂O), different from reaction (R1). So, N₂O can react with hydrogen or oxygen to form NO through reactions (R5) and (R6). Generally, this mechanism takes place in high-pressure conditions.

The Fenimore mechanism occurs in the combustion of hydrocarbons. Specially in fuel-rich combustion (MILLER, JAMES A AND BOWMAN, 1989), the NO formation rates exceeds that attributed to the thermal mechanism. This excess was first identified by Fenimore, which named it as prompt NO. This mechanism consists basically of the reactions between nitrogen and radicals, forming CN-based compounds, which will further form NO and CO. In a simple way, ignoring the CH formation steps, the Fenimore mechanism can be described as:



As pointed out by Turns (TURNS, 2013), for an equivalence ratio of 1.2 or less, the HCN conversion for NO formation corresponds to the following reactions:





Miller and Bowman (MILLER, JAMES A AND BOWMAN, 1989) pointed out that for equivalence ratios above 1.2, the HCN to NO conversion becomes slow and the NO is “recycled” to form HCN, which starts to inhibit the NO formation. Besides that, the reaction (R2) is shifted to the reverse direction, contributing also to the lowering in the NO production.

The NNH mechanism is an important mechanism for the combustion of hydrogen and hydrocarbons with high hydrogen concentration. The main reactions of the NNH mechanism are:



In the case of NO₂, although its production is far less than the NO, it can present a considerable emission. The elementary steps of its formation are:



Where the HO₂ radicals are formed in low-temperature regions by the reaction:



So, the NO₂ formation occurs when there is the transport of NO molecules from high-temperature regions to the ones with low temperature, which are generally, regions with air in excess (GALLEGO, ANTONIO GARRIDO AND MARTINS, GILBERTO AND GALLO, 2000; TURNS, 2013).

2.4 A brief description of the PAC chemical kinetics

It is well known in the literature (JU et al., 2016; JU; SUN, 2015; STARIKOVSKAIA, 2006) that plasmas can contribute to the improvement of combustion via three pathways: thermal, transport and kinetic effect. The thermal effect is related to the sensitivity of the reactions to the temperature rise via Arrhenius law. The transport effect is due to the fuel cracking into small fragments that change the fuel diffusivity, given that the small molecules reach the reaction zone faster. The consequence is a modification of the combustion process due to the acceleration of the flame propagation (JU; SUN, 2015; STARIKOVSKIY; ALEKSANDROV, 2013). Besides that, the ionic wind effect and instabilities generated by the plasma application can increase the flow turbulence and mixing. Finally, the kinetic effect is due to the plasma-produced species such as high energy electrons, ions, radicals and excited species that can change the chemical kinetics pathways, inducing reactions that can be hard to achieve in conventional chemical processes.

Here, two points are important to highlight. First is that often the three effects are coupled together and then, it is difficult to understand the isolated contribution of each effect for the combustion improvement. Second, although there are advances in PAC chemical kinetics literature, the kinetic mechanisms involved are still not well understood. Some advances in this task will be discussed in the following.

Sun et al. (SUN et al., 2011) studied a sub-atmospheric pressure (8 kPa) counter-flow burner integrated with a nanosecond discharge (NSPD) system to verify the role of atomic oxygen production on the extinction limits. The counter-flow burner is operated with O₂-Ar and CH₄. The discharge was generated in O₂-Ar in a frequency from 5 to 40 kHz. The

measurements of atomic oxygen at the exit of the oxidizer of the burner were performed using two-photon absorption laser-induced fluorescence (TALIF).

The results showed that the atomic oxygen concentration increases with the pulse repetition frequency. The increase in the discharge repetition frequency also affects the extinction limit of the flame, which can reach up to 90% for a frequency of 20 kHz. The authors showed that at frequencies of approximately 5 kHz, the comparison of the NSPD and an electrical heater at the same temperature indicates that the enhancement promoted by both devices is approximately the same. This result agrees well with the low atomic oxygen concentration measured in the above conditions and indicates that at this repetition frequency, the enhancement promoted by the discharge is mainly a thermal effect.

The simulation of the extinction limit of the plasma-assisted CH₄-air counter-flow combustion was performed using CHEMKIN applications OPPDIFF (diffusion counter-flow flame). The authors added a modified arc-length continuation method for the plug flow reactor, which fed the OPPDIFF module. The model used a fixed fuel stream temperature of 300 K and an oxidizer temperature varying between 528, 398 and 348 K. The plasma repetition frequency was set at 20 and 5 kHz.

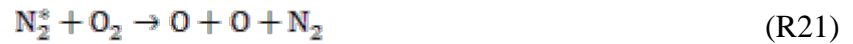
Although the model reproduced well the extinction limits without plasma, it underestimates the enhancement promoted by the plasma presence. This suggests the presence of additional kinetic enhancement from other excited species. The comparison with experimental results shows that there is a crossover temperature between 900 and 1000 K, above (below) which the kinetic enhancement by atomic oxygen production is governed by chain-branching (chain termination) reactions.

Uddi et al. (UDDI et al., 2009) measured the atomic oxygen concentration generated by air, methane-air and ethylene-air nanosecond pulsed discharges in low pressure (60 Torr) using TALIF. The results were compared with a proposed kinetic model. For an air NSPD, the model considers nitrogen and oxygen species, taking into account electron, atomic and molecular species. It also considers neutral, ionized and excited species.

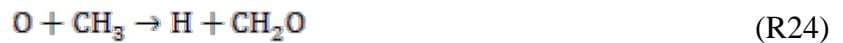
The sensitivity analysis showed that atomic oxygen is generated primarily via electron impact dissociation of O₂:



and by collisions between molecular oxygen and electronically excited nitrogen (N₂^{*}):



The model shows that the reaction (R21) occurs $\sim 10 \mu\text{s}$ after the pulse. The results also show that in methane-air and ethylene-air plasmas the loss of oxygen occurs mainly due to reactions involving H, HO₂, and CH₃ (both generated by the dissociation of methane):



The comparison between the model and the experimental results shows that the dissociation of CH₄ is mainly due to the direct impact of electrons:

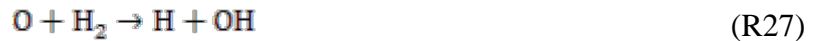


Zuzeek et al. (ZUZEEK et al., 2011) also studied NSPD generated in H₂-air mixtures at equivalence ratios from 0.05 to 1 and pressures < 100 Torr. The chemical model used in the study incorporates a non-equilibrium air plasma chemistry model (KOSSYI et al., 1992) expanded to include hydrogen dissociation processes by pulsed high current plasma, and the hydrogen-oxygen chemistry model (22 reactions among H, O, OH, H₂, O₂, H₂O, HO₂, and H₂O₂) developed by Popov (POPOV, 2008). Species concentration equations are coupled with the two-term expansion Boltzmann equation for the energy distribution function of plasma electron. The pulse shape used by the plasma chemistry model was adjusted to keep the coupled pulse energy per molecule constant (0.28 meV) during the burst. At these conditions, almost 50% of the coupled pulse energy in a hydrogen-air mixture at $\Phi = 0.5$ is spent on generation of O and H atoms.

The paper describes that at 300 K, the O and H are formed during, and after, the discharge pulse, mainly by electron impact and dissociation collisions with electronic metastable states of N₂. Subsequent fuel oxidation during the post-discharge stage (on a time scale from ~1 μs to ~ 1 ms) occurs primarily via a three process sequence, involving reactions (R22), (R23) and (R26):



So, at this low temperature, OH formation via the well-known “high temperature” chain processes:



is very low, while processes (R23) and (R26) are relatively fast, with activation barriers of 14.35 kJ/mol (1660 K) and essentially zero, respectively (POPOV, 2008).

In initial temperatures about 500 - 600 K, the rates of processes (R27) and (R28), as well as of the following three reactions:



increases rapidly, promoting a high acceleration of the overall plasma chemical oxidation. As the temperature increases, primarily due to the plasma chemical heat release, ignition occurs by the well-known chain mechanism of reactions (R27) and (R28).

Stancu et al. (STANCU et al., 2010) developed an NSPD discharge between two pin electrodes separated by 4 mm, in preheated atmospheric pressure air and nitrogen at 1000 K. Optical diagnostics showed that up to 50% of molecular oxygen was found to be dissociated by the discharge. The authors also point out that the main pathway of O formation is through the two-step mechanism for the formation of O atoms through reactions (R32) and (R21) respectively:



The measured temporal evolution of O and of the excited nitrogen species corroborates this affirmation.

It was found that the formation of O coincides with the loss of N_2^* and that the O density peak occurs after a few tens of nanoseconds of the discharge initiation and it decays in 25 μs , leading most probably to the formation of stable products such as O_3 and NO.

Ombrello et al. (OMBRELLO; JU, 2008) used a counter-flow burner with a coupled magnetic rotating gliding arc (MGA), for ignition of H_2 -air and H_2 - CH_4 blended air diffusion flames. The discharge was generated in a mixture of preheated air with small concentrations of H_2 and CH_4 . The upstream channel of the counter-flow burner was fed with nitrogen-diluted H_2 .

In the simulations, the species concentrations were fixed at 20% H_2 in 80% N_2 for the fuel side. For H_2 ignition, the model considers the H_2 oxidation and NO_x mechanisms. For ignition of CH_4 , the model uses the dimethyl-ether mechanism. The study did not take into account the presence of ions and excited species. Considering only the NO and NO_2 as the stable species capable of decreasing the ignition temperature.

The comparison of the numerical model with the measurements of ignition temperature and species concentration showed that NO enhanced ignition more than NO_2 and NO_x was the primary source of ignition enhancement by the plasma.

The authors argue that for an H_2 -air flame, without NO addition, the HO_2 produced by the reaction (R23) was not readily consumed. So, HO_2 became an inhibitor to the ignition. With NO addition, a new pathway for HO_2 consumption takes place by reaction (R16) to produce active OH radicals. Moreover, there is a catalytic cycle that converts the NO_2 to NO via reaction (R17).

In the case of H₂-fuel-blended air flames, the measurements showed that the ignition temperature increases with the H₂ content. Numerical and experimental results support that plasma-enhanced ignition in fuel-air mixtures increases the HO₂ consumption and therefore, can also suppress inhibitive effects of H₂O.

In CH₄-blended air, the results showed that the significant increase in the ignition temperature was mainly due to the unoxidized CH₄ consuming the active OH radicals and converting to CH₃ through the reaction (R33):



Other important reactions of CH₄ consuming the active radicals of O and H are:



The authors also point out that the active radical consumption by CH₄ inhibited ignition because they competed with the branching reactions for H₂ oxidation (R28) and (R36).



Simulations involved the measured concentration of CH₄, CO, CO₂, NO, NO₂, and H₂O was compared with the results of only CH₄, NO, and NO₂ addition. The results show that the exclusion of CO, CO₂, and H₂O do not change significantly the ignition temperatures. The addition of NO and NO₂ promote a reduction in the CH₄ production of OH by reaction (R34), due to the emergence of O consumption by the reaction (R18).

The model shows that reaction (R34) was a strong consumer of O without NO addition, while reaction (R18) became a significant consumer of O with NO addition. The authors also point out that reaction (R18) competes with reaction (R17) for the conversion of

NO₂ to NO. But reaction (R17) was a chain carrier of O to OH, whereas reaction (R18) converted O to O₂.

Dors et al. (DORS et al., 2014) presented a chemical kinetics modeling study of the methane pyrolysis by an atmospheric pressure microwave plasma. Experimental results were compared with the calculated ones. A set of 48 reactions was considered with 20 species. No soot formation neither electron reactions were considered in the model.

For the 1-D model, the Plug Flow Reactor (PFR) method was used and the plasma was represented by a simple cylinder. In this model, at an initial temperature of 2000 K, the numerical results fit quite well the experimental ones. However, the model still presents temperatures far from the experimental.

The authors point out that the H₂ concentration is higher than predicted by the model and that it is due to small amount of water vapor entering the plasma region, acting as an additional source of hydrogen.

The results show that the dissociation of the first C-H bond in the CH₄ molecule (R37) starts the chain of reactions.



H atoms originated from that reaction attack CH₄ causing the formation of H₂ through (R35). This reaction is responsible for the production of 74.6 % of the hydrogen, followed by reactions (R38) (10.8 %), (R39) (7.1 %) and (R40) (6.8%).



The authors point out that acetylene (C₂H₂) is involved in many reactions but is produced mostly by ethylene (C₂H₄) in direct reaction (R39) and through C₂H₃ radical in reaction (R41):



Ethylene is formed in reaction (R42) but is decomposed and so, acting as a source of acetylene in reaction (R39) and restoring methane through reaction (R43).



By using the model above, it can also be shown that the CH₄ pyrolysis does not occur in the plasma region but in the swirl gas flowing around the plasma.

One important aspect showed by the authors for their particular case is that, the chemical kinetics is controlled by thermal process and the products can be defined by considering thermodynamic equilibrium.

Korolev et al. (KOROLEV et al., 2014a) studied a DC gliding arc generated in a premixed mixture of CH₄ and air at atmospheric pressure. Electrical diagnostics and gas analysis show that increasing of the fuel content decreases the NO production by the discharge, which occurs due to the collisions between N₂^{*} and O:

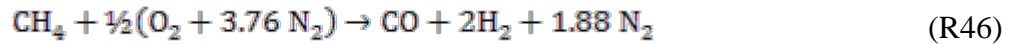
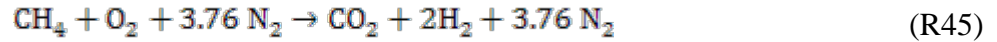


The decrease of NO production occurs due to the fact that methane oxidation competes with the NO formation for the consumption of oxygen. For an air excess coefficient (α) above 3.2 (which corresponds to equivalence ratios lesser than 0.31), the methane oxidation takes place at the plasma column.

The authors also show that for $\alpha \sim 3$ ($\Phi \sim 0.33$) the methane oxidation starts in the plasma jet and enhance the temperature of this region. Then the NO molecules can appear both in the plasma column and in the jet.

For the stoichiometric mixtures, the processes of NO formation are practically suppressed by the processes of methane oxidation. For $\alpha < 1$ (fuel-rich mixtures) the content

of CO₂ decrease and CO and hydrogen start being the main components in the exhaust gas, following the reactions (R45) and (R46):



Wu et al. (WU et al., 2015) characterized a GA for flame stabilization and the exhaust gas by means of optical emission spectroscopy and gas analysis. They showed that the complete oxidation of methane (R47) only occurs for equivalence ratios below 0.8:



When Φ is in the range of 0.8 to 1.1, the main dominant mechanism is the reaction (R45). So, in this range, the concentrations of CO and H₂ are nearly equal. For equivalence ratios above 1.1, the effect of reaction (R46) grows. The authors point out that the concentration of CH₄ on the exhaust gas is negligible in all conditions.

When the equivalence ratio is lower than 0.3, the intensities of OH are found to sharply increase with the increase of the equivalence ratio. This is due to the partial oxidation of methane, which produces OH radicals by reactions (R48) and (R49) (TANG; ZHAO; DUAN, 2011):



Where the CH₂O resulting from (R49) will further react with OH to form H₂O and HCO (LI et al., 2014; SÁNCHEZ et al., 2000) through the reaction (R50):



Besides that, OH also contributes to methane consumption through the reactions (R33) and reaction (R51):



The CH₃ generated by reaction (R33) reacts with atomic oxygen generating CH₂O and hydrogen through reaction (R52):



Cheng et al. (CHENG et al., 2018) developed a 2D model of a packed bed DBD reactor, considering plasma reactions of CH₄ and CO₂. An ns pulse voltage is used to drive plasma in this model.

The model indicates that the dissociation of CO₂ and CH₄ by electrons is the main production reactions of CO and H₂. The dominant pathway in H₂ production is the dissociation of CH₄ by electrons through reactions (R53) and (R54):



The comparison of the model with experimental results also shows that for dry reforming of natural gas, the nanosecond pulse packed bed DBD presents a higher conversion rate and high energy efficiency than the conventional AC DBD.

The discussed studies present the main possible reactions on plasma-assisted combustion. It can be seen that all papers converge to the action of the non-equilibrium plasma producing hydrogenated and oxygenated species, which modifies the oxidation pathways of hydrocarbons and CO. However, it needs to be pointed out that the PAC mechanism is not fully understood and there is much advance that still needs to be done.

2.5 Gliding arc discharges

The gliding arc (GA) is a non-stationary discharge that is set-up between two divergent electrodes. The breakdown occurs in the shortest gap between the electrodes and the plasma column is then dragged out by the gas flow. This push movement promotes the column elongation and it is cooled down until the applied voltage cannot sustain the discharge, so the plasma extinguishes and the cycle restarts at the shortest inter-electrode gap. The discharge can also be reignited if the breakdown voltage is reached again during a cycle. Figure 2.8 exemplifies the development of a gliding arc discharge.

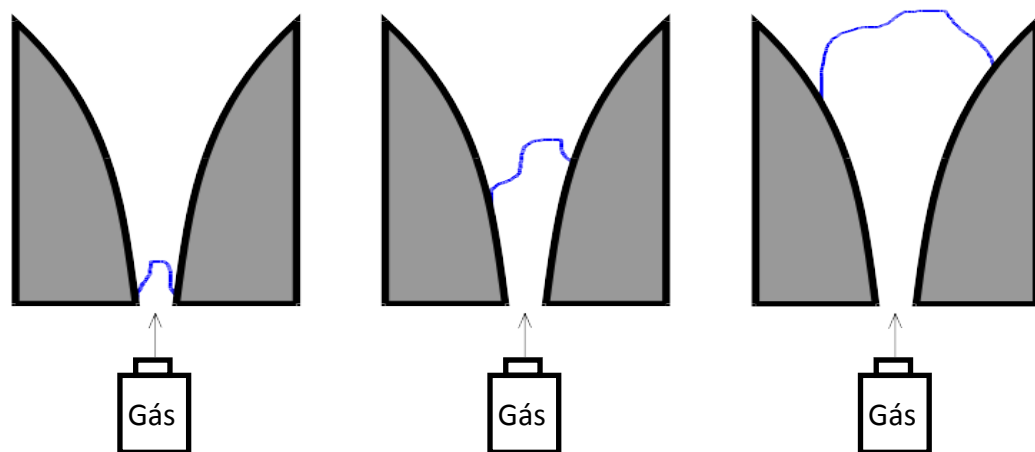


Figure 2.8 - Example of the development of a gliding arc discharge in 2D geometry.

The gliding arc discharge shows a high versatility: it can be powered by AC or DC power supplies, it can operate in a wide range of pressures (from few Torr to atmospheric pressure) and currents (from few mA to tens of A) and it can be constructed in various geometries: 2D or planar GA (KOROLEV et al., 2011; ZHU et al., 2017), coaxial (FULCHERI; ROLLIER; GONZALEZ-AGUILAR, 2007; KOROLEV et al., 2007b), forward vortex flow (FVF) (WU et al., 2015; ZHU et al., 2016) and the reverse vortex flow (RVF) (KALRA et al., 2005). This last promotes better gas mixing, improves the electrodes lifetime and lower heat losses through the walls.

Moreover the operational versatility of GA allows to reach different stages with different properties. For currents on the range of A, the arc starts close to the local thermal equilibrium (LTE), while near its extinction, it is far away from LTE (KOLEV; BOGAERTS, 2015a). When operating in the range of 100 mA or bellow, the discharge can suffer a transition and then shows characteristics of glow discharges, the so-called gliding glow (KOROLEV et al., 2007b, 2011). It occurs when the electric potential is not high enough to sustain the discharge via the field emission mechanism and so, the discharge is sustained by secondary electron emission. It is important to notice that both regimes (i.e, gliding arc and gliding glow) could be present in the same cycle of the discharge evolution. Theoretical studies comparing gliding arc and gliding glow show that the reduction in electrical potential, electric number density and temperature only change at the cathode region (KOLEV; BOGAERTS, 2015a). They also show that both regimes have energy exchange between the plasma column and the hot gas that surrounds it dominated by convection. In the case of the gliding arc regime, the energy transport is mainly due to the presence of gas eddies. In the case of the gliding glow regime, the energy transport occurs mainly due to the bulk motion of the neutral, charged and excited species (KOLEV; BOGAERTS, 2018).

One way to reach the gliding glow discharge mode is the preparation of the electrodes (KOLEV; BOGAERTS, 2015a; KOROLEV et al., 2014b). Clean and polished electrodes promote an electrical field that is not strong enough to establish the field emission and so, the discharge goes to gliding glow mode. Irregularities and impurities on the electrodes surfaces can promote a local amplification of the electric field and then, the discharge can be sustained by field emission, i.e., in gliding arc mode.

In the gliding arc mode, the plasma channel remains fixed at the electron emission point and is possible to take a plasma with a bigger volume (in comparison with gliding glow). However, this is a recent discussion in literature and there are few studies comparing these two regimes.

2.6 Gliding arc applied to PAC

There are a many studies about GA applied to combustion processes. Ombrello et al. (OMBRELLO et al., 2006) showed that in a counter-flow burner with air and nitrogen diluted methane, a gliding arc discharge disk-like generated in air with low power increases the extinction limits of the diffusive flame.

By means of planar laser-induced fluorescence (PLIF), electrical diagnostics and high-speed imaging, Zhu et al. (ZHU et al., 2015) points out that the use of an AC gliding arc discharge in a premixed mixture of air-methane integrated with a flame promotes the formation of OH and formaldehyde (CH_2O) in fuel-lean mixtures. The authors also point out that the presence of flame reduces the ignition voltage of the discharge.

Wu et al. (WU et al., 2015) showed that a methane-air premixed flame becomes more stable by the application of a gliding arc due to the feeding of the flame with species such as CO and H_2 . They also point out that the increase in applied power can improve the production of OH radicals and then, benefits the whole process.

Varella et al. (VARELLA; SAGÁS; MARTINS, 2016) used a gliding arc discharge generated in natural gas and air with equivalence ratios from 1.2 to 1.4. The authors showed that the applied power increase promotes growth of the plasma density, which improves the hydrocarbon cracking and so, the H_2 concentration, as shown in figure 2.9.

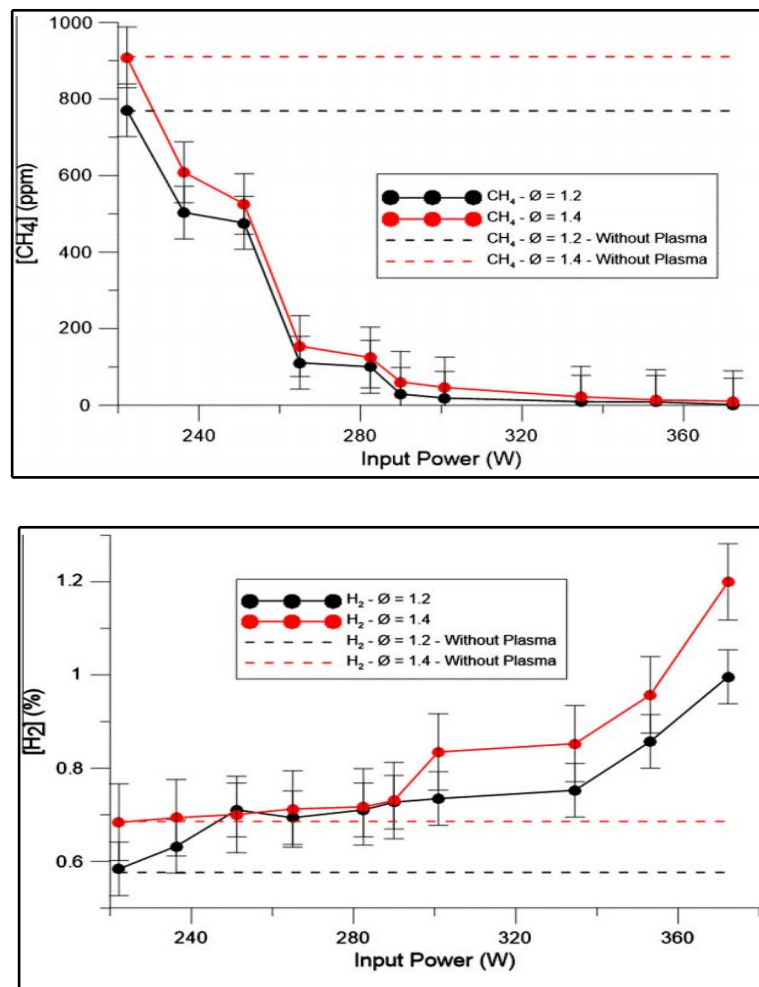


Figure 2.9 – CH_4 and H_2 concentrations as functions of the input power for different equivalence ratios (VARELLA; SAGÁS; MARTINS, 2016).

The increased power promotes higher hydrocarbon cracking to form H_2 . In this way, they found that the concentrations of methane (CH_4) and other hydrocarbons as ethane (C_2H_6) and propane (C_3H_8) diminish with the increase in applied power until 330 W, when these hydrocarbons are totally dissociated.

The carbon monoxide levels follow the hydrocarbon behavior. The CO oxidation is not so fast, but it can be improved by the plasma-produced H_2 which benefits the formation of hydroxyl radical (OH) which accelerates the CO oxidation. The concentration of NO increases with the applied power, rising from 30 ppm without plasma, to more than 200 ppm with plasma at 370 W.

Coupling an AC gliding arc reactor to an industrial low NO_x combustor, Lee et al. (LEE et al., 2013) and Song et al. (SONG et al., 2013) had obtained a decrease in the NO_x concentration due to the plasma produced hydrogen. It was shown also that the concentration of air in the gas mixture that feeds the plasma, has a significant impact on increasing the NO_x produced volume (SONG et al., 2013).

In fact, the plasma operated in fuel-rich conditions leads to the formation of CO and H_2 . The hydrogen-rich, high-temperature flow ignites the fuel-air mixture at the burner head. The expanded high-temperature gas detached the main flame from the burner rim (from about 5-15 cm above the burner head). The high burning velocity of hydrogen avoids the flame blow off.

This flame detachment provides time and space for better mixing and shifts the flame from a diffusion flame to a partially premixed flame. Both behaviors are favorable to the NO_x lowering (LEE et al., 2013).

Using optical emission spectroscopy of an AC powered GA generated in a premixed mixture of natural gas and air with equivalence ratios from 0.4 to 3.0, Sagás et al. (SAGÁS; MACIEL; LACAVA, 2016) showed that the intensity of the NO lines decreases with the equivalence ratio increase from 0.4 to 1.4. This is due to the greater hydrocarbon concentration in the inlet gas, lowering the NO produced by the plasma. The OH intensity is bigger close to the stoichiometric condition. The atomic hydrogen intensity increases with the equivalence ratio due to the hydrocarbon cracking in the plasma region, producing also molecular hydrogen, as could be verified in the plasma spectrum.

In their study, an analysis by high-speed camera shows that the flame ignition occurs at the plasma breakdown and the flame stabilizes axially inside the reactor while the plasma

column glides along the spiral electrode. After the discharge extinction, the visible flame remains inside the reactor from about 5 ms and extinguish itself if the mixture is out of the flammability limits without plasma.

The authors also pointed out that the H_2 produced in the plasma region is consumed in the flame. So, the GA generated in natural gas and air mixture is an efficient way to promote hydrogen enrichment of flames and consequently increase the flammability limits and the thermal energy release, intensifying the flame brightness.

3 Experimental Setup

3.1 System description

The gliding arc reactor was installed in the swirl burner. It is a typical reverse vortex flow plasma reactor, composed by a cylindrical chamber made of stainless steel with 50.0 mm in length, with an inner diameter of 25.7 mm and 10.1 mm of wall thickness. A convergent-divergent nozzle (throat diameter is 12 mm, inlet and outlet diameters are 16 mm) acts as the ground electrode while the reactor wall acts as the negative one. The smallest gap between the electrodes is 4 mm. The reactor is electrically insulated by a polytetrafluoroethylene (PTFE) sleeve. Figure 3.1 shows the schematics of the reactor and the burner.

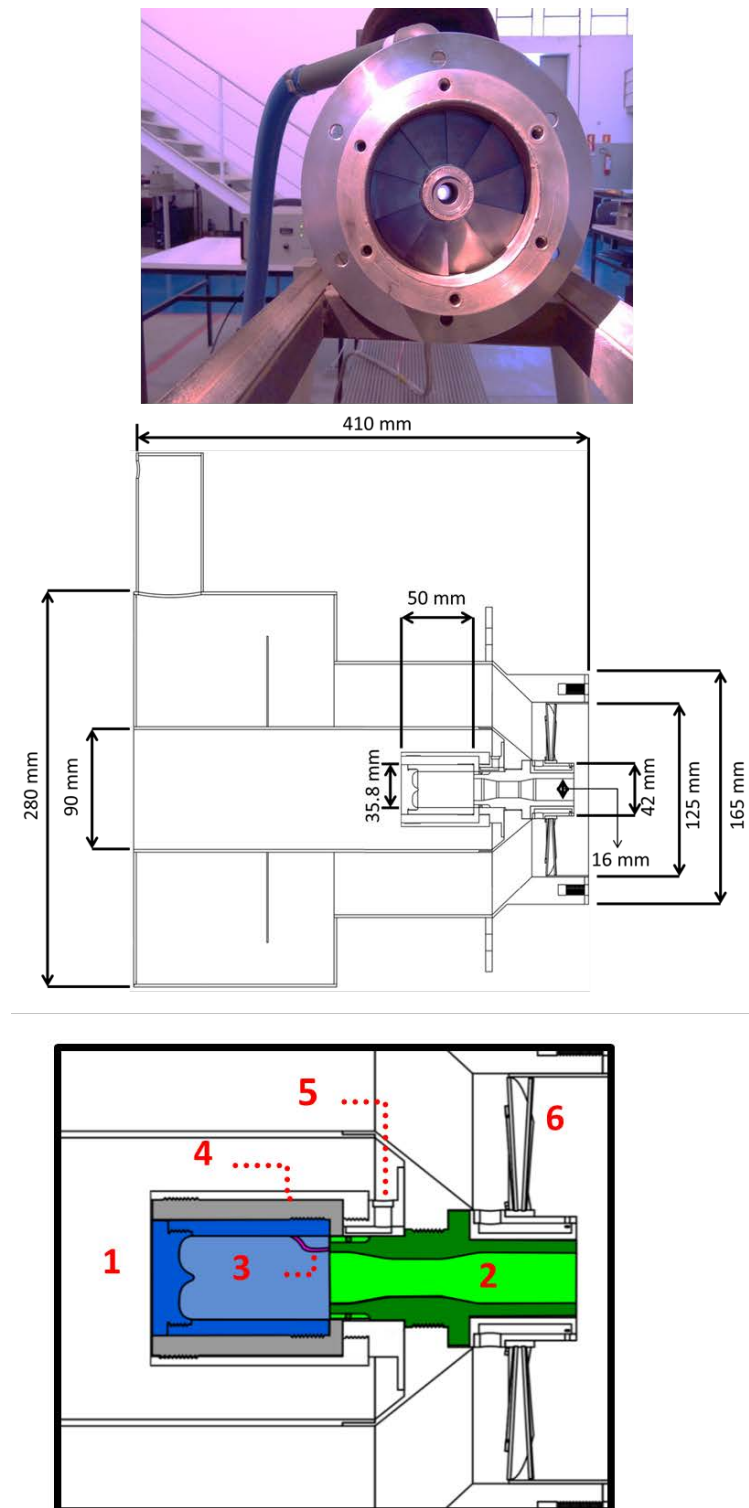


Figure 3.1 - Schematics of the burner and the plasma reactor. Upper panel - swirl burner. Central panel - a schematic of the whole system. Lower panel - a zoom of the reactor. On the lower panel: 1 - reactor wall, 2 - convergent-divergent nozzle, 3 - discharge breakdown, 4 - PTFE sleeve, 5 - reactor gas inlet, 6 - the swirler.

The burner is also made in stainless steel with a length of 410 mm, a bottom diameter of 280 mm and a gas exit diameter of 123 mm. The swirler of the burner is composed of 10 blades with a swirl angle of 80° . High swirl angles promote the generation of a high recirculation zone that enhances the mixture homogeneity in the combustion zone (SILVA, 2011), allowing the system to operate with global equivalence ratios lower than to 0.6. Figure 3.2 exemplifies the recirculation structure formed by the swirl and the flame produced by the present burner.

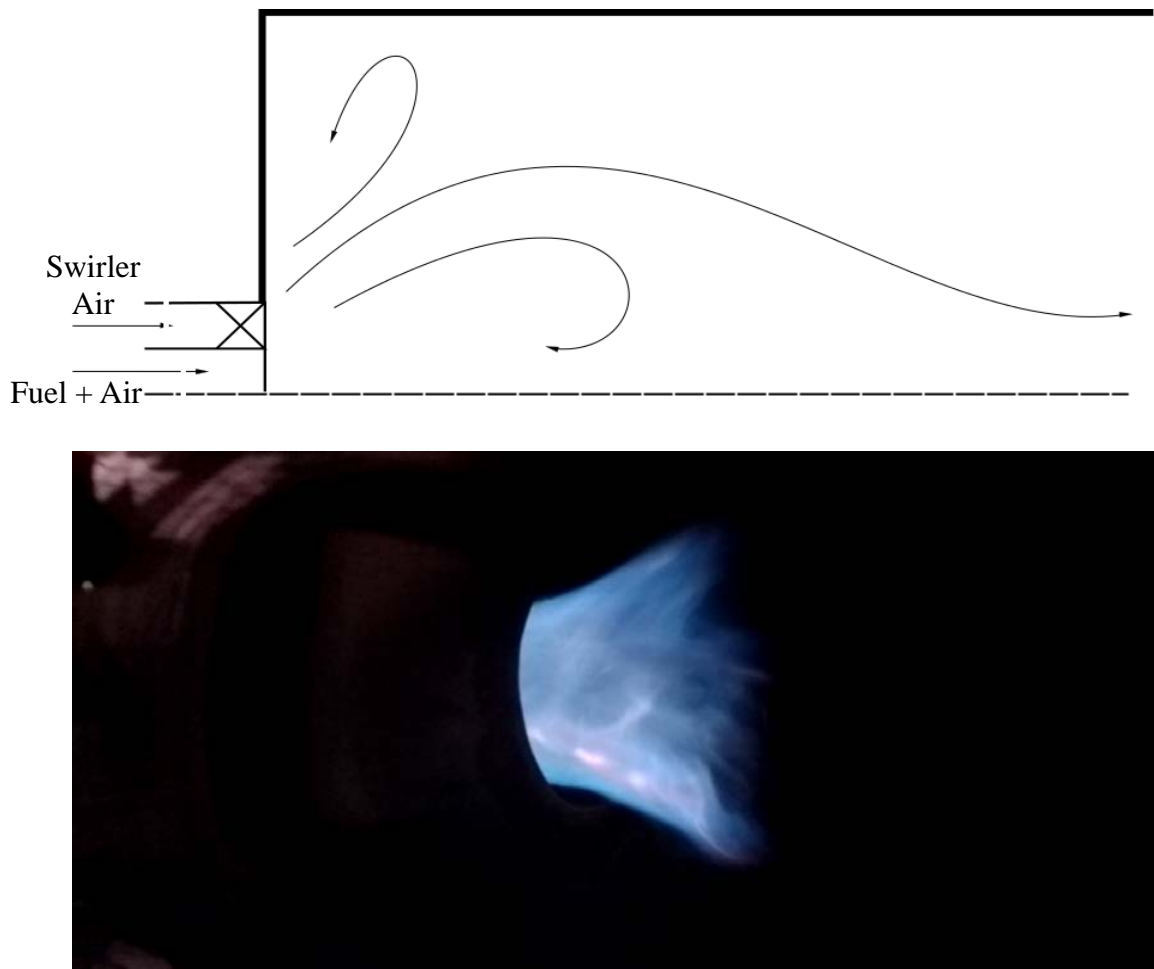


Figure 3.2 - Schematics of the recirculation structure generated by a swirl flow (top) and an example of the flame generated by the present burner without plasma.

It is worth to mention that the plasma application did not change any visual aspect of the flame during the tested conditions.

The swirl number is a dimensionless quantity, which quantifies the strength of the recirculation promoted in the device. It represents the ratio between the flow angular momentum and the flow linear momentum. It can be calculated following the methodology

exposed in (SILVA, 2011) and presented in appendix A. For the present experiments, the flame swirl number relies between 14.10 and 32.54. The variation of the flame swirl number (S') with the plasma reactor equivalence ratio is shown in figure 3.3.

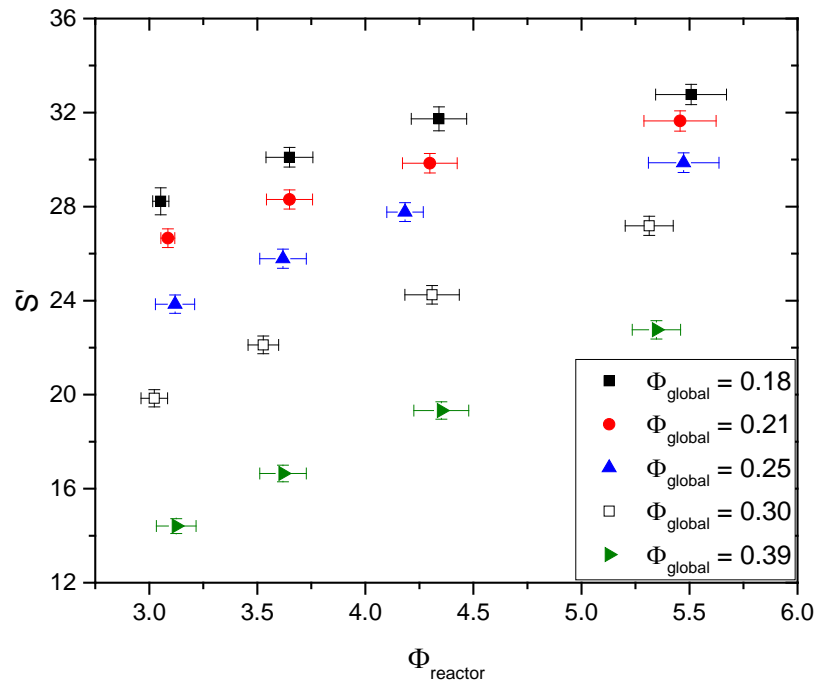


Figure 3.3 – Flame swirl number (S') as a function of the plasma reactor equivalence ratio Φ_{reactor} .

This is a very high swirl number that can promote an intense recirculation flow. Therefore the reactant mixing is improved and so, it is possible to sustain a flame in very lean conditions, below the flammability limits. It can be highlighted that for this calculation, it was considered that the flow that emerges from the reactor does not present a significant angular momentum and the plasma does not change considerably the flow dynamics in the reactor.

In this burner configuration, it is possible to change the fuel injection mode: it can be injected axially passing through the reactor, it can be injected radially to the swirl air flow and the fuel can be also injected combining these two modes, as shown in figure 3.4. However, in the present case, only the axial fuel injection was investigated, which means that all fuel injected passes through the plasma reactor.

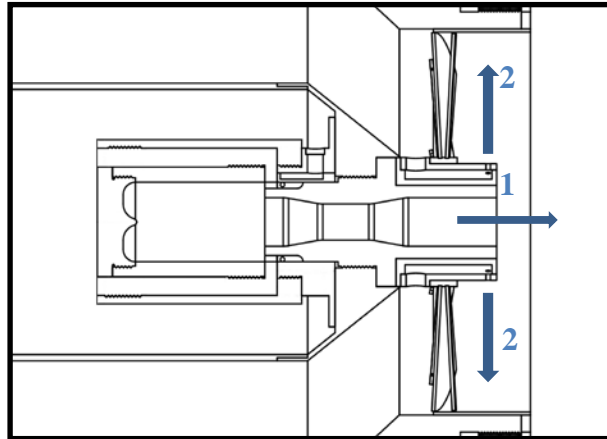


Figure 3.4 - Fuel injection modes of the burner. 1 - Axial fuel injection, 2 - radial fuel injection.

In spite of the air and fuel are not injected premixed, by the intense recirculation flow promoted by the swirler (high swirl number), it is possible to suppose that combustion happens in a turbulent global fuel-lean premixed swirling flame, whose aspect can be seen in figure 3.2. It is not possible to measure the local flame equivalence ratio in the present device; so that the combustion condition was characterized by the global equivalence ratio, calculated based on the fuel and air mass flow rate. In this context, it was supposed that flame local equivalence ratio follows the same tendency of the global equivalence ratio.

As the burner operates with very low equivalence ratios, the device promotes the formation of a very global fuel-lean flame. Although the flame temperature was not measured in this study, it is well known that in these conditions, flames typically have low temperatures, which promotes low formation of NO_x . This is due to the fact that in combustion systems, most of the NO_x is formed due to the thermal mechanism (also known as the Zeldovich mechanism), which presents a high-temperature dependence. However, low temperatures also slow the hydrocarbon and CO oxidation mechanism leading to high concentrations of carbon-based compounds on the exhaust gas.

The plasma-assisted burner is coupled to a combustion chamber with a square section of 500 mm and length of 600 mm. A convergent nozzle connects the chamber to the exhaust duct that has 550 mm of length and 300 mm of diameter. The chamber has two rectangular quartz windows for optical access (50 mm x 200 mm). The chamber has an entry to sample gas collecting at the exhaust duct. This entry is located 1000 mm from the burner exit. Figure

3.5 shows the burner coupled at the chamber and figure 3.6 shows their schematics with respective dimensions.

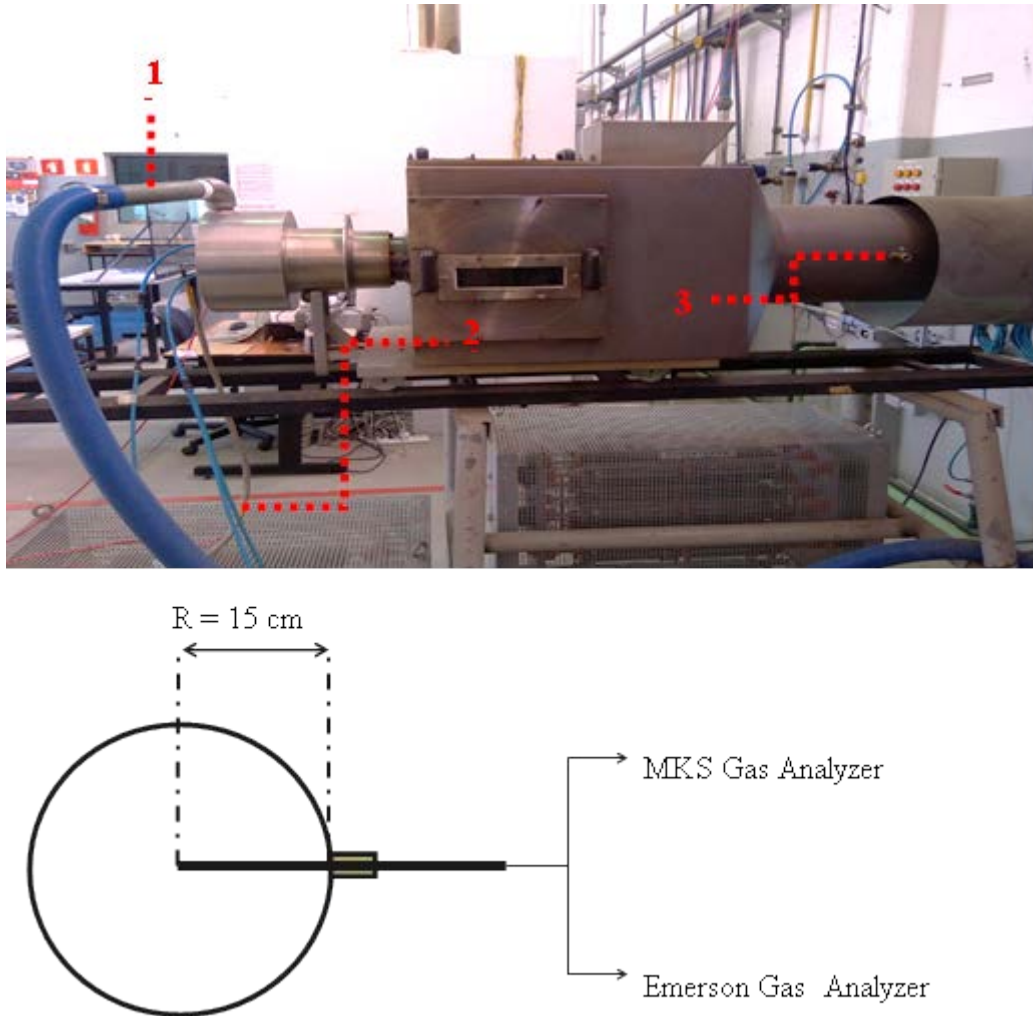


Figure 3.5 - Combustion chamber (on top) and the gas sample probe (bottom). At top panel: 1 - the swirler gas inlet, 2 - the reactor gas inlets and 3 - the gas sample probe entry. On the bottom panel, the indication of the gas sample probe on the exhaust duct.

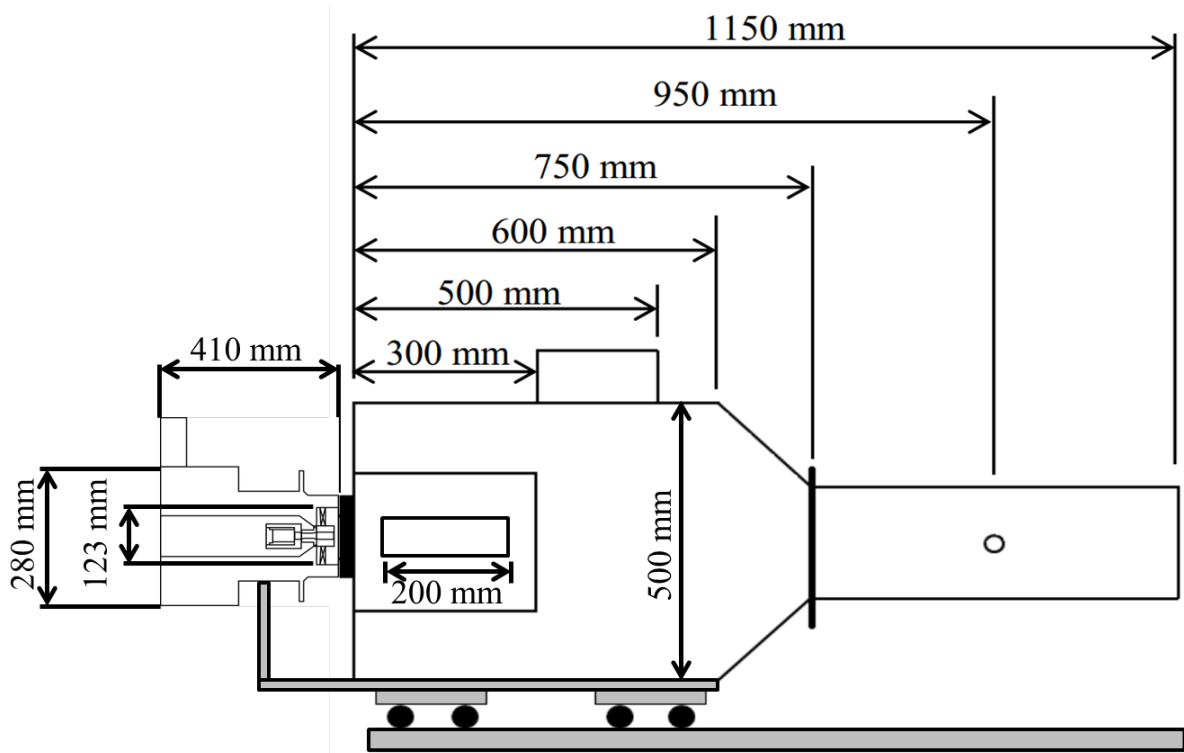


Figure 3.6 - Schematics of the combustion chamber and the burner with respective dimensions. Quartz window indicated by the double arrow of 200 mm. Exhaust duct has 300 mm diameter. Adapted from (ALVES, 2013).

The mass flow rates to the reactor were controlled by needle valves. The ranges of the mass flow meters are 0 - 1.00 g/s for natural gas and 0 - 15.00 g/s for air that feeds the plasma reactor, both with a 1.5 % precision of the full scale.

The swirler air mass flow rate was monitored by a Kurz 504FTS-24 mass flow meter with a 0-50.00 g/s range and precision of 1.3 % of the reading. A blower supplies the air and a frequency inverter controlled the air mass flow rate.

The assumed fuel gas composition for all tests was: CH₄ (88.683%), C₂H₆ (5.844%), C₃H₈ (2.339%), C₄H₁₀ (0.771%), C₅H₁₂ (0.128%), C₆H₁₄ (0.025%), CO₂ (1.616%), N₂ (0.594%) (COMPANHIA DE GÁS DE SÃO PAULO - COMGAS, 2014; TORRES, 2014).

For all conditions, the fuel mass flow rate was fixed at 0.50 g/s. So, the thermal power (product of the lower heating value and the fuel mass flow rate) of the burner was 23.2 kW for all tested conditions.

The equivalence ratio definition (E1) was used in order to identify separately the flame and the plasma. So, Φ_{reactor} was defined as the equivalence ratio of the mixture inside the reactor (with or without plasma) and Φ_{global} the equivalence ratio of the whole mixture that is

injected to the flame zone (i.e., it considers all the injected gas mass flow rates, including the reactor one). In this way, as the entire fuel passes through the reactor and feeds the flame, it is the air mass flow rate (in the reactor and in the swirler) that determines the difference between Φ_{reactor} and Φ_{global} .

The discharge was generated and sustained using a BRC 10 kV - 1 A Unipower DC power supply from Universal Voltronics with a 10 kW maximum output power in voltage regulation mode. A 50 k Ω - 2 kW ballast resistor was installed in series with the power supply in order to limit the discharge current to 200 mA.

A Tektronix TDS2024C oscilloscope with an impedance of 1 M Ω in parallel with 20 pF, 2 GS/s maximum sampling rate and two Tektronix P6015A 1000:1 voltage probes were used to obtain the voltage and current waveforms. The current waveforms were taken from the subtraction of the voltage signals measured at the two terminals of the ballast resistor, in accordance with Ohm's law.

3.2 Discharge characterization methodology

The GA characterization was performed measuring the current and voltage waveforms. The application of a Fast Fourier Transform (FFT) allowed the analysis of the discharge repetition frequency.

In an effort to compare the electrical power consumed by the discharge with the thermal power derived from the fuel burn, it was defined a quantity to represent the power of the discharge:

$$P' = U_m \cdot I_m \quad (\text{E2})$$

where U_m and I_m are respectively, the mean voltage and mean current of the discharge.

It can be noted that this quantity is taken as representative of the electrical power given that the voltage and current waveforms were not recorded at the same time. So, with no data about the phase between the two waveforms, P' could not correspond to the real value of the discharge electrical power.

In the first series of measurements, the GA reactor operated using two fixed fuel mass flow rates: 0.25 g/s and 0.49 g/s. For each one, the air mass flow rate was varied to achieve

equivalence ratios from 3.0 to 5.2 in the reactor. Therefore the total mass flow rate varied at the same time.

A set of additional experiments was performed using fixed total gas flow rates (1.85 g/s and 2.10 g/s), i.e. the air flow rate was reduced proportionally to the fuel flow rate increase, in order to change only the equivalence ratio. So, with this set of experiments, it was possible to verify the effects over the discharge characteristics promoted by the isolated increase of the fuel concentration in the reactor feed mixture.

All the error bars presented in the electrical graphs consider the standard deviation of the measurement as well as the equipment uncertainty (around 3% of the full scale).

3.3 Gas analysis methodology

The composition of the exhaust gas was monitored by an Emerson Rosemount Analytical MLT4 gas analyzer (for O₂ and H₂ measurements) and an MKS 2030 FTIR gas analyzer (for CO₂, CO, NO, NO₂, H₂O and hydrocarbon measurements).

In the present study, the total hydrocarbon content (THC) is composed by: methane (CH₄), ethane (C₂H₆), ethylene (C₂H₄), propane (C₃H₈), methanol (CH₃OH), acetaldehyde (C₂H₄O), propylene (C₃H₆), acrolein (C₃H₄O) and acetylene (C₂H₂). The calculation is performed by the MKS 2030 gas analyzer following the equation (E3):

$$\text{THC} = 2 [\text{C}_2\text{H}_4\text{O}] + 2 [\text{C}_3\text{H}_4\text{O}] + 2.4 [\text{C}_2\text{H}_2] + [\text{CH}_3\text{OH}] + 1.1 [\text{CH}_4] + 2 [\text{C}_2\text{H}_6] + 1.9 [\text{C}_2\text{H}_4] + 3 [\text{C}_3\text{H}_8] + 2.85 [\text{C}_3\text{H}_6] \quad (\text{E3})$$

where the multiplication coefficient of each considered specie is determined in the factory calibration by comparison with flame ionization results.

The MLT module performs electrochemical measurement of O₂ using a circuit arrangement where O₂ reacts with the analyzer electrodes generating a current proportional to the compound concentration in the gas sample.

The H₂ concentration is measured by the thermal conductivity technique. In this case, a metallic wire heated by an external circuit is immersed in a gas cell. If the gas that filled the gas cell contains hydrogen, it will promote cooling of the wire proportional to the hydrogen concentration.

The FTIR (Fourier Transform Infrared) analyzer uses infrared absorption spectroscopy to evaluate the concentration of the compounds. Since each polar molecule absorbs infrared (IR) light in specific wavelengths, each one has a unique fingerprint spectrum. Therefore, the raw data is processed using a Fourier transform algorithm, which turns the measured absorption values into concentration data.

Both gas analyzers have a heated gas probe and a diaphragm pump to collect the sample gas. The sampling rate is 0.25 Hz.

In order to verify the best location of the sample probe, it was performed a set of experiments varying the position of the probe radially to the exhaust duct. In the experiments, a 6 mm diameter stainless steel probe was placed in three different positions from the center of the exhaust duct in order to verify if the exhaust gas composition varied radially. The results are shown in figure 3.7.

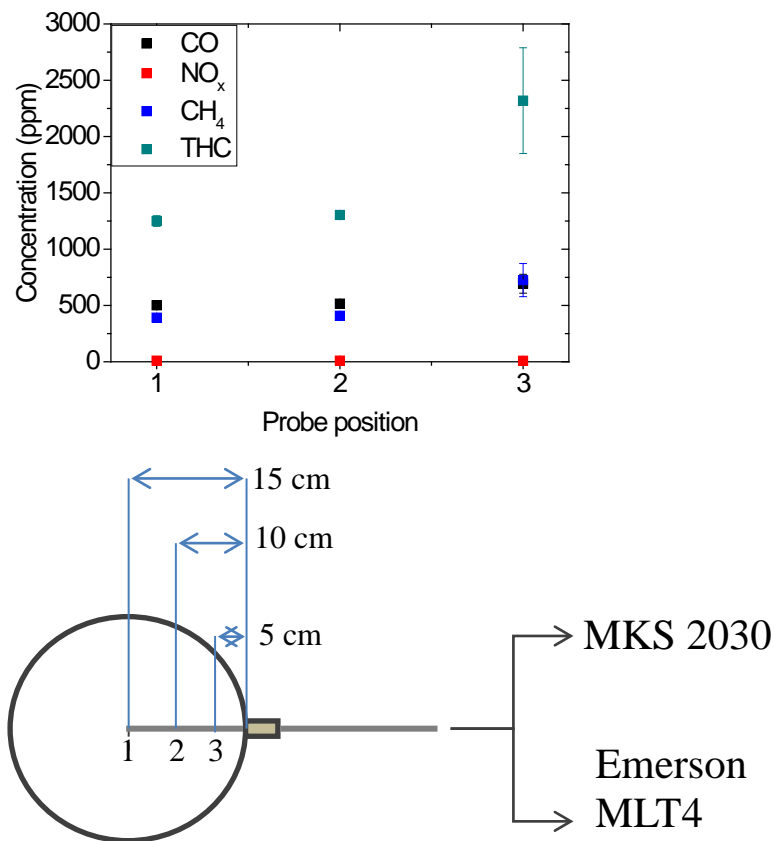


Figure 3.7 – Raw data concentration of the main compounds as a function of the sample probe position (1, 2 and 3). Condition: $\dot{m}_F = (0.50 \pm 0.01)$ g/s and $\dot{m}_{air} = (49.97 \pm 0.12)$ g/s. No plasma application. On the bottom panel, the three tested positions (1, 2 and 3) for the probe in relation to the center of the exhaust duct used to verify the radial homogeneity of the flow. The sample gas was divided between the two gas analyzers.

Thus, as the sample probe position could lead to different data, it was replaced by a 6 mm diameter stainless steel probe with 15 holes (with a diameter of 1 mm each, inter-spaced by 10 mm) placed transversally to the gas flow on the exhaust duct of the combustion chamber. Therefore, the collect sample is, in fact, a composition radially distributed of the exhaust gas. The gas sample was then distributed to the two gas analyzers.

For the gas analysis, the fuel mass flow rate was fixed at 0.50 g/s and the reactor air mass flow rate was varied from 1.6 to 2.8 g/s. This corresponds to Φ_{reactor} from (5.4 ± 0.1) to (3.1 ± 0.1) , respectively. The swirler air mass flow rate was varied from 20.00 to 50.00 g/s, which corresponds to Φ_{global} from (0.39 ± 0.01) to (0.18 ± 0.01) . The composition of the exhaust gas was monitored with and without plasma to define the role of the GA discharge at the combustion mechanism and to the exhaust gas compositions.

It is important to highlight that while the FTIR performed measurements are in wet basis, the MLT4 measurements are performed in dry basis. Thereby, the MLT4 O_2 measurements were corrected to wet basis following the equation (E4).

$$[\text{O}_2]_{\text{wet}} = [\text{O}_2]_{\text{measured}} \cdot \frac{100 - [\text{H}_2\text{O}]_{\text{measured}}}{100} \quad (\text{E4})$$

where the measured concentration of H_2O is given in %.

Moreover, to correct the gas concentration for the diluting effects caused by the excess of air, an O_2 reference value of 15 % was used. The correction was performed using equation (E5):

$$[\text{X}]_{15\% \text{O}_2} = [\text{X}]_{\text{measured}} \cdot \frac{20.9 - [\text{O}_2]_{\text{reference}}}{20.9 - [\text{O}_2]_{\text{wet}}} \quad (\text{E5})$$

where the O_2 concentration in wet basis is given in %.

All the concentration graphs presented in this study have error bars that comprise the standard deviation of the measurement, associated errors due to the corrections, as well as the equipment uncertainty (about 1% of the full scale for the MLT4 and a relative error of 5% for the MKS).

It is also important to verify the reliability of the concentration measurements. Thereby, the experimental measurements of the concentration of some calibration gases with the MKS FTIR gas analyzer were compared with the nominal value provided by the

manufacturer. The results and the comparison with the factory calibration are shown in table 3.1.

Table 3.1: Calibration gases experimental concentration and their nominal value.

Molecule	Calibration points (factory calibration)		LCPE calibration gases*	
	Minimum	Maximum	nominal	experimental**
CH ₄	40.1 ppm	20000 ppm	7997.00 ppm	(7931 ± 15) ppm
			84.42 ppm	(84.06 ± 0.05) ppm
CO low	4.8 ppm	5000 ppm	400.30 ppm	(392.9 ± 0.8) ppm
CO ₂	0.4 %	23.0 %	4.503 %	(4.43 ± 0.03) %
H ₂ O	2.03 %	20.57 %	-	-
N ₂ O	13.4 ppm	200.1 ppm	80.54 ppm	(85.13 ± 0.27) ppm
NO	19.4 ppm	2795 ppm	1307.00 ppm	(1290 ± 0.83) ppm
			87.80 ppm	(86.48 ± 0.73) ppm
NO ₂	32.6 ppm	488 ppm	81.70 ppm	(80.90 ± 0.38) ppm

* White Martins, dilution in N₂.

** average, 30 measurements (30 s)

It can be seen that the measured concentrations agree well with the nominal value, with deviations lesser than 6%.

Besides the good agreement of the measurements, which guarantees an assured calibration, it is important to define a cut point to prevent false positive values in the analysis. So, it was defined that concentrations which present values lesser than two times their standard deviation was not considered in the analysis.

4 Gliding arc discharge in fuel-rich conditions

The voltage waveform is the main feature to understand the GA discharge cyclical development. Figure 4.1 shows a typical waveform of the discharge.

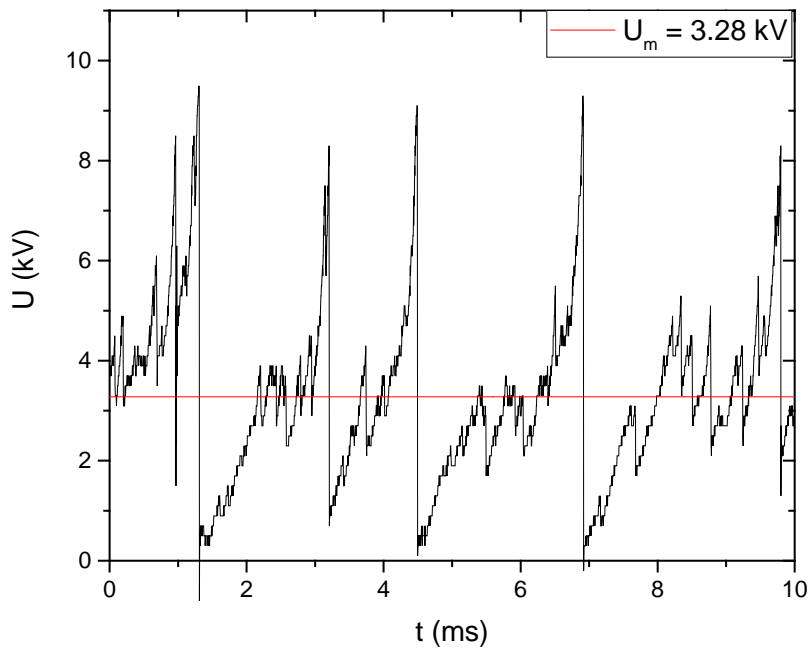


Figure 4.1 - Typical voltage waveform of the GA. Condition: $\dot{m}_F = (0.24 \pm 0.01)$ g/s and $\dot{m}_{air} = (0.79 \pm 0.02)$ g/s. Red line corresponds to the mean voltage (U_m). Voltage in absolute values.

From figure 4.1, it can be seen the cyclical behavior of the GA: the voltage increase until it reaches the breakdown, and then it drops down close to 221 V. After that, the plasma column elongation causes the voltage to rise until the breakdown voltage is reached again, restarting the cycle. As can be seen, at each cycle the shape of voltage rise is changed. Gliding arc discharges are quite unstable, due to the turbulent flow and the different paths the arc travels along the electrodes at each cycle. The voltage drops observed within a cycle can be caused by glow-to-spark transitions (KOROLEV et al., 2007a, 2011) or shortcuts (KOLEV; BOGAERTS, 2015b; PELLERIN et al., 1999). The former is caused by a momentaneous regime change in the discharge, while the second corresponds to an arc shortening. A

variation of breakdown voltage is also observed and can be related to a residual charge concentration from the previous cycle, temperature variations or even electrode irregularities.

The voltage waveforms can be seen as composed by one “low frequency” phenomenon (breakdown) and “high frequency” phenomena (regime transitions, shortcuts, turbulent motion, etc.). It indicates the importance of frequency analysis for this type of discharge, as will be discussed later.

The discharge current waveforms have an opposite behavior of the voltage: at the breakdown, the current in plasma column reaches its maximum value. Then, the elongation promotes the increase of the arc resistance and as a result, current begins to fall until the next breakdown. Figure 4.2 shows a typical current waveform of the GA. As in the case of voltage, high-frequency oscillations can be observed from current waveforms and are directly linked.

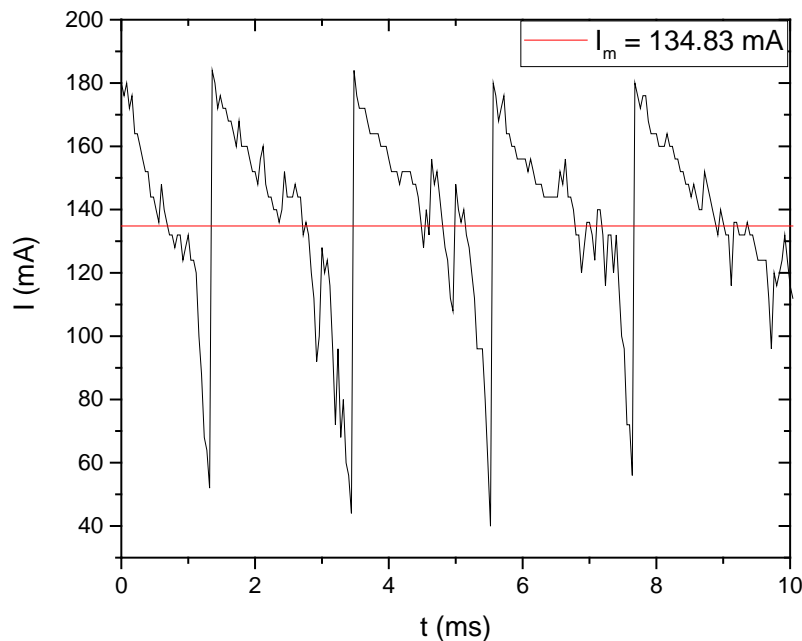


Figure 4.2 – Typical current waveform of the GA. Condition: $\dot{m}_F = (0.24 \pm 0.02)$ g/s and $\dot{m}_{air} = (0.83 \pm 0.01)$ g/s. Red line corresponds to the mean current for the plasma (I_m). Current in absolute values.

It is important to see the effect of the equivalence ratio and the total gas flow rate in the values of voltage and current. Therefore, in the first set of experiments, for a fixed equivalence ratio, the increase in the fuel mass flow rate (and, consequently, in the total gas flow rate) promotes only a small increase in mean voltage.

This increase is around 2.6 - 5.3% except for the equivalence ratio of 3.5, where the variation reached 15%, as shown in figure 4.3a. However, in all cases, the mean voltage variation is within the error bar, which includes the standard deviation and the equipment uncertainty (around 3% of the full scale).

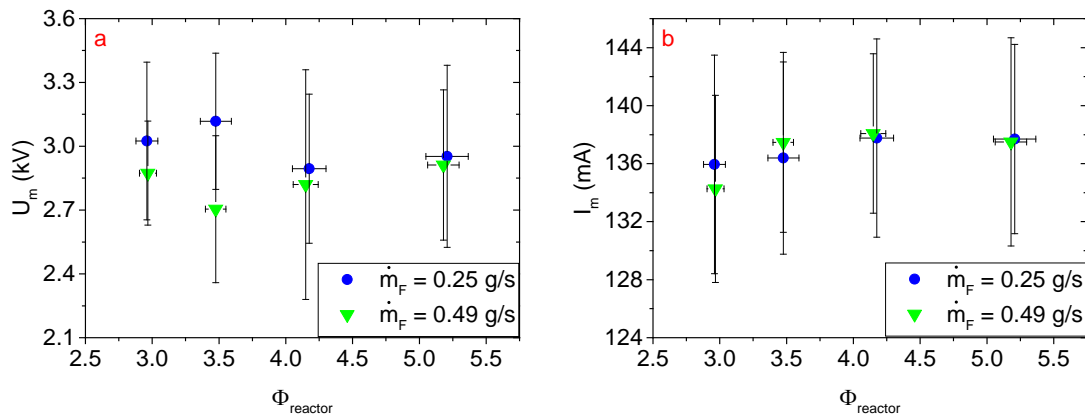


Figure 4.3 - Discharge mean voltage (a) and mean current (b) as functions of the reactor equivalence ratio for the two tested fuel mass flow rates. Mean voltage and mean current in absolute values.

Likewise, the mean discharge current does not change significantly, about 1% in all conditions, as shown in figure 4.3b. In the same way, the variation of the equivalence ratio (by increasing the air mass flow rate) does not significantly change the mean voltage and current.

For the conditions of figure 4.1, P' is between (399 ± 52) W and (425 ± 48) W for conditions with fuel mass flow rate of 0.25 g/s and (372 ± 50) W and (400 ± 53) W for the ones with fuel mass flow rate of 0.49 g/s. This indicates that the discharge power when $\dot{m}_F = 0.49$ g/s represents 1.60 % to 1.72 % of the thermal power.

Figure 4.4 shows the voltage waveforms and its respective FFTs, for two different total mass flow rates at an equivalence ratio of 3.0.

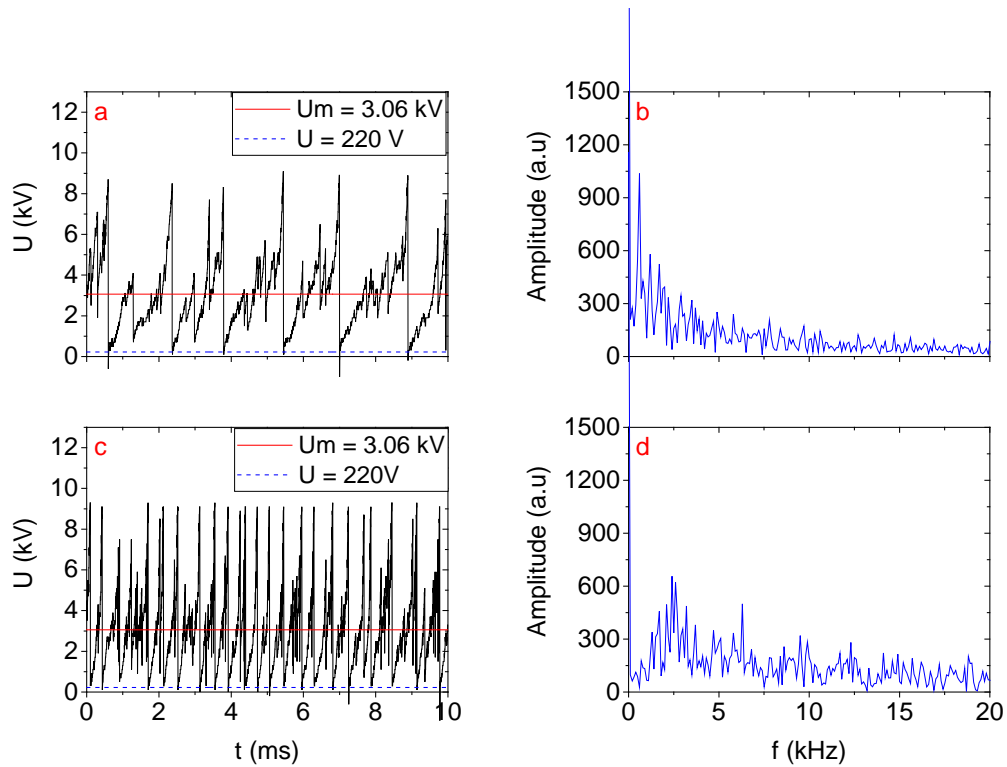


Figure 4.4 - Voltage waveforms (a,c) and respective FFTs (b,d) for two different conditions with $\Phi_{\text{reactor}} = (3.0 \pm 0.1)$. (a) and (b) $\dot{m}_F = (0.25 \pm 0.01)$ g/s, $\dot{m}_{\text{Air}} = (1.42 \pm 0.02)$ g/s (c) and (d) $\dot{m}_F = (0.49 \pm 0.01)$ g/s, $\dot{m}_{\text{Air}} = (2.80 \pm 0.02)$ g/s. Voltage in absolute values.

The breakdown voltage is between (7.72 ± 0.89) and (8.69 ± 0.78) kV. It can be seen that the period (time interval between successive breakdowns) changes slightly for each cycle. This is due to the fact that the plasma column glides along the cathodic wall by different paths in each cycle.

In the second set of experiments, for a total gas mass flow rate of 1.85 g/s, the breakdown voltage is about (6.46 ± 1.26) kV and (5.09 ± 1.00) kV when operating using 0.25 g/s and 0.49 g/s fuel flow rates, respectively. For a higher total flow rate of 2.10 g/s, the breakdown voltage is around (6.62 ± 1.54) kV and (5.81 ± 1.23) kV when the fuel flow rate is 0.25 g/s and 0.49 g/s, respectively. The increase in the breakdown voltage (U_B) with the total mass flow rate was also reported in the literature (SAGÁS et al., 2011) and it is related to the increase of the arc velocity. So, the critical length is reached in a shorter time.

An increase in the natural gas flow rate, for constant total flow rate, promotes a drop in the breakdown voltage, which results in a flattening of the voltage waveform as can be seen in figure 4.5.

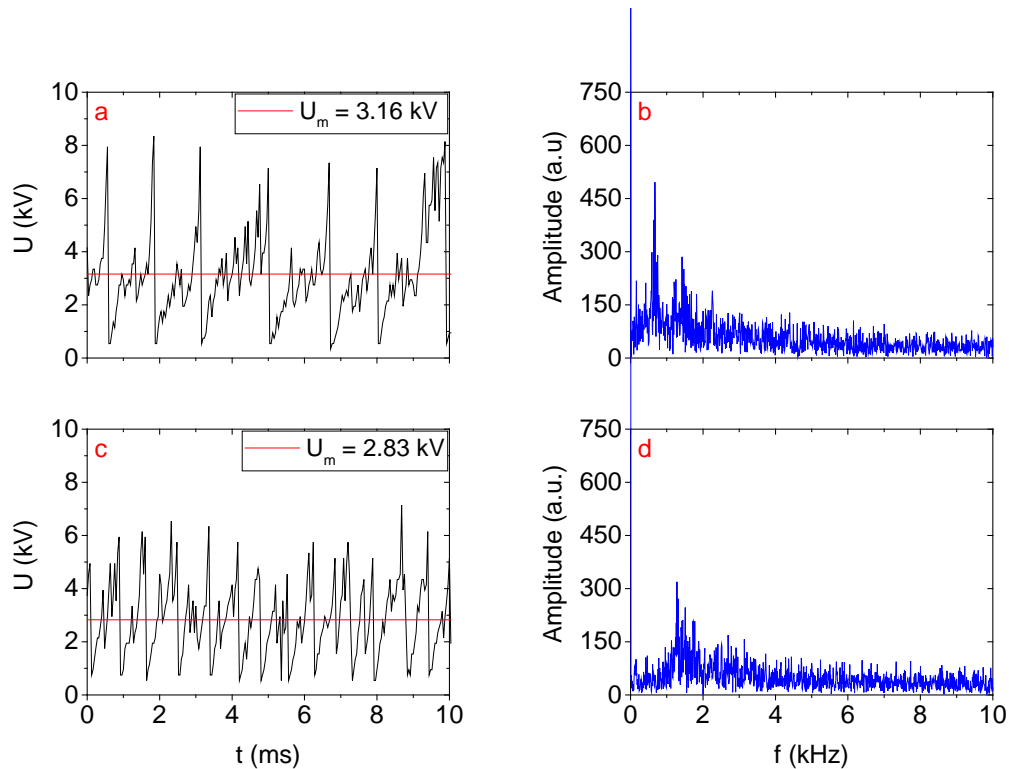


Figure 4.5 - Voltage waveforms and respective FFTs (in blue) for two conditions with a total mass flow rate of 1.85 g/s. (a) and (b) $\dot{m}_F = (0.25 \pm 0.01)$ g/s, $\dot{m}_{Air} = (1.59 \pm 0.02)$ g/s and $\Phi_{reactor} = (2.8 \pm 0.1)$; (c) and (d) $\dot{m}_F = (0.51 \pm 0.03)$ g/s, $\dot{m}_{Air} = (1.35 \pm 0.01)$ g/s and $\Phi_{reactor} = (6.5 \pm 0.4)$. Voltage in absolute values. The line corresponds to the mean discharge voltage (U_m).

This reduction in breakdown voltage can be associated with the lower ionization energies of the major components of natural gas (89% methane - 12.61 eV, 6% ethane - 11.52 eV and 2% propane - 10.94 eV, other components corresponds to 3%) when compared with those of air (78% N_2 - 15.58 eV, and 21% O_2 - 12.07 eV, the sum of the other components is closer to 1%) (LIAS, 2018). Besides that, the total ionization cross section for electron collisions is higher for methane (SONG et al., 2015) than for N_2 (ITIKAWA, 2006) and O_2 (ITIKAWA, 2009). A decrease in oxygen concentration along with an increase in equivalence ratio can also lead to decay of negative ion formation.

There is also the fact that the ignition of the mixture in the plasma environment increases the gas temperature in the reactor. Consequently, it reduces the gas density. The lower gas density reduces the breakdown voltage. Both effects increase the discharge repetition frequency (KONG et al., 2018).

The sum of these factors facilitates discharge ignition with increased equivalence ratio in this second set of experiments, i.e. a decrease in the breakdown voltage with an increase in natural gas concentration for a fixed total flow rate.

Figures 4.4 and 4.5 also shows the Fourier analysis performed on the voltage waveforms. This analysis allows the verification of the behavior of the discharge frequency as a function of the total mass flow rate and equivalence ratio. A DC component (0 Hz) is observed in the frequency spectrum in all conditions. As the GA is generated in a DC power supply, this component has the highest amplitude, as expected. A relatively high “noise” in the Fourier spectrum is observed, which is caused by the variations in the discharge voltage within each cycle, and corresponding to the “high frequency” phenomena discussed earlier. It can be seen that it is spread along all the analyzed frequency range. This “noise” is responsible by the typical electromagnetic interference generated by gliding arc discharges.

Although it is beyond the scope of this study to make a complete correlation between the frequency spectrum and the gliding arc phenomena, the discharge repetition frequency (or breakdown frequency) can be easily determined from the spectra. The discharge repetition frequency was determined by the peak with the maximum amplitude, excluding the DC component. The values obtained are in accordance with the estimative made by direct measurement of the period from voltage waveforms. Comparing figures 4.5b and 4.5d, it can be seen the shift of the peak to a higher frequency, while there is clearly an increase in frequency from the waveform in figure 4.5a to the one in figure 4.5c.

All the results regarding the discharge repetition frequency are summarized in figure 4.6, as a function of the equivalence ratio (figure 4.6a) and total mass flow rate (figure 4.6b).

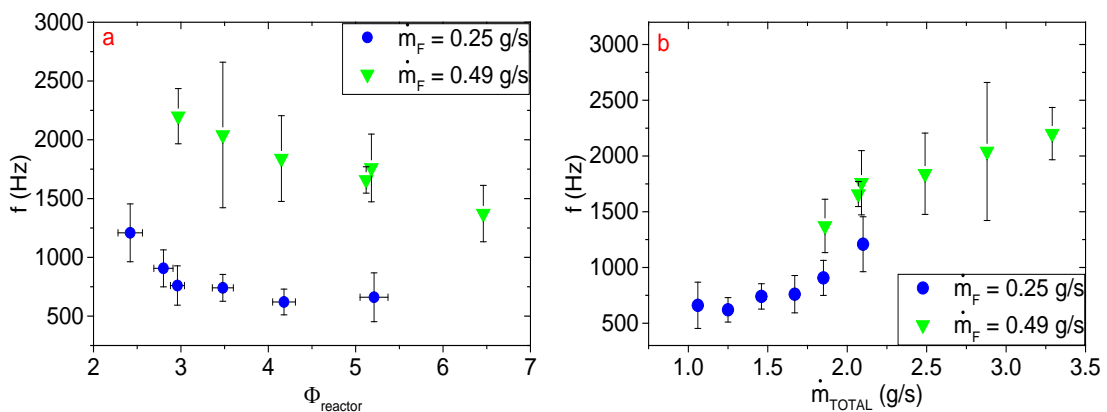


Figure 4.6 – Discharge repetition frequency as a function of the reactor equivalence ratio (a) and total mass flow rate (b).

By increasing the total gas mass flow rate for a constant natural gas flow, i.e. reducing the equivalence ratio, there is a growth in the discharge repetition frequency (figure 4.6a). From figure 4.6a, it is noted also that, for a constant equivalence ratio, there is an increase in the discharge repetition frequency with increased natural gas flow rate (and total gas flow rate). From this and from figure 4.6b (and figure 4.4), it is clear that when the gas flow rate increases, the discharge repetition frequency rises. This is due to the increase in the flow (and consequently in the arc) velocity, so the critical length is achieved in a shorter time. It leads to a new breakdown and restarts the cycle.

On the other hand, it can be seen from figure 4.6b (and figure 4.5) that for a given total mass flow rate, the discharge repetition frequency rises with the natural gas flow rate. This effect is caused by the reduction in the breakdown voltage observed in figure 4.5 with the increase in methane concentration on the gas mixture, which consequently reduces the time interval between breakdowns, increasing the discharge repetition frequency.

To verify if the presence of the flame downstream would influence the properties of the plasma upstream, electrical measurements of current and voltage of the discharge in the presence of the flame was performed. The repetition frequency for these conditions was also obtained. The results are summarized in figure 4.7:

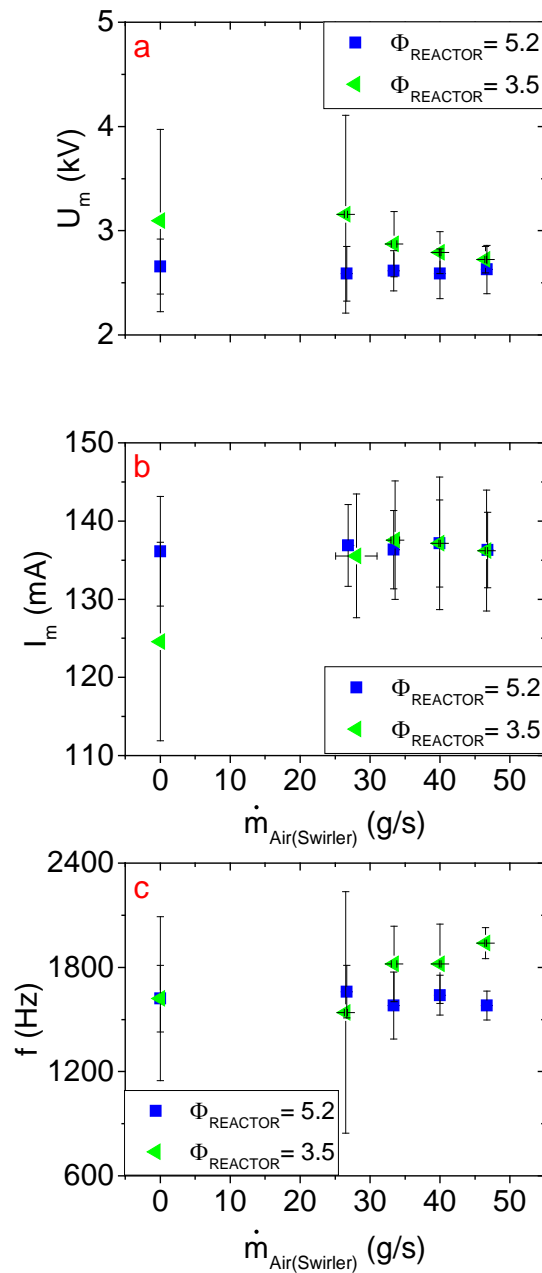


Figure 4.7 - Mean voltage (a), mean current (b) and discharge frequency (c) of the gliding arc discharge in the presence of the flame as function of the swirler air mass flow rate ($\dot{m}_{\text{Air(Swirler)}}$) for two plasma equivalence ratios: $\Phi_{\text{reactor}} = 5.2$ and 3.5 , both with fuel flow rate of 0.49 g/s. The swirler mass flow rate equals to zero corresponds to the plasma operation without flame.

As can be seen in figure 4.7, the mean current, the mean voltage and the repetition frequency of the discharge obtained in the presence of the flame are in accordance with the

measurements performed without flame. This shows that the discharge electrical properties are not influenced by the presence of the flame downstream, which permits to separate the effects of the plasma application and the effects due to the flame dynamics and kinetics.

As shown in this chapter, the discharge power on conditions with a fuel mass flow rate of 0.49 g/s corresponds to less than 1.75% of the calculated thermal power. The mean voltage and mean current of the discharge have no significant variation for the range of equivalence ratios and total mass flow rates used in this study. However, the discharge repetition frequency can increase up to 2.6 times. Both the increase in equivalence ratio (with constant total mass flow rate) and the increase in total mass flow rate (for constant equivalence ratio) lead to a rise in the discharge repetition frequency. In the first case, this is caused by the higher methane concentration, which has a lower ionization potential leading to a lower breakdown voltage (evidenced by a flattening in the voltage waveform) and so, to a higher discharge repetition frequency. In the second case, the rise in the discharge repetition frequency is a consequence of the increased arc velocity.

The decrease in the discharge repetition frequency with increased equivalence ratio (with constant fuel mass flow rate) could lead to a higher probability of failure in the flame ignition, causing the system to be unstable at high equivalence ratios. On the other hand, the increase in the total mass flow rate can lead to a flame blow off due to the increase in the flow velocity. Both phenomena must be considered when choosing an optimum operational condition for plasma-assisted burners.

It was shown also that the discharge electrical characteristics were not influenced by the flame downstream the reactor. Thus, it is reasonable to suppose that the changes on the exhaust gas composition in conditions with plasma are due only to the plasma kinetic enhancement and not by plasma regime variations or mutual effects between the flame and the discharge.

5 Plasma-assisted combustion results

Some papers (SAGÁS et al., 2011; SAGÁS; MACIEL; LACAVA, 2016; VARELLA; SAGÁS; MARTINS, 2016) argue that the GA discharge, operating with natural gas - air mixtures produces an OES spectrum dominated by H₂ bands, as well as peaks relatives to OH radicals and NO (SAGÁS et al., 2011). In those papers, it was shown that the discharge OES spectrum also presents CH, CN, C and H peaks.

Measurements of the exhaust gas concentration of fuel-rich GA showed that the hydrocarbon cracking is the main source of H₂. Although the plasma promotes an increase of NO_x, it was shown that the release of H₂ promotes a lowering in the CO and hydrocarbon concentrations, as well as an increase in the CO₂ at the plasma reactor exhaust gas (VARELLA; SAGÁS; MARTINS, 2016). It needs to be pointed out that due to the high H₂ content at the exit of the plasma reactor, the plasma is capable to sustain a pilot flame in this region.

On the other hand, the flame studied here works on high swirl numbers (with swirl number between 14.10 and 32.54), which allows to achieve flame in an environment with very lean global equivalence ratios (0.18 – 0.39). Besides that, this burner operates with high air in excess and thus, the flame lost a high amount of energy to heat this air. Therefore, there is a slowing in the NO_x thermal mechanism, as well as, in the hydrocarbons oxidation rates, both of them dependent on the temperature. As a consequence, the exhaust gas presents higher concentrations of THC and CO.

In this way, in the present arrangement, the plasma produced H₂, OH and NO species will feed the flame in an effort to accelerate the CO and hydrocarbons mechanism, maintaining the exhaust NO_x levels acceptable.

In this section, it was measured the exhaust gas composition of the burner with and without plasma application. For these tests, the fuel mass flow rate was fixed at (0.50 ± 0.1) g/s and the air mass flow rate was varied. In the swirler, the air mass flow rate varied from (21.65 ± 0.03) g/s to (49.33 ± 0.08) g/s and in the plasma reactor, the air mass flow rate was varied from (1.6 ± 0.1) g/s to (2.8 ± 0.1) g/s. These conditions allowed global equivalence ratios (Φ_{global}) between (0.18 ± 0.01) and (0.39 ± 0.01), and plasma reactor equivalence ratios (Φ_{reactor}) between (3.1 ± 0.1) and (5.4 ± 0.1).

The measured gas exhaust compositions are shown and discussed as a function of the plasma reactor equivalence ratio. All the presented graphs are related to $\Phi_{\text{global}} = 0.21$. However, the behavior of the concentrations is similar for all the range of Φ_{global} . All graphs relative to the other conditions of Φ_{global} are presented in the appendix B. Tables relative to the percentage variations promoted by the plasma application are presented in appendix C.

It needs also to be pointed that due to the high flammability of H_2 , no hydrogen content was detected at the exhaust gas.

5.1 O_2 and CO_2

Figure 5.1 shows the presence of oxygen and carbon dioxide in terms of concentration with and without plasma.

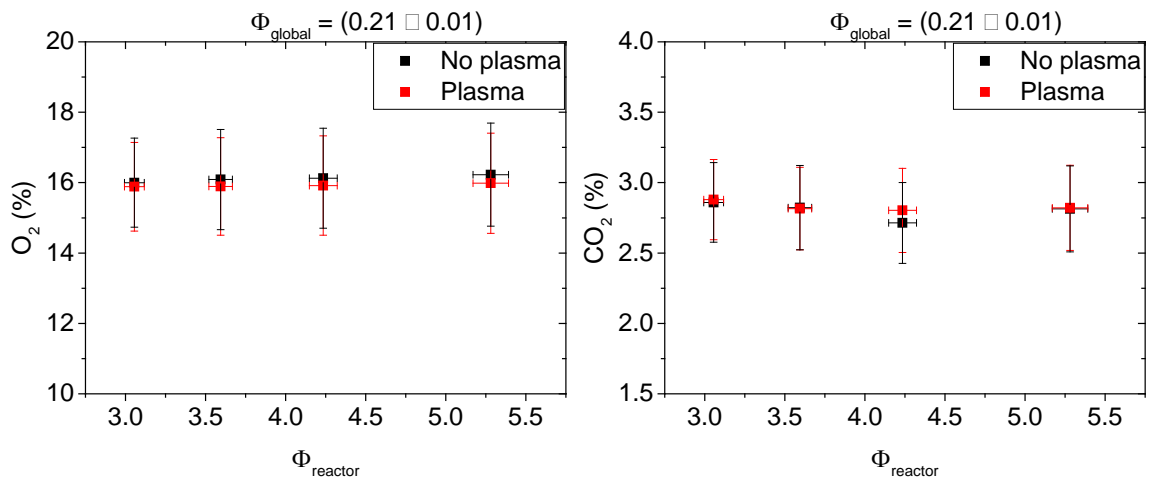


Figure 5.1 - Concentrations of O_2 , and CO_2 as functions of the reactor equivalence ratio (Φ_{reactor}) for $\Phi_{\text{global}} = 0.21$. Both concentrations are in wet basis. CO_2 was corrected for an excess of 15% of O_2 .

For these compounds, the plasma presence promotes slight variations on their concentrations. However, in all cases, the variation is within the measurement uncertainty.

5.2 THC and CO

THC and CO behaviors are shown in figure 5.2.

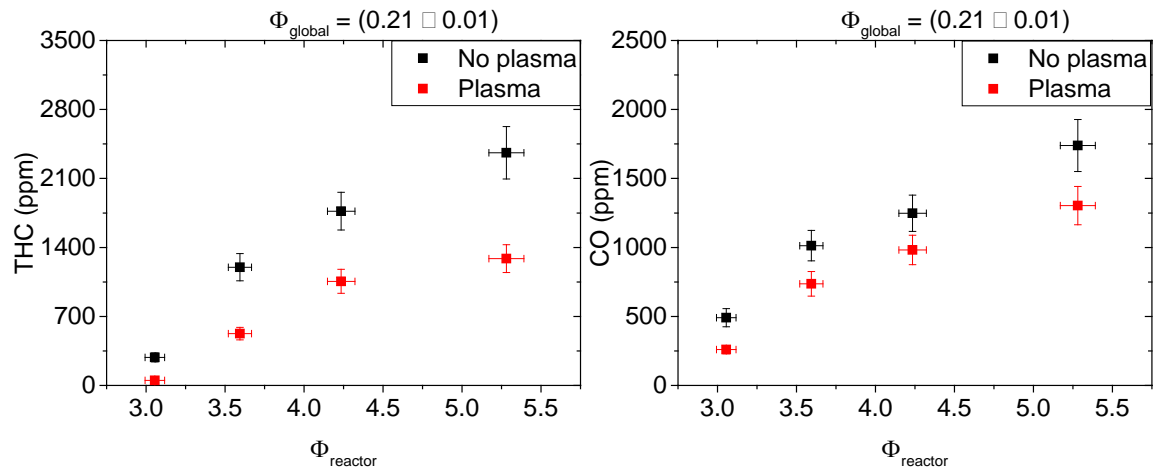


Figure 5.2 - THC and CO behaviors as a function of the reactor equivalence ratio (Φ_{reactor}) for $\Phi_{\text{global}} = 0.21$. All concentrations are in wet basis and were corrected for an excess of 15% of O_2 .

The plasma presence promoted faster oxidation of hydrocarbons in all conditions, lowering the THC concentration in the exhaust gas, reaching maximum decreases from 2982.2 ppm to 1518.1 ppm, which corresponds to a diminish of 49.1 %. This maximum decrease is reached when $\Phi_{\text{reactor}} = 5.4$ and $\Phi_{\text{global}} = 0.18$.

This faster oxidation is promoted by the electron dissociation of hydrocarbons (R25, R53 and R54) and by the plasma-generated species such as hydrogen (H_2 and H) and atomic oxygen. Many authors point out that non-equilibrium plasma is very efficient in producing atomic oxygen via electron (R20) and excited nitrogen (N_2^*) impact dissociation (R21).

Hydrogen is produced by the cracking of hydrocarbons through direct impact dissociation by electrons (R25, R53, and R54), atomic species (R24, R52), molecular species (R46, R47), and radicals (R33, R51).

As shown by Sagás et al. (SAGÁS; MACIEL; LACAVA, 2016), the gliding arc discharge in a natural gas - air premixed mixture is a source of H_2 , which is partially consumed in the flame conjugated to the plasma, i.e. inside the reactor. However, as shown by Varella et al. (VARELLA; SAGÁS; MARTINS, 2016), the H_2 content in the exhaust gas of a fuel-rich combustion increases using a gliding arc discharge, despite this internal

consumption. Therefore, the plasma reactor is injecting H₂ in the burner flame zone, which contributes to the fast hydrocarbon oxidation. Due to hydrogen great flammability, no H₂ content was measured in the exhaust gas, as expected.

Following the behavior of the THC, carbon monoxide (CO) concentration decreases with the plasma application. The maximum decrease is from 1185.0 ppm to 486.4 ppm, corresponding to a fall of 59.0 %. This occurs at the condition where $\Phi_{\text{reactor}} = 5.4$ and $\Phi_{\text{global}} = 0.30$.

As the plasma increases the amount of OH and H₂ due to the dissociation of the hydrocarbons, it also impacts the CO conversion in the flame zone. The faster oxidation of CO in the presence of H₂ was already shown by Kim et al. (KIM et al., 2009) in premixed flames. Varella et al. (VARELLA; SAGÁS; MARTINS, 2016) point out that the CO oxidation in the plasma process is due to the presence of OH radicals, which is known as one of the reactions most responsible for the heat release.



The carbon monoxide can also be oxidized by collision with O₂ (R56), and by the water shift reaction (R57).



In a medium with high H₂ concentration, as expected in the flame zone due to H₂ injection from the reactor, the reactions (R58) and (R59) can also be involved:



Meanwhile, as pointed by Varella et al. (VARELLA; SAGÁS; MARTINS, 2016), reaction (R56) is too slow, promoting not much contribution to the CO₂ formation. So, in the presence of the plasma, reaction (R55) is the predominant oxidation pathway to the CO decrease.

5.3 NO_x

The behavior of NO_x as a function of the reactor equivalence ratio is shown in figure 5.3.

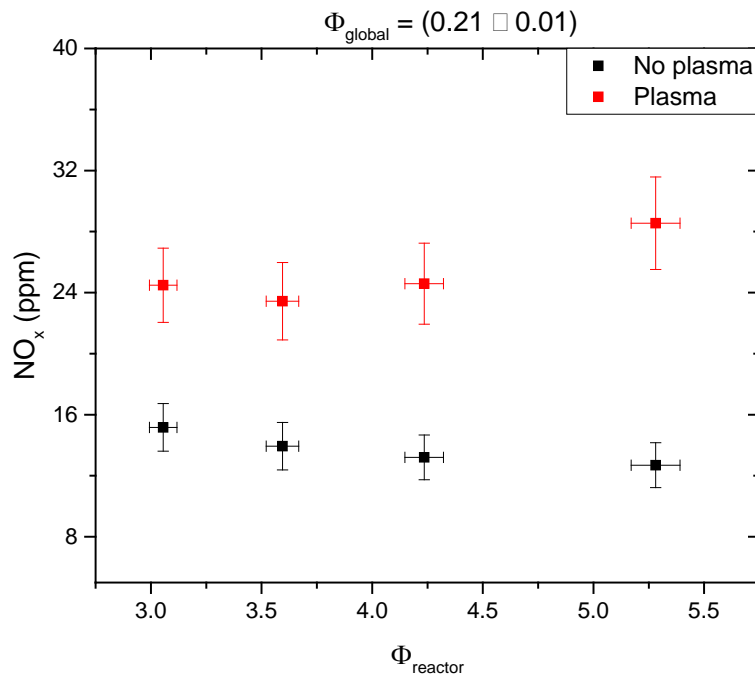


Figure 5.3 - NO_x concentration as function of the reactor equivalence ratio (Φ_{reactor}) for $\Phi_{\text{global}} = 0.21$. All concentrations are in wet basis and were corrected for an excess of 15% of O₂.

As the higher loss of heat to the excess of oxidant in the flame zone reduces the temperature of this region, low levels of NO_x are measured at the exhaust gas. However, the plasma application increases the NO_x concentration, reaching a maximum increase from 10.5 ppm to 28.8 ppm, corresponding to a rise of 174.3 %. This is reached in the condition where $\Phi_{\text{reactor}} = 5.4$ and $\Phi_{\text{global}} = 0.30$.

The generation of NO_x species, predominantly NO (VARELLA; SAGÁS; MARTINS, 2016), in plasmas at atmospheric pressure in mixtures containing air is well known

(KOROLEV et al., 2012a; WANG et al., 2017b). So, it is important to notice that in a discharge that produces NO and NO₂, the low-temperature NO_x catalytic reactions (R16 and R17) can convert radicals, such as HO₂ to OH radicals and thus, promote chain-branching reactions and extend ignition limits. The hydrogen combustion also promotes an increase in the temperature of the reaction zone, improving the thermal mechanism of NO formation. This hypothesis is reinforced by the fall of THC concentration with the plasma application.

5.4 Hydrocarbons

Looking for the THC components, acetaldehyde (C₂H₄O) and propylene (C₃H₆) and acrolein (C₃H₄O) remain below the cut point in all tested conditions and so, their measurements were not considered. For all hydrocarbon species, the plasma application decreased their concentrations.

As the main component of natural gas, methane (CH₄) concentration is also the bigger among the THC hydrocarbons as shown in figure 5.4.

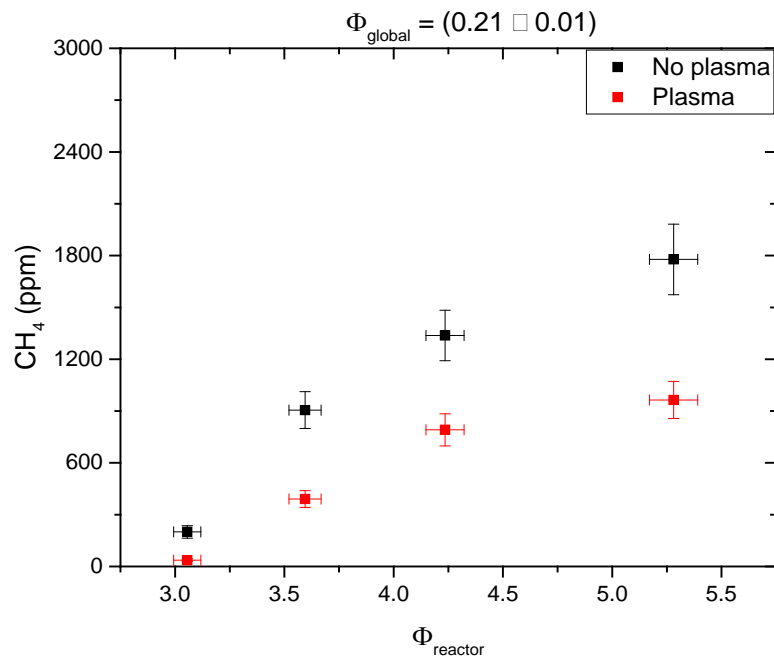


Figure 5.4 - CH₄ concentration as function of the reactor equivalence ratio (Φ_{reactor}) for $\Phi_{\text{global}} = 0.21$. All concentrations are in wet basis and were corrected for an excess of 15% of O₂.

The methane concentration falls with the plasma application reaching maximum decrease from 2201.5 ppm to 1131.3 ppm, corresponding to a fall of 48.6 %. This situation occurs when $\Phi_{\text{reactor}} = 5.4$ and $\Phi_{\text{global}} = 0.18$.

Ethane (C_2H_6) presents concentrations below 100 ppm in all conditions. Its behavior is shown in figure 5.5.

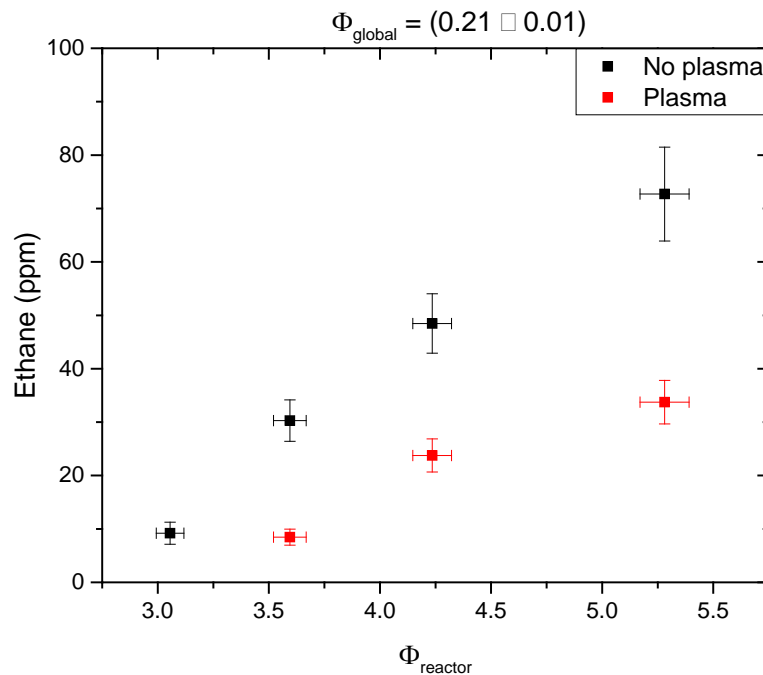


Figure 5.5 - Ethane concentration as function of the reactor equivalence ratio (Φ_{reactor}) for $\Phi_{\text{global}} = 0.21$. All concentrations are in wet basis and were corrected for an excess of 15% of O_2 .

The maximum decrease in the ethane concentration due to the plasma presence is from 97.1 ppm to 41.3 ppm, which corresponds to a fall of 57.5 %. This decrease is reached in the condition of $\Phi_{\text{reactor}} = 5.4$ and $\Phi_{\text{global}} = 0.18$.

The behavior of propane (C_3H_8) as a function of the reactor equivalence ratio is shown in figure 5.6.

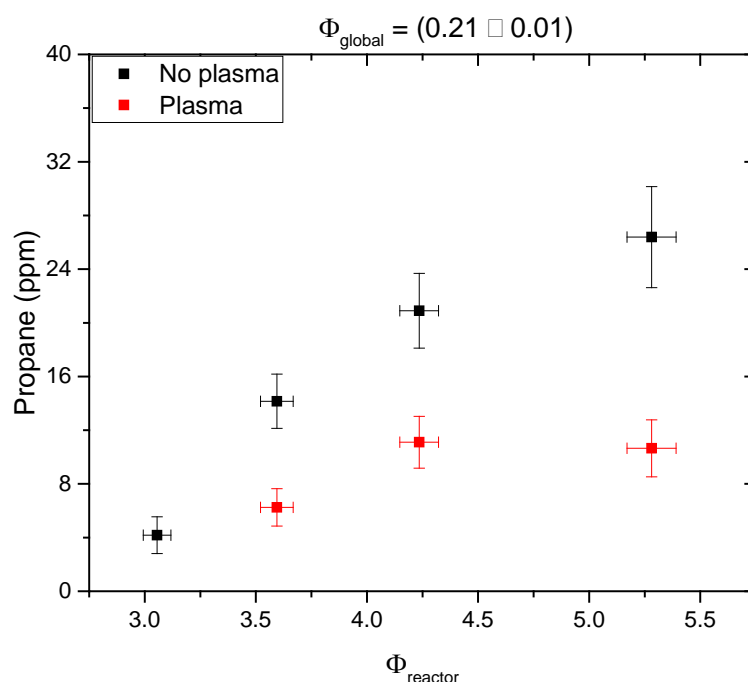


Figure 5.6 - Propane concentration as function of the reactor equivalence ratio (Φ_{reactor}) for $\Phi_{\text{global}} = 0.21$. All concentrations are in wet basis and were corrected for an excess of 15% of O_2 .

Propane concentration is less than 50 ppm in all conditions. When $\Phi_{\text{reactor}} = 5.4$ and $\Phi_{\text{global}} = 0.18$, the plasma application promotes a maximum decrease from 48.9 ppm to 13.6 ppm, a corresponding diminish of 72.2 %.

It is important to notice that although in absolute values the methane concentration shows the high decrease (about 1070.2 ppm) the plasma influence is bigger in propane and ethane, which present higher percentage decreases: 72.2 % and 57.5 %, respectively. This result can be linked to the lower dissociation energy for propane and ethane in relation to methane. For example, at 298 K the bond dissociation energy for the first C-H bond of propane is 98.6 kcal/mol, while for ethane and methane it is respectively 101.1 kcal/mol and 104.99 kcal/mol (BLANKSBY; ELLISON, 2003; RUSCIC, 2015). So in the plasma environment, it is energetically easier to achieve the dissociation of propane and ethane, which turns them more sensitive to the plasma application.

The plasma action over methane corresponds to its dissociation by direct impact of electrons (R25, R53, and R54), or collisions with other molecules (R37) to form radicals (CH_3 , CH_2 and CH). The dissociation of methane is the main source of hydrogen in the mixture. Besides that, the consumption of CH_4 can occur to form hydrogen (R45, R46), or in

reactions with the hydroxyl radical (R33) and atomic species (O and H) through reactions (R34) and (R35). It is important to say that in the range of equivalence ratios used in this study, a portion of methane is cracked in the plasma environment. However, there is an excess of methane that is not decomposed in the reactor and reaches the flame zone, where it can be consumed. As pointed out by Sagás et al. (SAGÁS; MACIEL; LACAVA, 2016), for plasma reactor equivalence ratios higher than 1.9, the OH intensity in the OES spectrum of the plasma disappears, due to the lower oxygen concentration in the mixture and the C peak appears due to the natural gas cracking in the plasma.

The reactions between methane and atomic oxygen (R34 and R48) promote the increase of radical OH in the medium. The increase of molecular hydrogen also has contribution from other hydrocarbons reaction such as ethane (R39) and ethylene (R40 and R41) in the plasma environment.

Varella et al. (VARELLA; SAGÁS; MARTINS, 2016) show that the propane concentration diminishes with the increase of the discharge applied power. Korolev et al. (KOROLEV et al., 2012b) points out that propane is converted to acetylene (C_2H_2) in the discharge area, without the participation of oxygen on the reactions.

Acetylene (C_2H_2) and ethylene (C_2H_4) behaviors are shown in figure 5.7.

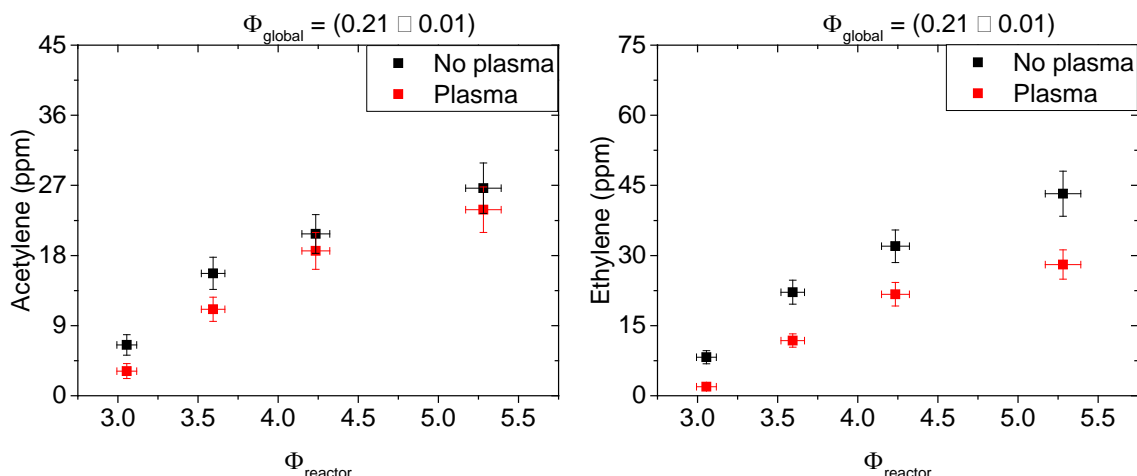


Figure 5.7 - Acetylene and ethylene concentrations as function of the reactor equivalence ratio (Φ_{reactor}) for $\Phi_{\text{global}} = 0.21$. All concentrations are in wet basis and were corrected for an excess of 15% of O_2 .

Considering all the tested conditions, acetylene and ethylene are always lower than 35 ppm and 55 ppm respectively. The plasma promotes a maximum decrease in the

concentration of acetylene from 12.4 ppm to 5.5 ppm and for ethylene from 52.5 ppm to 30.5 ppm. These decreases correspond to a fall of 55.6 % for acetylene (when $\Phi_{\text{reactor}} = 5.4$ and $\Phi_{\text{global}} = 0.30$) and 41.9 % for ethylene (when $\Phi_{\text{reactor}} = 5.4$ and $\Phi_{\text{global}} = 0.18$). However, it is important to notice that for a same condition, ethylene always present decreases bigger than acetylene, as can be seen in the tables of appendix C.

The fact that ethylene is more sensitive to the plasma presence than acetylene is linked to the bigger concentration of ethylene, but the structure of the compounds cannot be neglected. While ethylene presents a double C-C bond, acetylene presents a triple C-C bond. This also reflects in their C-H dissociation energy: 110.7 kcal/mol (at 298 K) for the ethylene and 133.32 kcal/mol (at 298 K) for acetylene (BLANKSBY; ELLISON, 2003). So, as the C-C bond becomes strong, the C-H bond dissociation energy increases, which makes the ethylene dissociation easier in the plasma environment.

As shown by Dors et al. (DORS et al., 2014), acetylene is generated from ethylene (R39) and from C_2H_3 (R41) in the plasma environment. It probably is decomposed in smaller species and oxidized by oxygen in the flame zone.

Formaldehyde (CH_2O) and methanol (CH_3OH) concentrations are shown in figure 5.8.

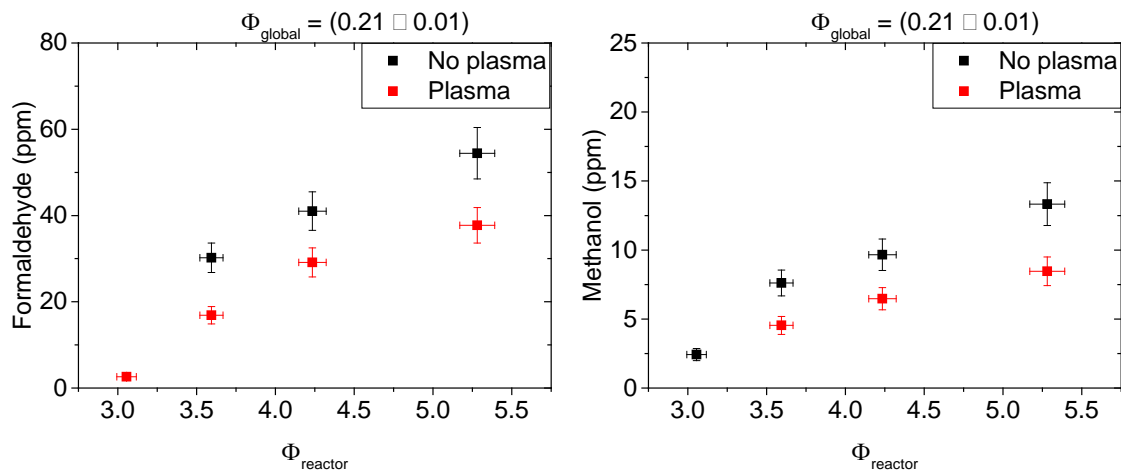


Figure 5.8 - Formaldehyde and methanol concentrations as a function of the reactor equivalence ratio (Φ_{reactor}) for $\Phi_{\text{global}} = 0.21$. All concentrations are in wet basis and were corrected for an excess of 15% of O_2 .

Looking for all conditions, both formaldehyde and methanol present concentrations less than 65 ppm and 20 ppm respectively. Their maximum lowering is from 46.3 ppm to 10.7 ppm for formaldehyde and from 17.5 ppm to 9.9 for methanol. These decreases correspond to

diminishes of 36.4 % and 43.4 % respectively, and occur in the conditions where $\Phi_{\text{reactor}} = 5.4$ and $\Phi_{\text{global}} = 0.30$ for formaldehyde and $\Phi_{\text{reactor}} = 5.4$ and $\Phi_{\text{global}} = 0.18$, for methanol.

Formaldehyde reacts with OH radical through reaction (R49) and (R50) and also generates more atomic hydrogen and methyl radicals (CH_3) through reaction (R52).

Methanol probably reacts with oxygen to form formaldehyde and dissociated in methyl (CH_3) and OH radicals (JU et al., 2016).

As discussed, the plasma effect in the combustion process is hugely related to feeding the flame with hydrogen and oxygen plasma-generated species, which promotes fast oxidation of the hydrocarbons. The dissociation of hydrocarbons in the plasma environment is the main source of H_2 . The generation of H_2 also affects the Zeldovich mechanism in the flame zone.

The greater hydrocarbons decrease occurs for the higher plasma reactor equivalence ratio ($\Phi_{\text{reactor}} = 5.3$), the same point where the increase in NO_x concentration with plasma is maximum. This point is also where lesser carbon-based compounds are converted in the flame region, and so, the greater concentration of these compounds is measured without plasma. Both behaviors are related to the increase in the amount of fuel in the inlet gas concentration. For the very low global equivalence ratio, an increase in the reactor equivalence ratio leads to more hydrocarbons in the exhaust gas. At the same time, as more hydrocarbons are present in the reactor environment, it increases the H_2 and OH produced by the plasma leading to higher hydrocarbon and CO oxidation in the flame zone, as well as more NO_x . A summary of these effects is schematized in figure 5.9:

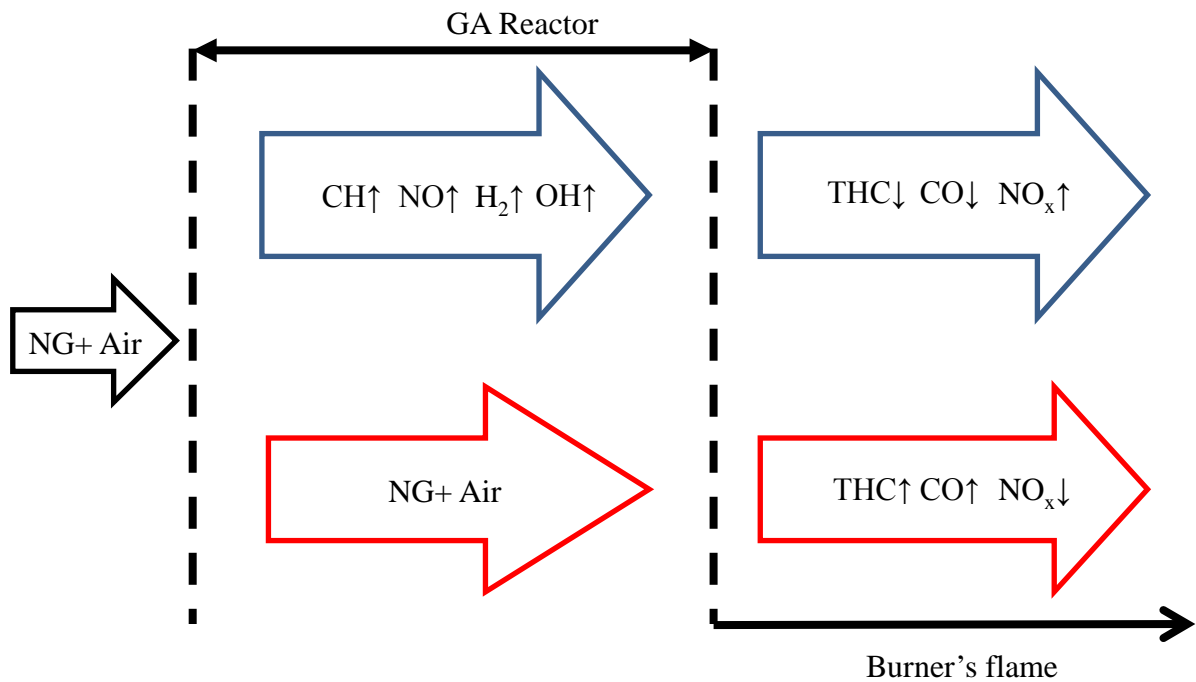


Figure 5.9 - Scheme of the plasma action over the flame exhaust gas. Blue arrows represent the conditions with plasma application, while red arrows represent the conditions without plasma. NG corresponds to natural gas. The black arrows near to the compounds chemical description represent the increase or decrease in its concentration inside the GA reactor or in the exhaust gas.

In the present chapter, it was shown the results from the monitoring of the exhaust gas concentration of a global fuel-lean swirl flame assisted by a reverse vortex flow gliding arc discharge. Both, the plasma and the flame operate with natural gas and air. The plasma was generated in a fuel-rich premixed mixture with equivalence ratios from 3.1 to 5.3, as well as the global equivalence ratio of the entire system varied from 0.18 to 0.39.

The concentrations of O₂, CO₂, CO, NO_x and hydrocarbon content in the exhaust gas were monitored with and without plasma application to verify the effect of the discharge on this gas composition.

The results showed that the concentrations of THC, CH₄, and CO decrease with the plasma application. The NO_x always increases with plasma application. However, this increase is only from 18.3 ppm at its maximum, while in some conditions the plasma application can lower the level of THC from hundreds of ppm. NO_x concentration always remains below 40 ppm.

The plasma promotes the cracking of the hydrocarbons to generate hydrogen and OH, accelerating the oxidation of the fuel. The results also show that some hydrocarbons are more

sensitive to the plasma presence than others. For example, propane and ethane present higher decreases than methane. This behavior is linked to the lower C-H bond dissociation energy of propane and ethane in comparison with methane. This discussion can also be extended to ethylene and acetylene, where the first is more sensitive to the plasma application than the second.

The higher variations of hydrocarbons, CO and NO_x, as well as their condition of occurrence are summarized in table 5.1.

Table 5.1: NO_x, CO and hydrocarbon variation with plasma application. In the variation column, a negative value is equivalent to a decrease in concentration, as well as a positive value is equivalent to its increase.

Compound	Φ_{reactor}	Φ_{global}	Concentration (no plasma)	Concentration (plasma)	Variation
			ppm	ppm	%
THC	5.4	0.18	2982.2 ± 338.6	1518.1 ± 171.5	-49.1 ± 0.2
CO	5.4	0.30	1185.0 ± 124.7	486.4 ± 57.9	-59.0 ± 0.2
NO _x	5.4	0.30	10.5 ± 1.3	28.8 ± 3.0	174.3 ± 0.2
CH ₄	5.4	0.18	2201.5 ± 255.7	1131.3 ± 130.2	-48.6 ± 0.2
C ₂ H ₆	5.4	0.18	97.1 ± 11.5	41.3 ± 5.2	-57.5 ± 0.2
C ₃ H ₈	5.4	0.18	48.9 ± 6.2	13.6 ± 2.7	-72.2 ± 0.2
C ₂ H ₂	5.4	0.30	12.4 ± 1.6	5.5 ± 0.9	-55.6 ± 0.2
C ₂ H ₄	5.4	0.18	52.5 ± 5.9	30.5 ± 3.5	-41.9 ± 0.2
CH ₂ O	5.4	0.30	46.3 ± 5.4	10.7 ± 1.4	-76.9 ± 0.2
CH ₃ OH	5.4	0.18	17.5 ± 2.0	9.9 ± 1.2	-43.4 ± 0.2

From table 5.1 it is clear that the higher decreases of the hydrocarbons at the exhaust gas occur when $\Phi_{\text{reactor}} = 5.4$. This same reactor equivalence ratio also implies the higher increase of the NO_x content.

The use of the GA plasma to assist global fuel-lean combustion improves the hydrocarbon oxidation by generating hydrogen and oxygen species such as H, H₂, O and OH. All of these species accelerates the hydrocarbon oxidation mechanism, by improving the heat release in the flame zone and cracking hydrocarbons in lighter species. The fuel-rich gliding arc applied to combustion shows itself as an alternative to highly improve hydrocarbon

combustion in global fuel-lean flames without a big increase in the nitrogen oxides concentration.

6 Conclusions and suggestions for future studies

6.1 Conclusions

The main objective of this study was to verify the effect of a gliding arc discharge in the emissions of a global fuel-lean swirl flame. To accomplish this goal, a direct comparison between conditions with and without plasma application was performed.

The electrical characterization of the discharge showed that its repetition frequency increased with the equivalence ratio and gas mass flow rate. These behaviors are linked with the fall of the breakdown voltage and the increase of the gas velocity, respectively. Although the increase in the discharge frequency can impact the ignition and flame stability, such problems were not verified in this study. Also, the mean current and the mean voltage showed no significant variation with the plasma reactor equivalence ratio or total mass flow rate. The FFT analysis of voltage waveforms showed to be a useful tool to characterize the breakdown frequency, with possible application to study other “high frequency” phenomena in gliding arc discharge.

The measurements also show that the flame in the burner had no significant effect on the electrical characteristics of the discharge. So, it is reasonable to consider that the changes on the exhaust gas composition are due only to the plasma kinetic enhancement, and not to variations on the flame structure or in the plasma regime.

From the gas analysis, it can be concluded that the main plasma action, relies on the hydrocarbon and CO oxidation, as well as in the NO_x formation.

The hydrocarbons and CO concentrations decrease rapidly when the plasma was turned on. In fact, the gliding arc promotes the cracking of hydrocarbons to form H₂ and OH species, as well as some radicals such as CH₃, CH₂ and CH. The increase of the amount of H₂ in the flame improves the hydrocarbon cracking. The H₂ oxidation also releases energy that helps to sustain the combustion chain-reactions in the global-lean regime. This energy release thus improves the hydrocarbon consumption on the flame zone. The increase of the OH specie improves the hydrocarbons and CO oxidation. On the other hand, there is an increase in the NO_x concentration, but it still remains below 40 ppm (corrected by O₂ 15%).

Although the plasma promotes the decrease of all hydrocarbons, it can be seen that some of them are more sensitive to the plasma application. For example, although methane

shows the higher absolute decreases, propane and ethane present higher percentage decreases than methane when plasma is applied. This behavior is linked to the lower C-H bond dissociation energy of propane and ethane in comparison with methane. So, it is energetically easier to dissociate ethane and propane molecules than methane. The same is true when comparing ethylene and acetylene, where the first is more sensitive to the plasma than the second.

The comparison of emissions with and without plasma at the same burner system and conditions proves that gliding arc discharges can be efficiently used to accelerate the hydrocarbon oxidation in global fuel-lean flames, while leaving the NO_x levels acceptable. The main plasma action relies on the release of H₂ and OH radicals, as well as promoting the hydrocarbon cracking. The sum of these factors facilitates the hydrocarbon oxidation in the flame zone.

6.2 Recommendations for future studies

- Studies of the flame structure by means of laser techniques, which could help in the understanding of the role of the fluid dynamics in the exhaust gas composition.
- Numerical simulation of the gliding arc development by using Computational Fluid Dynamics (CFD) to estimate and understand the plasma properties when operating in natural gas-air mixtures. This effort can provide valuable data to chemical kinetics models.
- Measurements of the plasma-generated intermediary species such as H, O, OH, O₃, etc. in an effort to refine the kinetics mechanism understanding related to the plasma-produced species.
- Analysis of the effect of the plasma on flame stabilization in conditions where thermo-acoustic instabilities occur.
- Simultaneous monitoring of the discharge voltage and current to accurate calculation of the discharge electrical power. This data allows evaluating the energetic cost of the plasma-assisted combustion by comparison of the discharge power and the thermal power of the flame.
- Analysis of the effects of the gliding arc in global fuel-rich flame conditions and low swirl flame conditions too.
- Study of the fuel-staged conditions.
- Study of glow-to-spark transitions and shortcuts using FFT analysis and high-speed imaging.
- A deeper analysis of the sensitivity of hydrocarbons to the plasma application by exhaust gas analysis of the plasma reactor when the discharge is generated in mixtures of hydrocarbons with controlled composition.

Bibliography

- ALVES, A. **Estudo Experimental da Estabilização de Chamas em Escoamentos com Baixa Rotação para Aplicações em Turbinas a Gás.** [s.l.] Instituto Tecnológico de Aeronáutica, 2013.
- BLANKSBY, S. J.; ELLISON, G. B. Bond dissociation energies of organic molecules. **Accounts of Chemical Research**, v. 36, n. 4, p. 255–263, 2003.
- BOULOS, M. I. New frontiers in thermal plasma processing. **Pure and Applied Chemistry**, v. 68, n. 5, p. 1007–1010, 1996.
- BRANDENBURG, R. Dielectric barrier discharges: progress on plasma sources and on the understanding of regimes and single filaments. **Plasma Sources Science and Technology**, v. 26, n. 5, p. 053001, 2017.
- CHA, M. S. et al. Soot suppression by nonthermal plasma in coflow jet diffusion flames using a dielectric barrier discharge. **Combustion and Flame**, v. 141, n. 4, p. 438–447, 2005.
- CHENG, H. et al. Nanosecond pulse plasma dry reforming of natural gas. **Catalysis Today**, 2018.
- COMPANHIA DE GÁS DE SÃO PAULO - COMGAS. **Anexos Comgas - Versão 2014.** [s.l.: s.n.]. Disponível em: <https://www.comgas.com.br/wp-content/uploads/2017/05/RIP-2014__-9-_Anexos.pdf>.
- COUTO, H. S. .; MUNIZ, W. F. .; BASTOS-NETTO, D. **Geometrical parameters for flows across axial swilers.** Proceedings of the 3rd Asian-Pacific International Symposium on Combustion and Energy Utilization. **Anais...**1995
- DEREK DUNN-RANKIN PETER THERKELSEN. **Lean combustion: technology and control.** Second Edi ed. [s.l.] Academic Press, 2016.
- DORS, M. et al. Chemical Kinetics of Methane Pyrolysis in Microwave Plasma at Atmospheric Pressure. **Plasma Chemistry and Plasma Processing**, v. 34, n. 2, p. 313–326, 2014.
- EUROPEAN COMISSION CLIMATE ACTION. **EU Emissions Trading System.** [s.l.: s.n.]. Disponível em: <https://ec.europa.eu/clima/policies/ets_en>.
- FRIDMAN, A. **Plasma Chemistry.** [s.l.] Cambridge university press, 2008.
- FRIDMAN, A.; KENNEDY, L. A. **Plasma physics and engineering.** [s.l.] CRC press, 2004.
- FULCHERI, L.; ROLLIER, J.-D.; GONZALEZ-AGUILAR, J. Design and electrical charaterization of a low current–high voltage compact arc plasma torch. **Plasma Sources**

- Science and Technology**, v. 16, n. 1, p. 183–192, 1 fev. 2007.
- GALLEGO, ANTONIO GARRIDO AND MARTINS, GILBERTO AND GALLO, W. L. Emissões de NO_x em turbinas a gás: mecanismos de formação e algumas tecnologias de redução. **Revista de Ciência & Tecnologia**, v. 15, p. 13–22, 2000.
- GAO, J. et al. Visualization of instantaneous structure and dynamics of large-scale turbulent flames stabilized by a gliding arc discharge. **Proceedings of the Combustion Institute**, v. 000, p. 1–8, 2018.
- GLEIZES, ALAIN AND GONZALEZ, JEAN-JACQUES AND FRETON, P. Thermal plasma modelling. **Journal of Physics D: Applied Physics**, v. 153, n. 9, 2005.
- GOMEZ, E. et al. Thermal plasma technology for the treatment of wastes : A critical review. **Journal of Hazardous Materials**, v. 161, n. 2–3, p. 614–626, 2009.
- HICKS, A. et al. Singlet oxygen generation in a high pressure non-self-sustained electric discharge. **Journal of Physics D: Applied Physics**, v. 38, n. 20, p. 3812–3824, 2005.
- ITIKAWA, Y. Cross Sections for Electron Collisions with Nitrogen. **Journal of Physical and Chemical Reference Data**, v. 35, n. 1, p. 31–53, 2006.
- ITIKAWA, Y. Cross Sections for Electron Collisions with Oxygen Molecules. **Journal of Physical and Chemical Reference Data**, v. 38, n. 1, p. 1–20, 2009.
- JAMES, S. R. et al. Hominid Use of Fire in the Lower and Middle Pleistocene: A Review of the Evidence [and Comments and Replies]. **Current Anthropology**, v. 30, n. 1, p. 1–26, 1989.
- JU, Y. et al. Plasma Assisted Low Temperature Combustion. **Plasma Chemistry and Plasma Processing**, v. 36, n. 1, p. 85–105, 2016.
- JU, Y.; SUN, W. Plasma assisted combustion : Dynamics and chemistry. **Progress in Energy and Combustion Science**, v. 48, p. 21–83, 2015.
- KALRA, C. S. et al. Gliding arc in tornado using a reverse vortex flow. **Review of Scientific Instruments**, v. 76, n. 2, p. 025110, 2005.
- KIM, H. S. et al. Hydrogen addition effects in a confined swirl-stabilized methane-air flame. **International Journal of Hydrogen Energy**, v. 34, n. 2, p. 1054–1062, 2009.
- KOLEV, S.; BOGAERTS, A. Similarities and differences between gliding glow and gliding arc discharges. **Plasma Sources Science and Technology**, v. 24, n. 6, p. 064023, 2015a.
- KOLEV, S.; BOGAERTS, A. A 2D model for a gliding arc discharge. **Plasma Sources Science and Technology**, v. 24, n. 1, 2015b.
- KOLEV, S.; BOGAERTS, A. 3D modeling of energy transport in a gliding arc discharge in argon. **Plasma Sources Science and Technology**, 2018.

- KONG, C. et al. Characteristics of a Gliding Arc Discharge Under the Influence of a Laminar Premixed Flame. **IEEE Transactions on Plasma Science**, p. 1–7, 2018.
- KOROLEV, Y. D. et al. Glow-to-Spark Transitions in a Plasma System for Ignition and Combustion Control. v. 35, n. 6, p. 1651–1657, 2007a.
- KOROLEV, Y. D. et al. Glow-to-Spark Transitions in a Plasma System for Ignition and Combustion Control. **IEEE Transactions on Plasma Science**, v. 35, n. 6, p. 1651–1657, dez. 2007b.
- KOROLEV, Y. D. et al. Low-Current Gliding Arc in an Air Flow. **IEEE Transactions on Plasma Science**, v. 39, n. 12, p. 3319–3325, 2011.
- KOROLEV, Y. D. et al. Low-Current Plasmatron as a Source of Nitrogen Oxide Molecules. **IEEE Transactions on Plasma Science**, v. 40, n. 11, p. 2837–2842, 2012a.
- KOROLEV, Y. D. et al. Propane oxidation in a plasma torch of a low-current nonsteady-state plasmatron. **IEEE Transactions on Plasma Science**, v. 40, n. 2, p. 535–542, 2012b.
- KOROLEV, Y. D. et al. Methane oxidation in a low-current nonsteady-state plasmatron. **IEEE Transactions on Plasma Science**, v. 42, n. 6, p. 1615–1622, 2014a.
- KOROLEV, Y. D. et al. Features of a near-cathode region in a gliding arc discharge in air flow. **Plasma Science and Technology**, v. 23, p. 1–10, 2014b.
- KOSAREV, I. N. et al. **Comparative Study of Nonequilibrium Plasma Generation and Plasma-Assisted Ignition for Different C2 Hydrocarbons**. Plasma Science (ICOPS), 2016 IEEE International Conference on. **Anais...IEEE**, 2016
- KOSSYI, I. et al. Kinetic scheme of the non-equilibrium discharge in nitrogen-oxygen mixtures. **Plasma Sources Science and Technology**, v. 1, n. 3, p. 207, 1992.
- LAW, C. J. **Principles of Combustion Engineering and Boilers**. [s.l.] Academic Press, 1987.
- LEE, D. H. et al. Plasma-Assisted Combustion Technology for NO_x Reduction in Industrial Burners. **Environmental Science and Technology**, v. 47, p. 10964–10970, 2013.
- LI, X. et al. Study on stretch extinction limits of CH₄/CO₂ versus high temperature O₂/CO₂ counterflow non-premixed flames. **Combustion and Flame**, v. 161, n. 6, p. 1526–1536, 2014.
- LIAS, S. G. Ionization Energy Evaluation. In: LINSTROM, P.J.; MALLARD, W. G. (Ed.). . **NIST Chemistry Webbook, NIST Standard Reference Database Number 69**. [s.l.] National Institute of Standards and Technology, 2018.
- LIN, B. et al. Experimental investigation of gliding arc plasma fuel injector for ignition and extinction performance improvement. **Applied Energy**, v. 235, p. 1017–1026, 2019.

- MEDEIROS, H. DE S. **Desenvolvimento e operação de um sistema de plasma excitado por micro-ondas para reforma de naftaleno.** [s.l.] Instituto Tecnológico de Aeronáutica, 2016.
- MILLER, JAMES A AND BOWMAN, C. T. Mechanism and modeling of nitrogen chemistry in combustion. **Progress in Energy and Combustion Science**, v. 15, n. 4, p. 287–338, 1989.
- MUNIZ, W. F. . et al. **Flame holding performance of axial swirlers.** Proceedings of the 5th Asian-Pacific International Symposium on Combustion and Energy Utilization. **Anais...2000 NATIONAL ENVIRONMENT COUNCIL - CONAMA. CONAMA Resolutions.** [s.l.: s.n.].
- OMBRELLO, T. et al. Combustion Enhancement via Stabilized Piecewise Nonequilibrium Gliding Arc Plasma Discharge. **AIAA Journal**, v. 44, n. 1, p. 142–150, 2006.
- OMBRELLO, T.; JU, Y. Kinetic Ignition Enhancement of H₂ Versus Fuel-Blended Air Diffusion Flames Using Nonequilibrium Plasma. **IEEE Transactions on Plasma Science**, v. 36, n. 6, p. 2924–2932, 2008.
- PELLERIN, S. et al. Backbreakdown Phenomenon in low current discharge at atmospheric pressure in transversal flow. **High Temperature Material Processes: An International Quarterly of High-Technology Plasma Processes**, v. 3, n. 2–3, 1999.
- PILLA, G. et al. Stabilization of a Turbulent Premixed Flame Using a Nanosecond Repetitively Pulsed Plasma. **IEEE Transactions on Plasma Science**, v. 34, n. 6, p. 2471–2477, 2006.
- POPOV, N. A. Effect of a Pulsed High-Current Discharge on Hydrogen – Air Mixtures. **Plasma Physics Reports**, v. 34, n. 5, p. 376–391, 2008.
- PRESIDENCY OF THE REPUBLIC OF BRAZIL. **RESOLUTION No. 420, December 28, 2009 Published in Official Gazette 249 on 12/30/2009, pp. 81-84 Official Gazette.** [s.l.: s.n.].
- RUSCIC, B. Active Thermochemical Tables: Sequential Bond Dissociation Enthalpies of Methane, Ethane, and Methanol and the Related Thermochemistry. **Journal of Physical Chemistry A**, v. 119, n. 28, p. 7810–7837, 2015.
- SAGÁS, J. C. **Caracterização de Descargas de Arco Deslizante.** [s.l.] Instituto Tecnológico de Aeronáutica, 2009.
- SAGÁS, J. C. et al. Basic characteristics of gliding-arc discharges in air and natural gas. **IEEE Transactions on Plasma Science**, v. 39, n. 2, p. 775–780, 2011.
- SAGÁS, J. C. **Combustão Assistida A Plasma Gerado por Descarga de Arco Deslizante para Produção de Gases Ricos em Hidrogênio.** [s.l.] Instituto Tecnológico de Aeronáutica, 2013.

- SAGÁS, J. C.; MACIEL, H. S.; LACAVALA, P. T. Effects of non-steady state discharge plasma on natural gas combustion: Flammability limits, flame behavior and hydrogen production. **Fuel**, v. 182, p. 118–123, 2016.
- SÁNCHEZ, A. L. et al. The Reduced Kinetic Description of Lean Premixed Combustion. **Combustion and Flame**, v. 123, n. 4, p. 436–464, 2000.
- SILVA, D. DE A. **Análise de Instabilidades Termoacústicas e Emissões de Poluentes em Combustores do Tipo Duplo-estágio para Aplicações em Turbinas a Gás**. [s.l.] Instituto Tecnológico de Aeronáutica, 2011.
- SONG, M. et al. Cross Sections for Electron Collisions with Methane. **Journal of Physical and Chemical Reference Data**, v. 44, n. 2, p. 023101, 2015.
- SONG, Y. H. et al. Clean combustion using rotating arc. **International Journal of Plasma Environmental Science and Technology**, v. 7, n. 2, p. 97–103, 2013.
- STANCU, G. D. et al. Atmospheric pressure plasma diagnostics by OES , CRDS and TALIF. **Journal of Physics D: Applied Physics**, v. 43, n. 12, p. 124002, 2010.
- STARIKOVSKAIA, S. M. Plasma assisted ignition and combustion. **Journal of Physics D: Applied Physics**, v. 39, n. 16, p. R265–R299, 2006.
- STARIKOVSKAIA, S. M. Plasma-assisted ignition and combustion : nanosecond discharges and development of kinetic mechanisms. **Journal of Physics D: Applied Physics**, v. 47, n. 35, p. 353001, 2014.
- STARIKOVSKII, A. Y. et al. Plasma-assisted combustion. **Pure and Applied Chemistry**, v. 78, n. 6, p. 1265–1298, 2006.
- STARIKOVSKIY, A.; ALEKSANDROV, N. Plasma-assisted ignition and combustion. **Progress in Energy and Combustion Science**, v. 39, n. 1, p. 61–110, 2013.
- SUN, W. et al. Effects of non-equilibrium plasma discharge on counterflow diffusion flame extinction. **Proceedings of the Combustion Institute**, v. 33, n. 2, p. 3211–3218, 2011.
- SUN, Z. W. et al. Optical diagnostics of a gliding arc. **Optics Express**, v. 21, n. 5, p. 6028–6044, 2013.
- TANG, J.; ZHAO, W.; DUAN, Y. Some observations on plasma-assisted combustion enhancement using dielectric barrier discharges. **Plasma Sources Science and Technology**, v. 20, n. 4, p. 045009, 2011.
- TORRES, F. A. **Medida de Velocidade de Chama em Combustão parcialmente Pré-misturada**. [s.l.] Instituto Tecnológico de Aeronáutica, 2014.
- TU, X.; WHITEHEAD, J. C. Plasma dry reforming of methane in an atmospheric pressure AC gliding arc discharge: Co-generation of syngas and carbon nanomaterials. **International**

Journal of Hydrogen Energy, v. 39, n. 18, p. 9658–9669, 2014.

TURNS, S. R. **An Introduction to Combustion: Concepts and Applications**. Third Edit ed. [s.l.] McGraw-hill New York, 2013.

UDDI, M. et al. Atomic oxygen measurements in air and air / fuel nanosecond pulse discharges by two photon laser induced fluorescence. **Proceedings of the Combustion Institute**, v. 32, n. 1, p. 929–936, 2009.

UNITED NATIONS. **United Nations Framework Convention On Climate Change**. [s.l: s.n.]. Disponível em: <<https://unfccc.int/resource/docs/convkp/conveng.pdf>>.

UNITED NATIONS. **Adoption of the Paris Agreement**. [s.l: s.n.].

UNITED NATIONS. **Kyoto Protocol To the United Nations Framework Kyoto Protocol To the United Nations Framework**. [s.l: s.n.]. Disponível em: <<http://unfccc.int/resource/docs/convkp/kpeng.pdf>>.

VARELLA, R. A. **Analysis of Plasma Assisted Combustion Under Rich-fuel Conditions**. [s.l.] Instituto Tecnológico de Aeronáutica, 2015.

VARELLA, R. A.; SAGÁS, J. C.; MARTINS, C. A. Effects of plasma assisted combustion on pollutant emissions of a premixed flame of natural gas and air. **Fuel**, v. 184, p. 269–276, 2016.

WANG, W. et al. Gliding arc plasma for CO₂ conversion: Better insights by a combined experimental and modelling approach. **Chemical Engineering Journal**, v. 330, n. June, p. 11–25, 2017a.

WANG, W. et al. Nitrogen Fixation by Gliding Arc Plasma: Better Insight by Chemical Kinetics Modelling. **ChemSusChem**, v. 10, n. 10, p. 2145–2157, 2017b.

WEINER, S. et al. Evidence for the use of fire at Zhoukoudian, China. **Science**, v. 281, n. 5374, p. 251–253, 1998.

WU, W.; FUH, C. A.; WANG, C. Comparative Study on Microwave Plasma-Assisted Combustion of Premixed and Nonpremixed Methane / Air Mixtures. **Combustion Science and Technology**, v. 187, n. 7, p. 999–1020, 2015.

WU, W. W. et al. Experimental Investigation of Premixed Methane-Air Combustion Assisted by Alternating-Current Rotating Gliding Arc. **IEEE Transactions on Plasma Science**, v. 43, n. 12, p. 3979–3985, 2015.

XIA, Y. et al. Dry reforming of CO₂-CH₄ assisted by high-frequency AC gliding arc discharge: Electrical characteristics and the effects of different parameters. **International Journal of Hydrogen Energy**, v. 42, n. 36, p. 22776–22785, 2017.

ZHAO, F. et al. Investigation of mechanisms in plasma-assisted ignition of dispersed coal

particle streams. **Fuel**, v. 186, p. 518–524, 2016.

ZHU, F. et al. Destruction of toluene by rotating gliding arc discharge. **Fuel**, v. 176, p. 78–85, 2016.

ZHU, J. et al. **Effects of gliding arc discharge penetrating a premixed flame**. Proceedings of the European Combustion Meeting. **Anais...**2015

ZHU, J. et al. Spatiotemporally resolved characteristics of a gliding arc discharge in a turbulent air flow at atmospheric pressure. **Physics of Plasmas**, v. 24, n. 1, 2017.

ZUZEEK, Y. et al. Pure rotational CARS studies of thermal energy release and ignition in nanosecond repetitively pulsed hydrogen-air plasmas. **Proceedings of the Combustion Institute**, v. 33, n. 2, p. 3225–3232, 2011.

Appendix A – Mathematical calculation of the Swirl number

The swirl number corresponds to the ratio between the angular momentum flow and the linear momentum flow. Here is present the methodology used to calculate the swirl number in the present study, and it follows the one proposed by Lawn (LAW, 1987), Muniz et al. (MUNIZ et al., 2000) and Couto et al. (COUTO; MUNIZ; BASTOS-NETTO, 1995) apud Almeida (SILVA, 2011).

The angular (G_φ) and the linear (G_x) momentum are conserved and both can be written as follow:

$$G_\varphi = \int_{R_1}^{R_2} 2\pi\rho u\omega r^2 dr = \text{constant} \quad (\text{A1})$$

$$G_x = \int_{R_1}^{R_2} 2\pi r(p + \rho u^2) dr = \text{constant} \quad (\text{A2})$$

where ρ is the flow specific mass, u and ω are respectively, the axial and tangential components of the velocity in a transversal section of the flow. The inferior and superior radius that limit this transversal section are R_1 and R_2 , respectively. The parameter p corresponds to the static pressure. Thus, the swirl number can be calculated as:

$$S = \frac{G_\varphi}{RG_x} \quad (\text{A3})$$

where R is the radius of the exit duct of the burner. Since it can be hard to obtain the static pressure downstream the burner, it is convenient to adopt an “alternative swirl number” (S')

based in the velocity distribution of the swirler itself. So, the alternative swirl number can be written as:

$$S' = \frac{G_{\varphi}}{R G_x'} \quad (\text{A4})$$

where,

$$G_x' = \int_{R_1}^{R_2} 2\pi\rho u^2 r dr \quad (\text{A5})$$

Supposing a uniform distribution of velocity in the transversal section of the duct and integrating equation (A5):

$$G_x' = \pi\rho u^2 (R_2 - R_1) \quad (\text{A6})$$

or,

$$G_x' = m \cdot \bar{u} \quad (\text{A7})$$

where m is the mass flow rate and \bar{u} the mean axial velocity.

The alternative swirl number can be extended to situations where there is a central primary flow (subscript p) and an annular secondary flow (subscript s):

$$S' = \frac{G_{\varphi p} + G_{\varphi s}}{R(G_{xp}' + G_{xs}')} \quad (\text{A8})$$

Writing S' for the primary and secondary flows:

$$S_p' = \frac{G_{\varphi p}}{R_p G_{xp}'} \quad (\text{A9})$$

$$S_s' = \frac{G_{\varphi s}}{R_s G'_{\varphi s}} \quad (\text{A10})$$

So, from equations (A8) and (A7):

$$S' = \frac{(\mu)_p \left(\frac{R_p}{R_s}\right) S'_p + G'_{\varphi s} S'_s}{(\mu)_p + (\mu)_s} \quad (\text{A11})$$

If M_r is the ratio between the linear and angular momentum flow of the primary and secondary flows, so:

$$M_r = \frac{(\mu)_p}{(\mu)_s} \quad (\text{A12})$$

and replacing in equation (A11):

$$S' = \left(\frac{M_r}{1 + M_r}\right) \left(\frac{R_p}{R_s}\right) S'_p + \left(\frac{1}{1 + M_r}\right) S'_s \quad (\text{A13})$$

Figure A.1 shows a general schematics of a swirl burner:

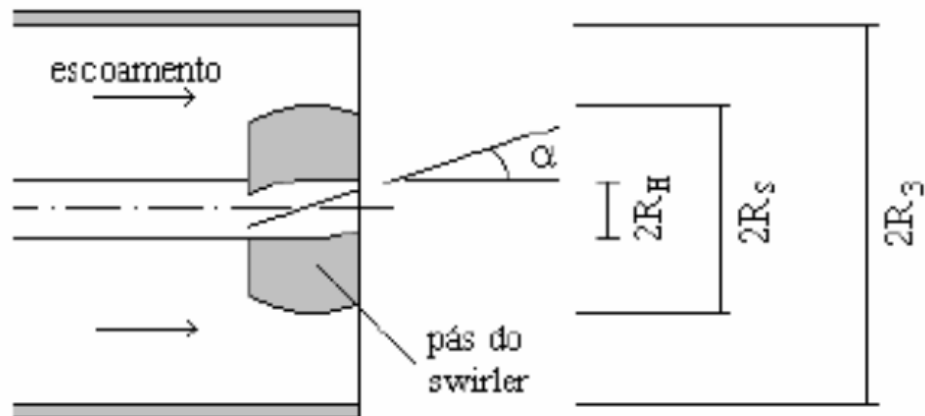


Figure A.1 – General schematics of a swirl burner (SILVA, 2011).

For this burner, equations (A1) and (A5) become:

$$G_{\varphi} = \int_{R_H}^{R_S} 2\pi r \omega r^2 dr \quad (\text{A14})$$

and

$$G'_{x} = \int_{R_H}^{R_S} 2\pi \rho u^2 r dr \quad (\text{A15})$$

The tangential component of velocity (ω) can be written as $\omega = u \cdot \tan(\alpha)$, where α is the angle of the swirler blades. So, equation (A14) and (A16) become:

$$G_{\varphi} = 2\pi(\text{CB})\rho u^2 \tan(\alpha) \left(\frac{R_S^3 - R_H^3}{3} \right) \quad (\text{A16})$$

$$G'_{x} = \pi \rho u^2 (R_S^3 - R_H^3) \quad (\text{A17})$$

where CB is the block coefficient due to the thickness of the blades, R_s is the radius of the swirler, R_H is the fuel injector radius and R_3 is the radius of the duct of the burner.

From equations (A16) and (A17):

$$\frac{G_\varphi}{G'_x} = \frac{2(\text{CB})\text{tg}(\alpha)(R_s^3 - R_H^3)}{3(R_3^2 - R_H^2)} \quad (\text{A18})$$

As only the secondary flow passes through the swirler, from equation (A13), S' becomes:

$$S' = \frac{S'_s}{1 + M_x} \quad (\text{A19})$$

which is the equation used in this study to calculate the swirl number.

Writing the mean axial velocity for the primary and secondary flows:

$$\bar{u}_p = \left(\frac{m}{\rho A} \right)_p \quad (\text{A20})$$

and

$$\bar{u}_s = \left(\frac{m}{\rho A} \right)_s \quad (\text{A21})$$

A_p and A_s can be written as follow:

$$A_p = \pi R_1^2 \quad (\text{A22})$$

and

$$A_s = \pi(R_3^2 - R_H^2) \quad (\text{A23})$$

where R_1 is the radius of the fuel injector role. Thus, the equation (A12) becomes:

$$M_r = \frac{\left(\frac{\rho}{m^2}\right)_s \left(\frac{m^2}{\rho}\right)_p (R_3^2 - R_H^2)}{R_1^2} \quad (A24)$$

Given that $(R_3 - R_H)$ corresponds to the transversal section through which the flow passes, the alternative swirl number of the secondary flow can be written as:

$$S'_s = \frac{G_\phi}{(R_3 - R_H)G_x} \quad (A25)$$

The blocking coefficient can be calculated as showed by Muniz et al. (MUNIZ et al., 2000) apud Almeida (SILVA, 2011), which considers that the influence of the Reynolds number is small. In this way, CB only depends on the geometric dimension of the blades in the perpendicular direction of the duct axis. So:

$$CB = \frac{1}{1 - \sigma} \quad (A26)$$

where σ is the blocking factor and is calculated as:

$$\sigma = \frac{A_s - A_{ef}}{A_{3a} - A_s} \quad (A27)$$

The parameter A_s corresponds to the area of the swirler, A_{3a} is the annular area between the swirler and the duct wall. A_{ef} is the effective area of the flow and is calculated as:

$$A_{ef} = 2 (R_s - R_H)(K - 2T)\cos(\alpha) \quad (A28)$$

where

$$K = \cos\left(\frac{\pi}{2Z}\right) \left[R_S \sin\left(\frac{\pi}{2Z}\right) + R_H \tan\left(\frac{\pi}{2Z}\right) \right] \quad (\text{A27})$$

in which Z is the number of blades of the swirler and T is its thickness.

Appendix B – Concentration graphs of the exhaust gas components

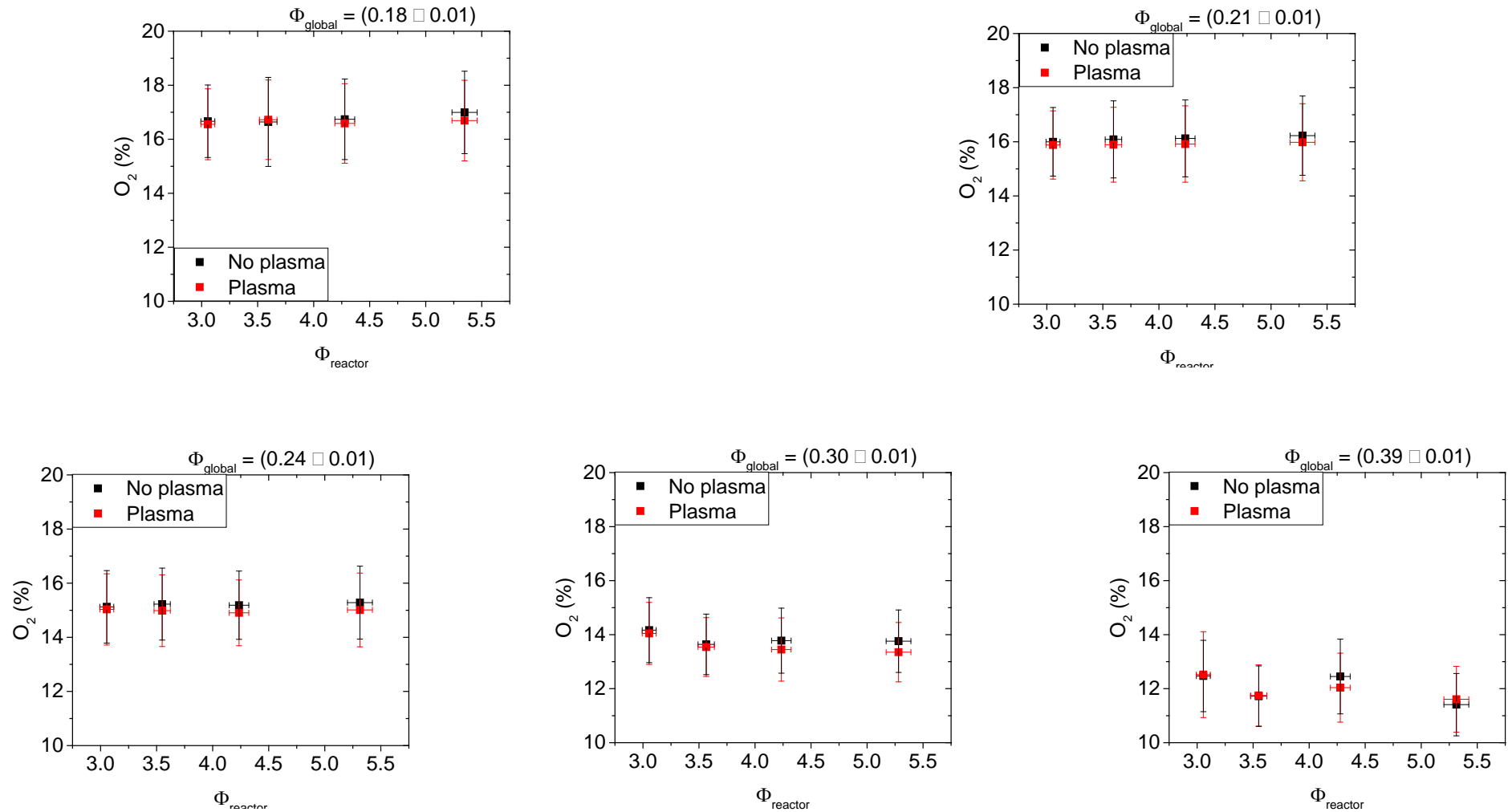


Figure B.1 – O_2 behavior as a function of the reactor equivalence ratio (Φ_{reactor}) for all tested Φ_{global} range.

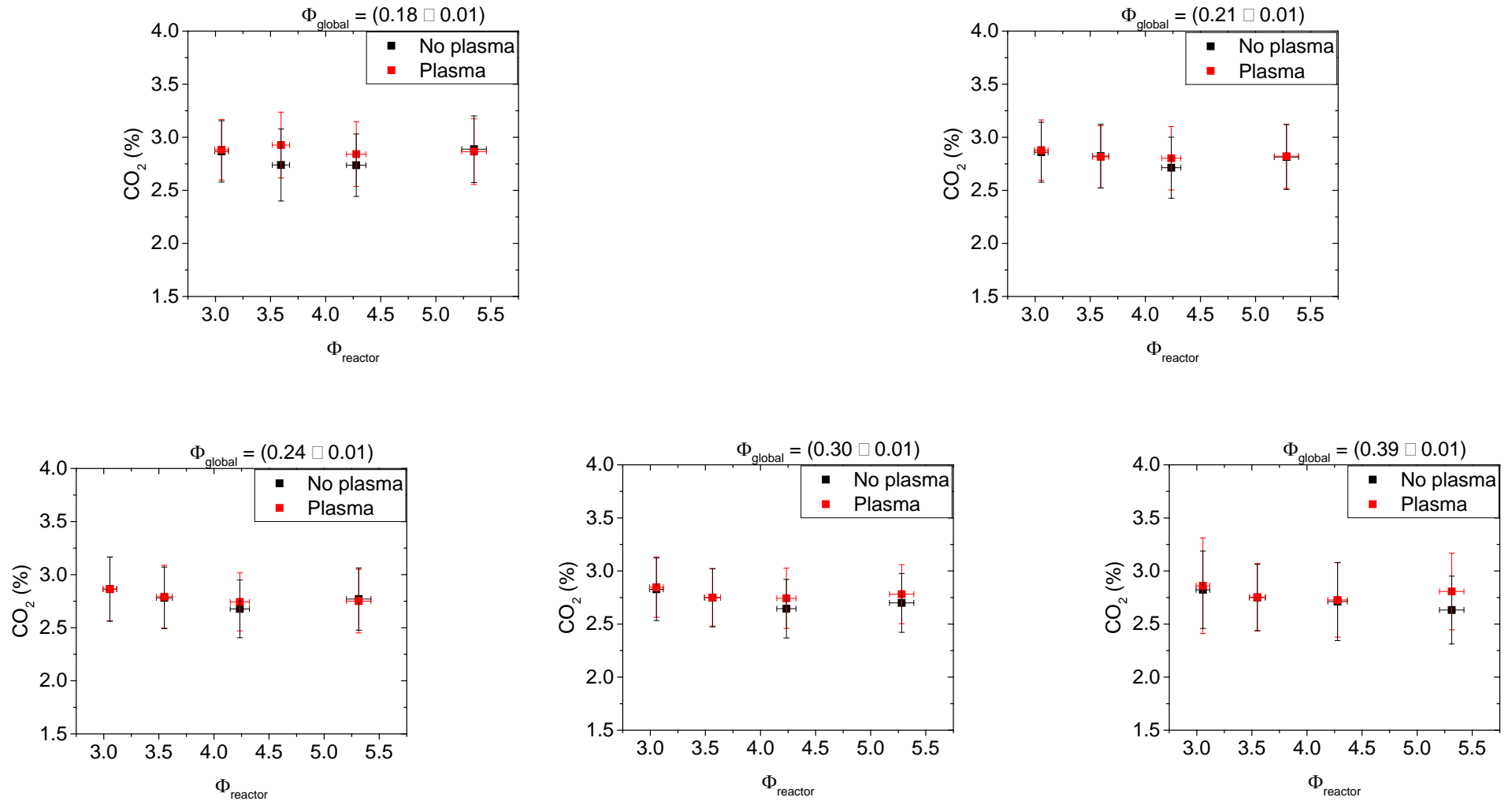


Figure B.2 – CO₂ behavior as a function of the reactor equivalence ratio (Φ_{reactor}) for all tested Φ_{global} range. All concentrations are in wet basis and were corrected for an excess of 15% of O₂.

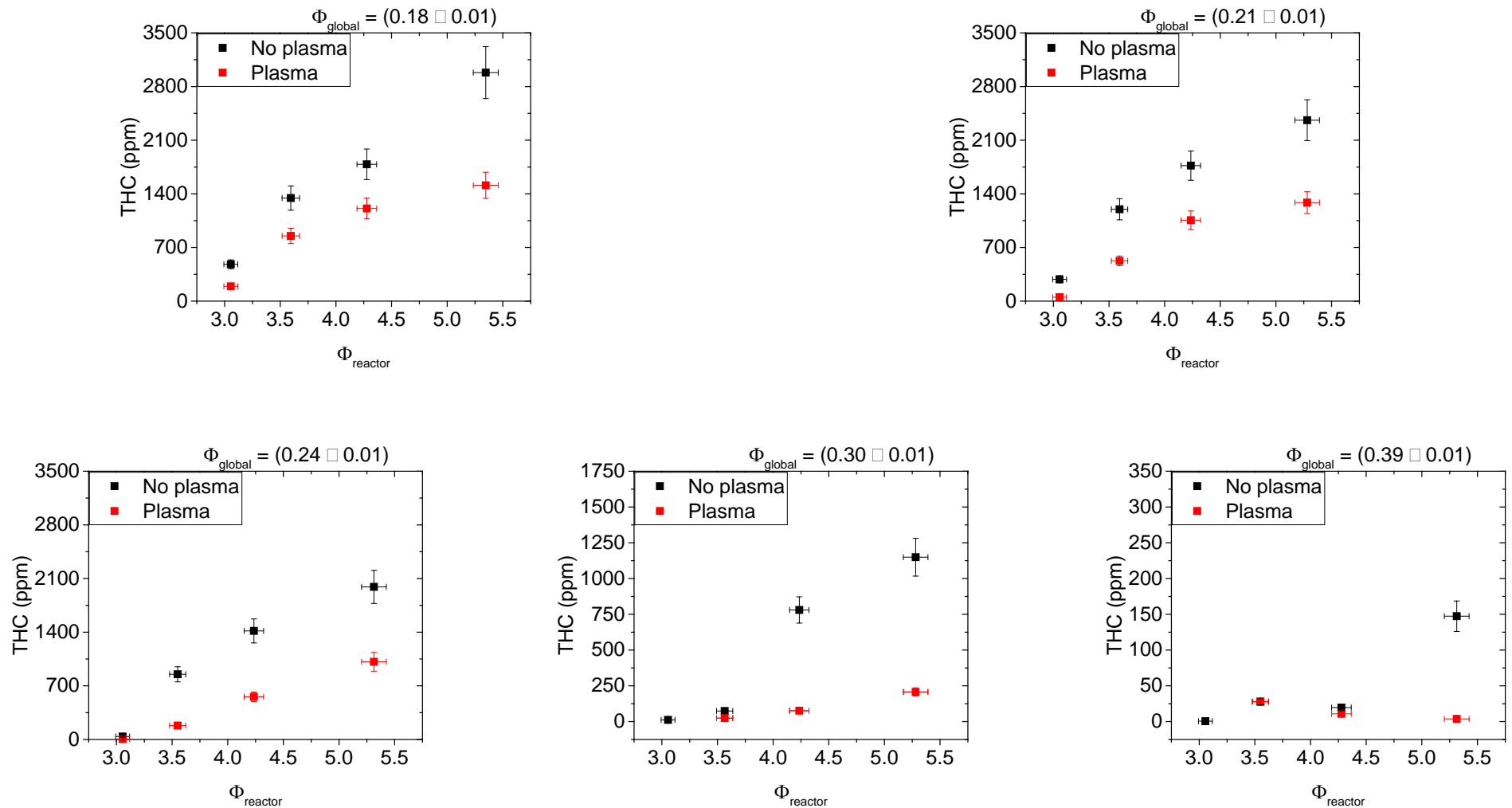


Figure B.3 – THC behavior as a function of the reactor equivalence ratio (Φ_{reactor}) for all tested Φ_{global} range. All concentrations are in wet basis and were corrected for an excess of 15% of O_2 .

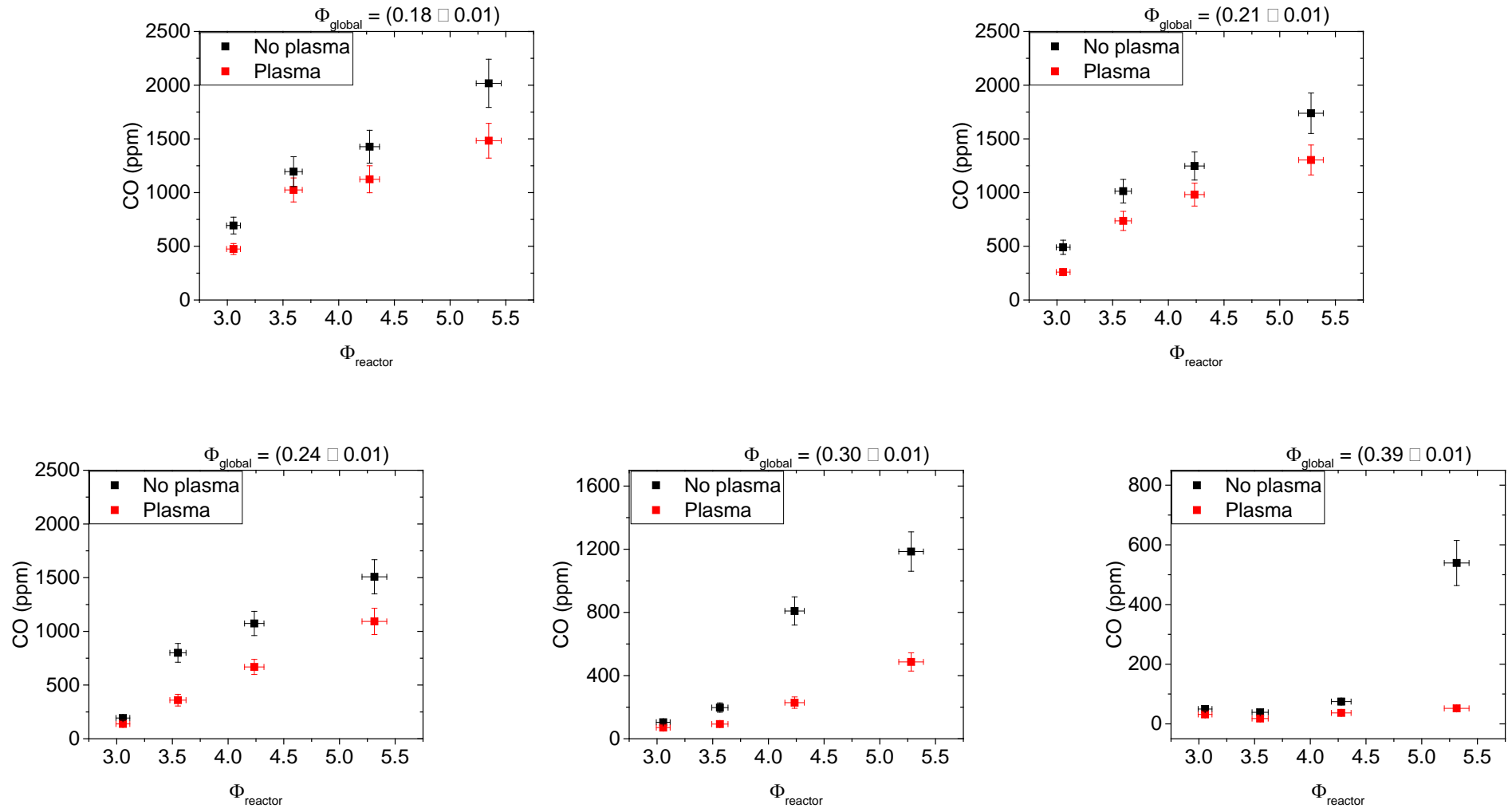


Figure B.4 – CO behavior as a function of the reactor equivalence ratio (Φ_{reactor}) for all tested Φ_{global} range. All concentrations are in wet basis and were corrected for an excess of 15% of O_2 .

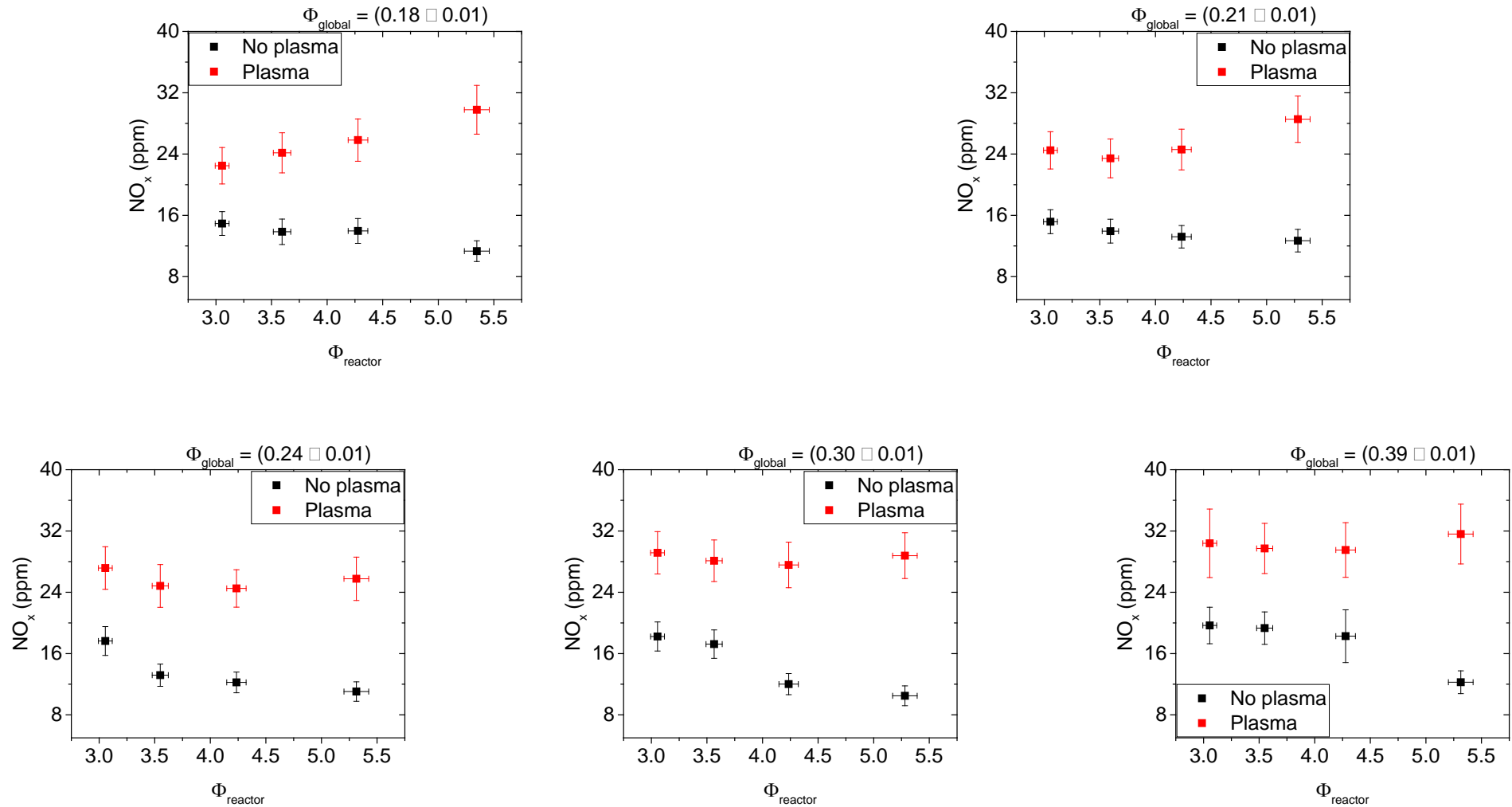


Figure B.5 – NO_x behavior as a function of the reactor equivalence ratio (Φ_{reactor}) for all tested Φ_{global} range. All concentrations are in wet basis and were corrected for an excess of 15% of O_2 .

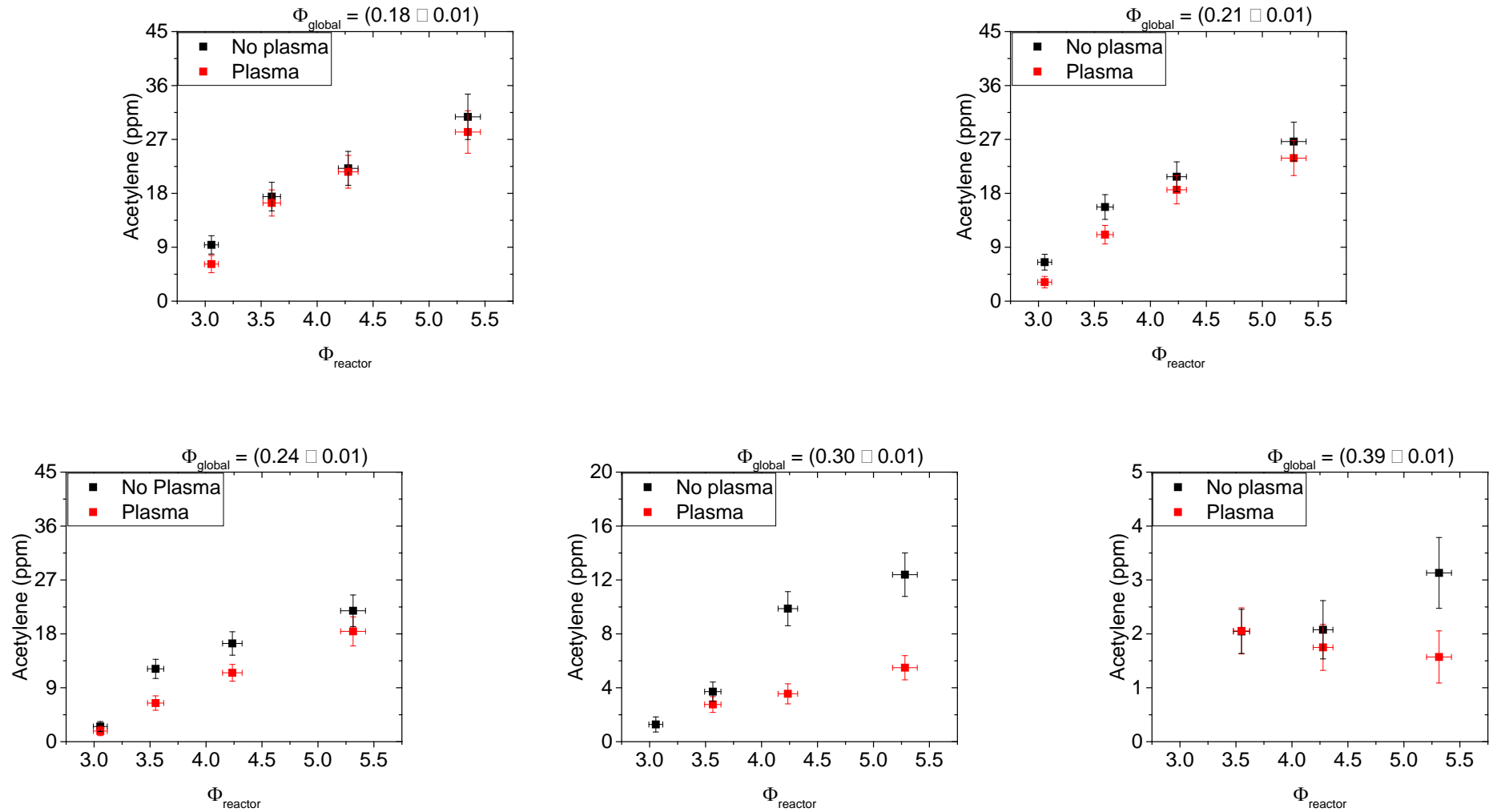


Figure B.6 – Acetylene (C_2H_2) behavior as a function of the reactor equivalence ratio (Φ_{reactor}) for all tested Φ_{global} range. All concentrations are in wet basis and were corrected for an excess of 15% of O_2 .

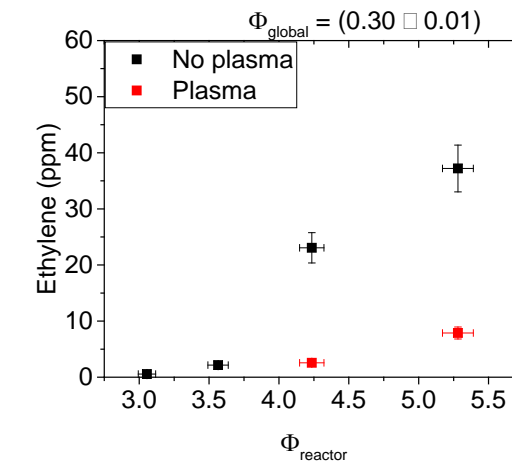
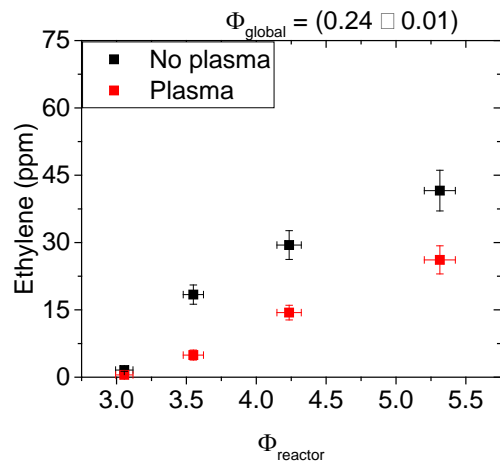
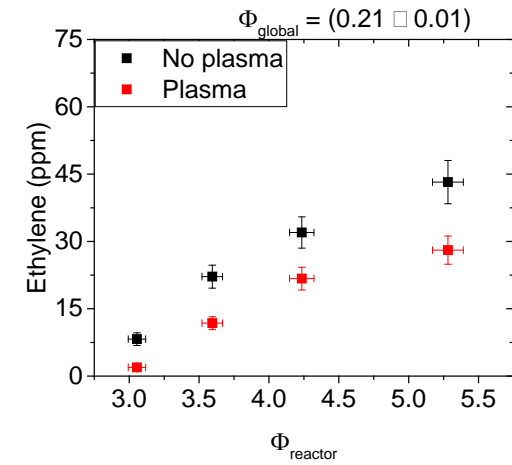
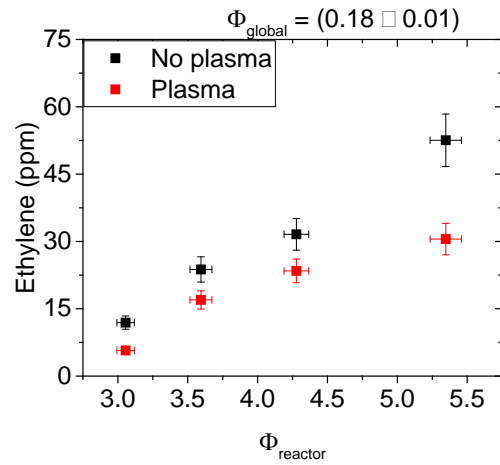


Figure B.7 – Ethylene (C_2H_4) behavior as a function of the reactor equivalence ratio (Φ_{reactor}) for all tested Φ_{global} range. All concentrations are in wet basis and were corrected for an excess of 15% of O_2 .

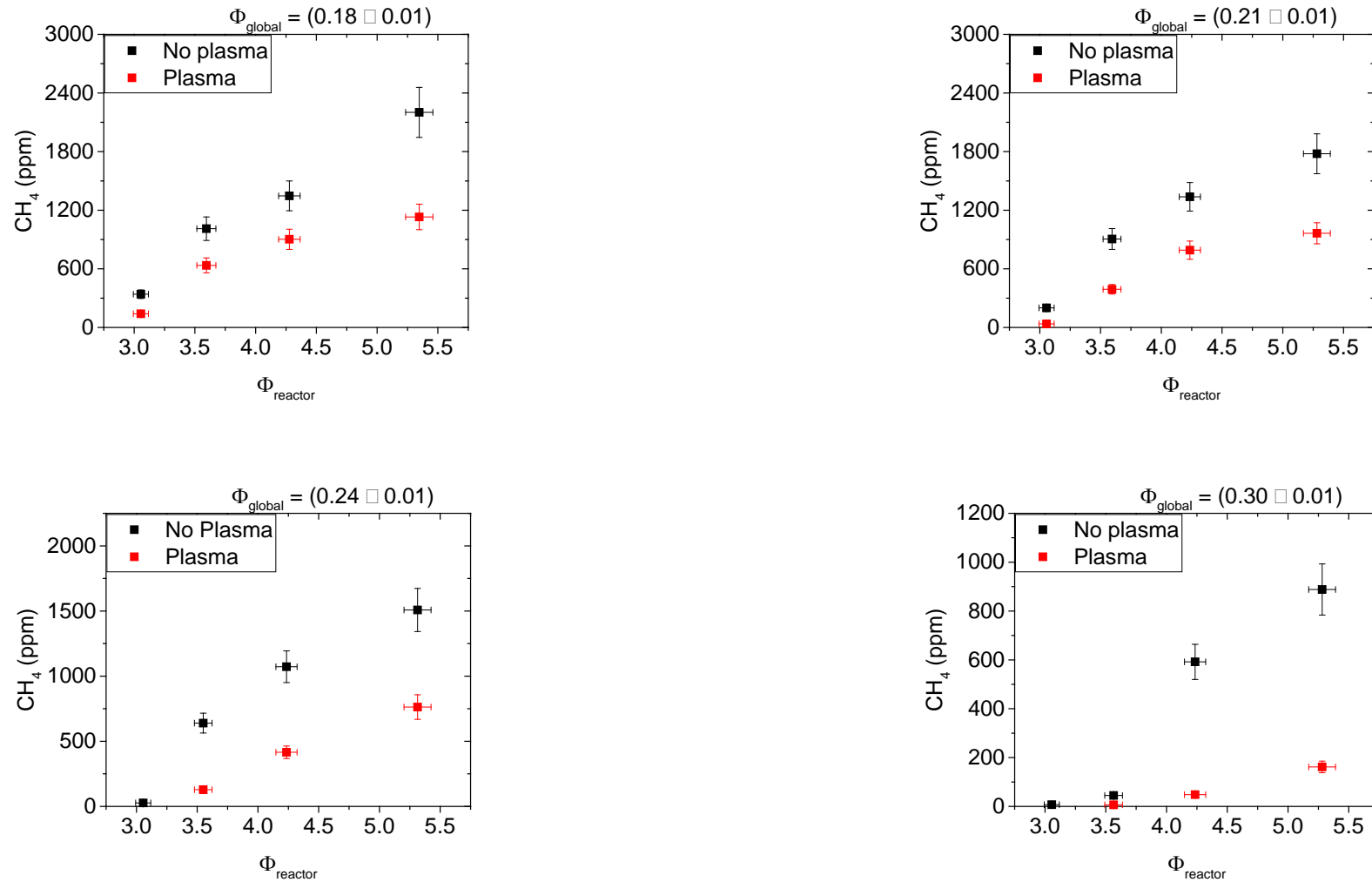


Figure B.8 – CH_4 behavior as a function of the reactor equivalence ratio (Φ_{reactor}) for all tested Φ_{global} range. All concentrations are in wet basis and were corrected for an excess of 15% of O_2 .

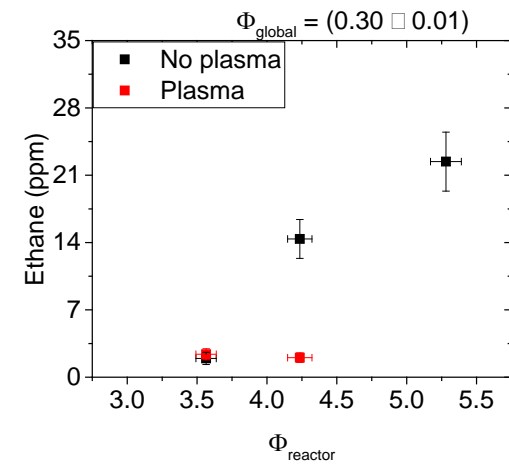
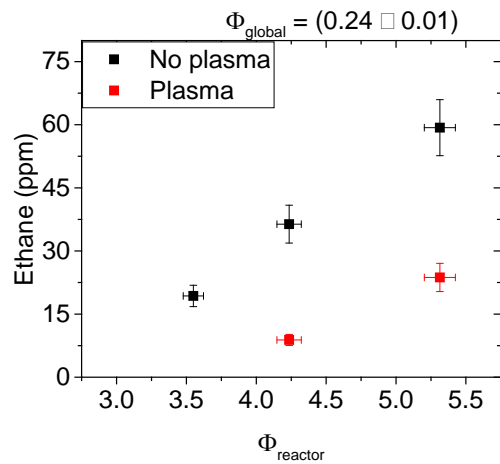
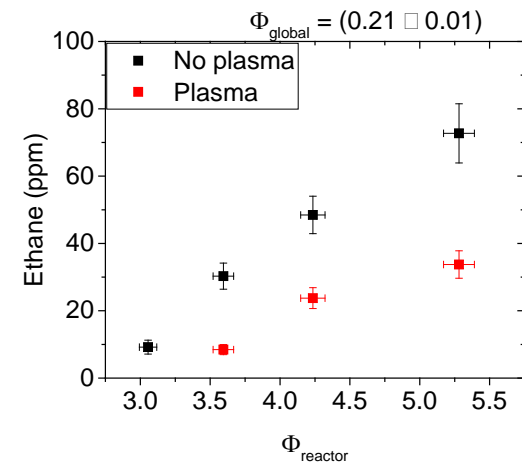
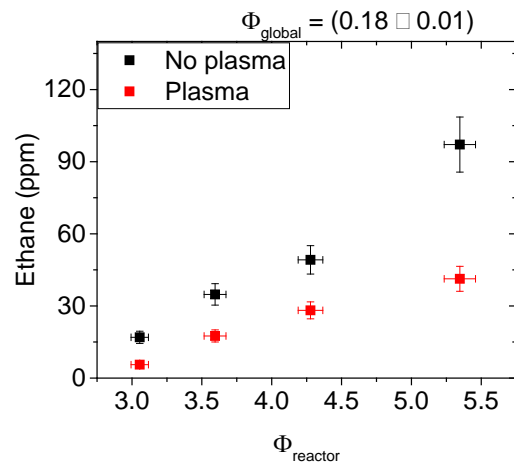


Figure B.9 – Ethane (C_2H_6) behavior as a function of the reactor equivalence ratio (Φ_{reactor}) for all tested Φ_{global} range. All concentrations are in wet basis and were corrected for an excess of 15% of O_2 .

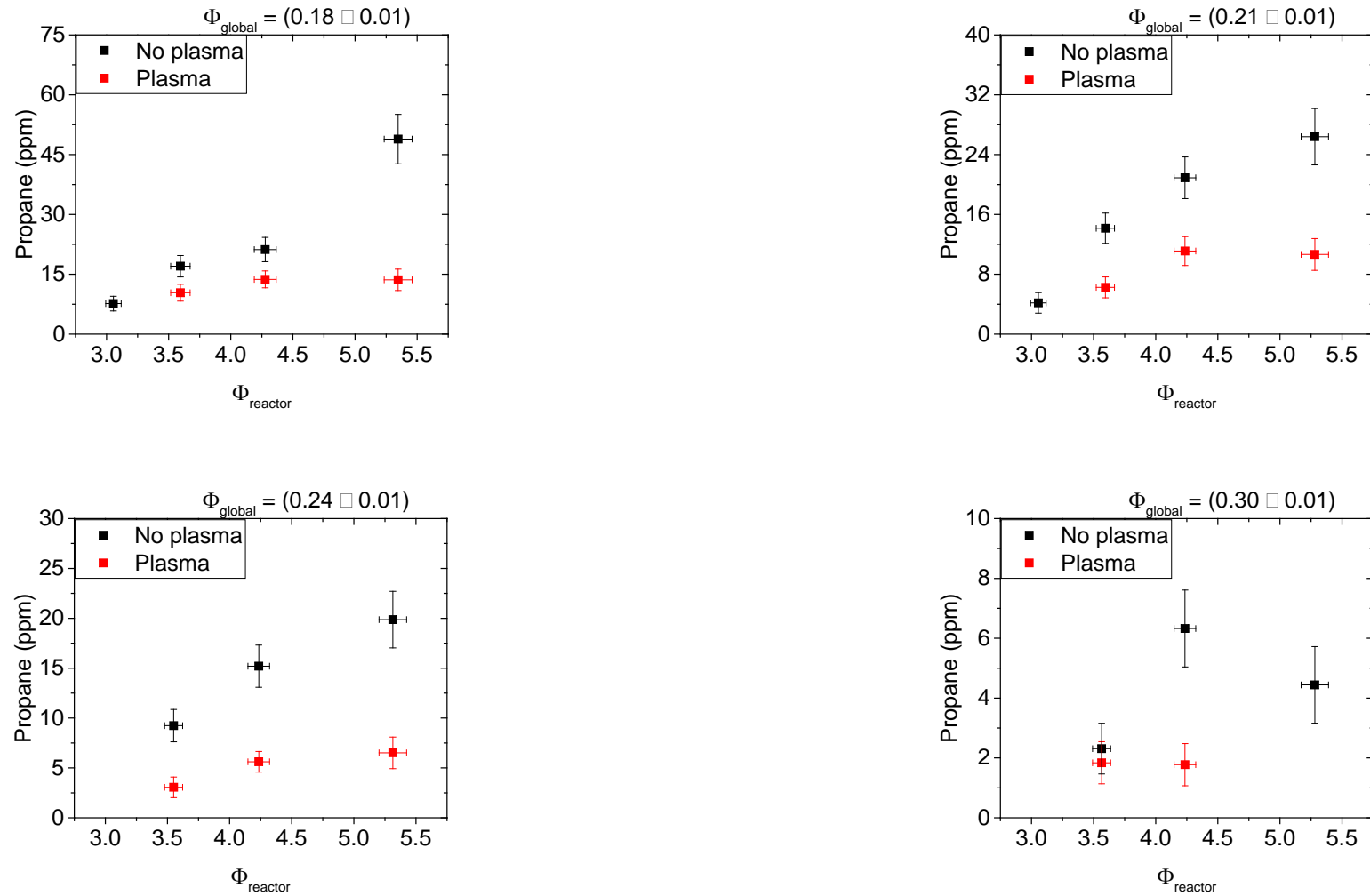


Figure B.10 – Propane (C_3H_8) behavior as a function of the reactor equivalence ratio (Φ_{reactor}) for all tested Φ_{global} range. All concentrations are in wet basis and were corrected for an excess of 15% of O_2 .

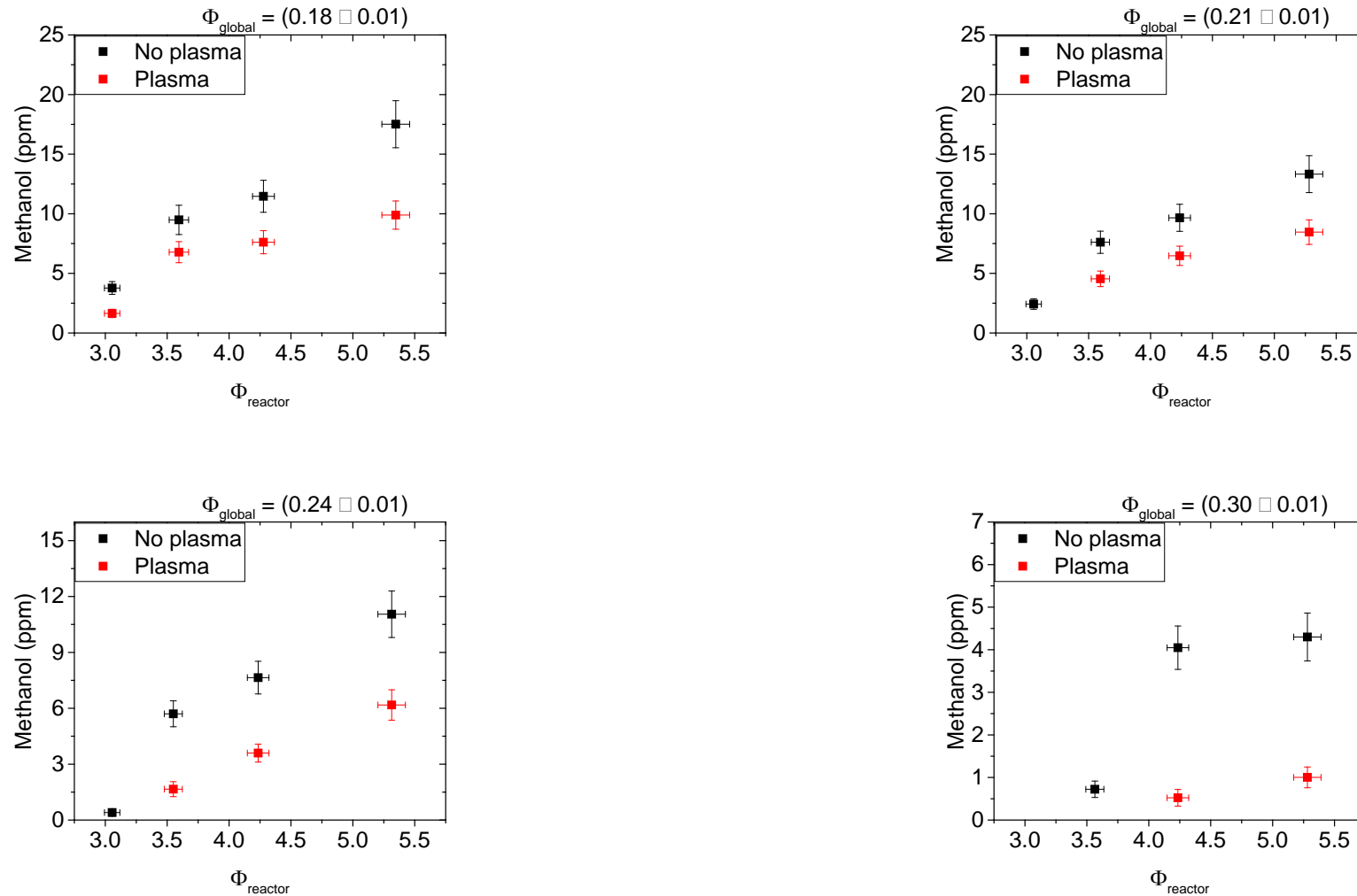


Figure B.11 – Methanol (CH_3OH) behavior as a function of the reactor equivalence ratio (Φ_{reactor}) for all tested Φ_{global} range. All concentrations are in wet basis and were corrected for an excess of 15% of O_2 .

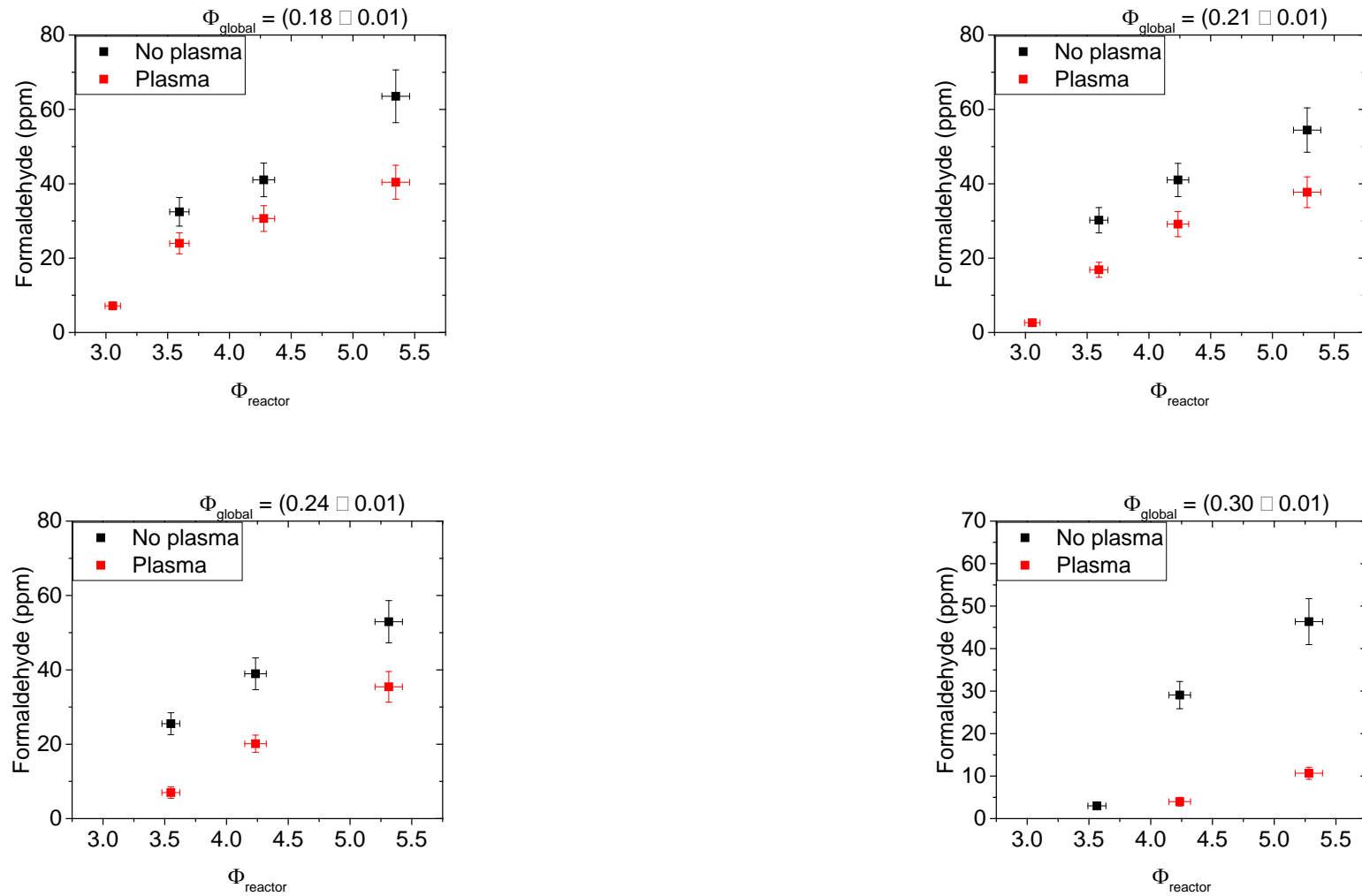


Figure B.12 – Formaldehyde (CH_2O) behavior as a function of the reactor equivalence ratio (Φ_{reactor}) for all tested Φ_{global} range. All concentrations are in wet basis and were corrected for an excess of 15% of O_2 .

Appendix C – Tables referent to the variations on the concentration of the exhaust gas composition

Tabel C.1: O₂ variation with plasma application.

O ₂				
Φ_{reactor}	Φ_{global}	Concentration (no plasma)	Concentration (plasma)	Variation
		%	%	%
5.4	0.18	17.0±1.5	16.7±1.5	-1.8±0.1
4.3	0.18	16.7±1.5	16.6±1.5	-0.6±0.1
3.6	0.18	16.6±1.6	16.7±1.5	0.6±0.1
3.1	0.18	16.66±1.3	16.6±1.3	-0.6±0.1
5.4	0.21	16.2±1.5	16.0±1.4	-1.2±0.1
4.3	0.21	16.1±1.4	15.9±1.4	-1.2±0.1
3.6	0.21	16.1±1.4	15.9±1.4	-1.2±0.1
3.1	0.21	16.0±1.3	15.9±1.3	-0.6±0.1
5.4	0.24	15.3±1.35	15.0±1.4	-2.0±0.1
4.3	0.24	15.2±1.26	14.9±1.2	-2.0±0.1
3.6	0.24	15.2±1.33	15.0±1.3	-1.3±0.1
3.1	0.24	15.1±1.34	15.0±1.3	-0.7±0.1
5.4	0.30	13.8±1.2	13.4±1.1	-2.9±0.1
4.3	0.30	13.8±1.2	13.4±1.2	-2.9±0.1
3.6	0.30	13.6±1.1	13.5±1.1	-0.7±0.1
3.1	0.30	14.2±1.2	14.0±1.2	-1.4±0.1
5.4	0.39	11.4±1.2	11.6±1.2	1.8±0.1
4.3	0.39	12.4±1.4	12.0±1.3	-3.2±0.2
3.6	0.39	11.7±1.1	11.8±1.1	0.9±0.1
3.1	0.39	12.5±1.3	12.5±1.6	0.0±0.2

Tabel C.2: CO₂ variation with plasma application

CO ₂				
Φ_{reactor}	Φ_{global}	Concentration (no plasma)	Concentration (plasma)	Variation
		%	%	%
5.4	0.18	2.9±0.3	2.9±0.3	0.0±0.1
4.3	0.1	2.7±0.3	2.8±0.3	3.7±0.2
3.6	0.18	2.7±0.3	2.9±0.3	7.4±0.2
3.1	0.18	2.9±0.3	2.9±0.3	0.0±0.1
5.4	0.21	2.8±0.3	2.8±0.3	0.0±0.2
4.3	0.21	2.7±0.3	2.8±0.3	3.7±0.2
3.6	0.21	2.8±0.3	2.8±0.3	0.0±0.2
3.1	0.21	2.9±0.3	2.9±0.3	0.0±0.1
5.4	0.24	2.8±0.3	2.8±0.3	0.0±0.2
4.3	0.24	2.7±0.3	2.7±0.3	0.0±0.2
3.6	0.24	2.8±0.3	2.8±0.3	0.0±0.2
3.1	0.24	2.9±0.3	2.9±0.3	0.0±0.1
5.4	0.30	2.7±0.3	2.8±0.3	3.7±0.2
4.3	0.30	2.6±0.3	2.7±0.3	3.8±0.2
3.6	0.30	2.8±0.3	2.8±0.3	0.0±0.2
3.1	0.30	2.8±0.3	2.8±0.3	0.0±0.2
5.4	0.39	2.6±0.3	2.8±0.4	7.7±0.2
4.3	0.39	2.7±0.4	2.7±0.4	0.04±0.2
3.6	0.39	2.8±0.3	2.8±0.3	3.7±0.2
3.1	0.39	2.8±0.4	2.9±0.5	3.6±0.2

Tabel C.3: THC variation with plasma application

THC				
Φ_{reactor}	Φ_{global}	Concentration (no plasma)	Concentration (plasma)	Variation
		ppm	ppm	%
5.4	0.18	2982.2±338.6	1518.1±171.5	-49.1±0.2
4.3	0.18	1787.9±199.3	1212.4±136.0	-32.2±0.2
3.6	0.18	1346.4±158.7	854.5±100.3	-36.5±0.2
3.1	0.18	482.5±58.7	205.1±28.1	-57.5±0.2
5.4	0.21	2367.0±266.8	1293.9±142.5	-45.3±0.2
4.3	0.21	1772.7±191.4	1058.8±121.6	-40.3±0.2

3.6	0.21	1199.9±138.2	530.2±63.8	-55.8±0.2
3.1	0.21	287.6±45.8	63.4±12.3	-78.0±0.3
5.4	0.24	2002.2±217.3	1019.3±122.4	-49.1±0.2
4.3	0.24	1420.8±157.1	560.8±62.7	-60.5±0.2
3.6	0.24	852.2±98.4	183.3±37.0	-78.5±0.2
3.1	0.24	49.1±9.9	20.3±7.5	-58.7±0.4
5.4	0.30	1154.1±132.3	214.0±29.8	-81.5±0.2
4.3	0.30	783.1±92.1	82.3±15.4	-89.5±0.2
3.6	0.30	78.0±14.1	28.0±6.1	-64.1±0.3
3.1	0.30	19.0±6.5	15.8±6.1	-16.8±0.5
5.4	0.39	149.7±21.9	8.5±4.3	-94.3±0.5
4.3	0.39	25.7±5.5	17.2±4.8	-33.1±0.4
3.6	0.39	31.3±5.4	33.8±5.8	8.0±0.2
3.1	0.39	10.2±4.6	13.0±5.3	27.5±0.6

Tabel C.4: CO variation with plasma application

CO				
Φ_{reactor}	Φ_{global}	Concentration (no plasma)	Concentration (plasma)	Variation
		ppm	ppm	%
5.4	0.18	2017.2±224.4	1482.8±161.4	-26.5±0.2
4.3	0.18	1427.2±152.7	1123.9±125.6	-21.3±0.2
3.6	0.18	1195.3±138.6	1024.6±112.1	-14.3±0.2
3.1	0.18	693.3±78.2	474.8±50.7	-31.5±0.2
5.4	0.21	1738.6±188.5	1303.2±139.3	-25.0±0.2
4.3	0.21	1247.8±131.2	981.2±106.6	-21.4±0.2
3.6	0.21	1013.0±110.2	736.4±88.8	-27.3±0.2
3.1	0.21	490.7±65.9	259.4±29.4	-47.1±0.2
5.4	0.24	1507.9±159.3	1092.4±122.3	-27.6±0.2
4.3	0.24	1073.8±112.8	669.0±70.2	-37.7±0.1
3.6	0.24	800.2±87.4	359.5±54.8	-55.1±0.2
3.1	0.24	193.5±22.4	138.0±15.2	-28.7±0.2
5.4	0.30	1185.0±124.7	486.4±57.9	-59.0±0.2
4.3	0.30	808.9±89.2	228.8±35.8	-71.7±0.2
3.6	0.30	197.5±29.8	93.0±10.0	-52.9±0.2
3.1	0.30	104.5±11.4	70.9±7.4	-32.2±0.2

5.4	0.39	539.1±75.5	51.9±8.1	-90.4±0.2
4.3	0.39	74.7±11.0	36.6±5.9	-51.0±0.2
3.6	0.39	38.7±4.6	17.8±2.2	-54.0±0.2
3.1	0.39	49.7±6.7	31.4±5.1	-36.8±0.2

Tabel C.5: NO_x variation with plasma application

NO _x				
Φ_{reactor}	Φ_{global}	Concentration (no plasma)	Concentration (plasma)	Variation
		ppm	ppm	%
5.4	0.18	11.3±1.4	29.8±3.2	163.7±0.2
4.3	0.18	14.0±1.6	25.8±2.8	84.3±0.2
3.6	0.18	13.9±1.7	24.2±2.6	74.1±0.2
3.1	0.18	14.9±1.6	22.5±2.4	51.0±0.2
5.4	0.21	12.7±1.5	28.5±3.0	124.4±0.2
4.3	0.21	13.2±1.5	24.6±2.7	86.4±0.2
3.6	0.21	13.9±1.6	23.4±2.5	68.3±0.2
3.1	0.21	15.2±1.6	24.5±2.4	61.2±0.1
5.4	0.24	11.0±1.3	25.8±2.8	134.5±0.2
4.3	0.24	12.2±1.4	24.5±2.4	100.8±0.2
3.6	0.24	13.2±1.5	24.8±2.8	87.9±0.2
3.1	0.24	17.6±1.9	27.2±2.8	54.5±0.1
5.4	0.30	10.5±1.3	28.8±3.0	174.3±0.2
4.3	0.30	12.0±1.4	27.6±3.0	130.0±0.2
3.6	0.30	17.2±1.9	28.1±2.7	63.4±0.1
3.1	0.30	18.2±1.9	29.2±2.8	60.4±0.1
5.4	0.39	12.3±1.5	31.6±3.9	156.9±0.2
4.3	0.39	18.3±3.4	29.5±3.6	61.2±0.2
3.6	0.39	19.3±2.1	29.7±3.3	53.9±0.2
3.1	0.39	19.7±2.4	30.4±4.5	54.3±0.2

Tabel C.6: Acetylene (C₂H₂) variation with plasma application

Acetylene				
Φ_{reactor}	Φ_{global}	Concentration (no plasma)	Concentration (plasma)	Variation
		ppm	ppm	%
5.4	0.18	30.8±3.8	28.2±3.6	-8.4±0.2
4.3	0.18	22.2±2.8	21.6±2.7	-2.7±0.2
3.6	0.18	17.5±2.4	16.4±2.2	-6.3±0.2
3.1	0.18	9.4±1.5	6.2±1.4	-34.0±0.3
5.4	0.21	26.6±3.2	23.9±2.9	-10.2±0.2
4.3	0.21	20.8±2.5	18.6±2.4	-10.6±0.2
3.6	0.21	15.7±2.1	11.1±1.6	-29.3±0.2
3.1	0.21	6.5±1.3	3.2±1.0	-50.8±0.4
5.4	0.24	21.9±2.6	18.4±2.4	-16.0±0.2
4.3	0.24	16.4±2.0	11.5±1.4	-29.9±0.2
3.6	0.24	12.2±1.6	6.5±1.2	-46.7±0.2
3.1	0.24	2.5±0.8	1.8±0.8	-28.0±0.5
5.4	0.30	12.4±1.6	5.5±0.9	-55.6±0.2
4.3	0.30	9.9±1.3	3.6±0.8	-63.6±0.3
3.6	0.30	3.7±0.7	2.8±0.6	-24.3±0.3
3.1	0.30	-	-	-
5.4	0.39	3.1±0.7	1.6±0.5	-48.4±0.4
4.3	0.39	2.1±0.5	1.8±0.4	-14.3±0.3
3.6	0.39	2.1±0.4	2.1±0.4	0.0±0.3
3.1	0.39	-	-	-

Tabel C.7: Ethylene (C₂H₄) variation with plasma application

Ethylene				
Φ_{reactor}	Φ_{global}	Concentration (no plasma)	Concentration (plasma)	Variation
		Ppm	ppm	%
5.4	0.18	52.5±5.9	30.5±3.5	-41.9±0.2
4.3	0.18	31.6±3.5	23.4±2.6	-25.9±0.2
3.6	0.18	23.8±2.8	17.0±2.0	-28.6±0.2
3.1	0.18	11.9±1.5	5.7±0.8	-52.1±0.2
5.4	0.21	43.2±4.8	28.1±3.1	-35.0±0.2
4.3	0.21	32.0±3.5	21.7±2.5	-32.2±0.2

3.6	0.21	22.2±2.6	11.8±1.4	-46.8±0.2
3.1	0.21	8.2±1.4	1.9±0.4	-76.8±0.3
5.4	0.24	41.6±4.5	26.1±3.1	-37.3±0.2
4.3	0.24	29.5±3.2	14.4±1.6	-51.2±0.2
3.6	0.24	18.4±2.1	4.9±1.1	-73.4±0.3
3.1	0.24	1.6±0.3	0.5±0.2	-68.8±0.4
5.4	0.30	37.2±4.2	7.9±1.1	-78.8±0.2
4.3	0.30	23.1±2.7	2.6±0.6	-88.7±0.3
3.6	0.30	-	-	-
3.1	0.30	-	-	-
5.4	0.39	-	-	-
4.3	0.39	-	-	-
3.6	0.39	-	-	-
3.1	0.39	-	-	-

Tabel C.8: CH₄ variation with plasma application

CH ₄				
Φ_{reactor}	Φ_{global}	Concentration (no plasma)	Concentration (plasma)	Variation
		Ppm	ppm	%
5.4	0.18	2201.5±255.7	1131.3±130.2	-48.6±0.2
4.3	0.18	1347.0±152.6	902.4±103.1	-33.0±0.2
3.6	0.18	1011.0±120.3	635.0±76.6	-37.2±0.2
3.1	0.18	340.2±43.5	140.5±20.1	-58.7±0.2
5.4	0.21	1777.8±204.0	964.1±107.4	-45.8±0.2
4.3	0.21	1337.3±146.0	791.2±93.1	-40.8±0.2
3.6	0.21	905.5±106.8	390.5±48.6	-56.9±0.2
3.1	0.21	200.0±35.9	36.2±7.6	-81.9±0.3
5.4	0.24	1508.0±165.7	763.1±94.3	-49.4±0.2
4.3	0.24	1072.4±121.7	416.0±48.0	-61.2±0.2
3.6	0.24	639.7±75.9	128.5±30.2	-79.9±0.3
3.1	0.24	-	-	-
5.4	0.30	888.1±104.6	161.7±23.7	-81.8±0.2
4.3	0.30	591.9±71.7	48.2±11.3	-91.9±0.3
3.6	0.30	44.7±10.1	6.4±2.8	-85.7±0.5
3.1	0.30	-	-	-

5.4	0.39	-	-	-
4.3	0.39	-	-	-
3.6	0.39	-	-	-
3.1	0.39	-	-	-

Tabel C.9: Ethane (C₂H₆) variation with plasma application

Ethane				
Φ_{reactor}	Φ_{global}	Concentration (no plasma)	Concentration (plasma)	Variation
		ppm	ppm	%
5.4	0.18	97.1±11.5	41.3±5.2	-57.5±0.2
4.3	0.18	49.2±5.9	28.2±3.5	-42.7±0.2
3.6	0.18	34.8±4.5	17.5±2.5	-49.7±0.2
3.1	0.18	17.0±2.5	5.6±1.2	-67.1±0.3
5.4	0.21	72.7±8.8	33.7±4.1	-53.6±0.2
4.3	0.21	48.5±5.6	23.8±3.1	-50.9±0.2
3.6	0.21	30.3±3.9	8.5±1.5	-71.9±0.2
3.1	0.21	-	-	-
5.4	0.24	59.3±6.7	23.7±3.4	-60.0±0.2
4.3	0.24	36.4±4.5	8.9±1.3	-75.5±0.2
3.6	0.24	-	-	-
3.1	0.24	-	-	-
5.4	0.30	-	-	-
4.3	0.30	14.4±2.0	2.0±0.5	-86.1±0.3
3.6	0.30	2.0±0.6	2.4±0.6	20.0±0.4
3.1	0.30	-	-	-
5.4	0.39	-	-	-
4.3	0.39	2.1±0.5	1.9±0.5	-9.5±0.4
3.6	0.39	3.8±0.6	3.9±0.6	2.6±0.2
3.1	0.39	-	-	-

Tabel C.10: Propane (C₃H₈) variation with plasma application

Propane				
Φ_{reactor}	Φ_{global}	Concentration (no plasma)	Concentration (plasma)	Variation
		Ppm	Ppm	%
5.4	0.18	48.9±6.2	13.6±2.7	-72.2±0.2
4.3	0.18	21.2±3.0	13.7±2.1	-35.4±0.2
3.6	0.18	17.0±2.7	10.4±2.1	-38.8±0.3
3.1	0.18	-	-	-
5.4	0.21	26.4±3.8	10.7±2.1	-59.5±0.2
4.3	0.21	20.9±2.8	11.1±1.9	-46.9±0.2
3.6	0.21	14.2±2.0	6.3±1.4	-55.6±0.3
3.1	0.21	-	-	-
5.4	0.24	19.9±2.8	6.5±1.6	-67.3±0.3
4.3	0.24	15.2±2.1	5.6±1.0	-63.2±0.2
3.6	0.24	9.2±1.6	3.1±1.0	-66.3±0.4
3.1	0.24	-	-	-
5.4	0.30	-	-	-
4.3	0.30	6.3±1.3	1.8±0.7	-71.4±0.4
3.6	0.30	2.3±0.9	1.8±0.7	-21.7±0.6
3.1	0.30	-	-	-
5.4	0.39	-	-	-
4.3	0.39	-	-	-
3.6	0.39	3.1±0.6	3.1±0.7	0.0±0.3
3.1	0.39	-	-	-

Tabel C.11: Methanol (CH₃OH) variation with plasma application

Methanol				
Φ_{reactor}	Φ_{global}	Concentration (no plasma)	Concentration (plasma)	Variation
		ppm	Ppm	%
5.4	0.18	17.5±2.0	9.9±1.2	-43.4±0.2
4.3	0.18	11.5±1.3	7.6±1.0	-33.9±0.2
3.6	0.18	9.5±1.2	6.8±0.9	-28.4±0.2
3.1	0.18	3.8±0.5	1.6±0.4	-57.9±0.3
5.4	0.21	13.3±1.6	8.5±1.0	-36.1±0.2
4.3	0.21	9.7±1.1	6.5±0.8	-33.0±0.2

3.6	0.21	7.6±0.9	4.5±0.7	-40.8±0.2
3.1	0.21	-	-	-
5.4	0.24	11.1±1.3	6.2±0.8	-44.1±0.2
4.3	0.24	7.7±0.9	3.6±0.5	-53.2±0.2
3.6	0.24	5.7±0.7	1.7±0.4	-70.2±0.3
3.1	0.24	-	-	-
5.4	0.30	4.3±0.6	1.0±0.2	-76.7±0.2
4.3	0.30	4.1±0.5	0.5±0.2	-87.8±0.4
3.6	0.30	-	-	-
3.1	0.30	-	-	-
5.4	0.39	-	-	-
4.3	0.39	-	-	-
3.6	0.39	-	-	-
3.1	0.39	-	-	-

Tabel C.12: Formaldehyde (CH₂O) variation with plasma application

Formaldehyde				
Φ_{reactor}	Φ_{global}	Concentration (no plasma)	Concentration (plasma)	Variation
		ppm	ppm	%
5.4	0.18	63.5±7.1	40.4±4.6	-36.4±0.2
4.3	0.18	41.1±4.5	30.7±3.5	-25.3±0.2
3.6	0.18	32.5±3.8	24.0±2.8	-26.2±0.2
3.1	0.18	-	-	-
5.4	0.21	54.5±6.0	37.7±4.1	-30.8±0.2
4.3	0.21	41.0±4.5	29.1±3.4	-29.0±0.2
3.6	0.21	30.2±3.4	16.9±2.0	-44.0±0.2
3.1	0.21	-	-	-
5.4	0.24	52.9±5.7	35.4±4.1	-33.1±0.2
4.3	0.24	39.0±4.3	20.1±2.3	-48.5±0.2
3.6	0.24	25.5±2.9	7.0±1.6	-72.5±0.3
3.1	0.24	-	-	-
5.4	0.30	46.3±5.4	10.7±1.4	-76.9±0.2
4.3	0.30	29.1±3.2	4.0±1.0	-86.3±0.3
3.6	0.30	-	-	-
3.1	0.30	-	-	-

5.4	0.39	-	-	-
4.3	0.39	-	-	-
3.6	0.39	-	-	-
3.1	0.39	-	-	-

FOLHA DE REGISTRO DO DOCUMENTO			
1. CLASSIFICAÇÃO/TIPO TD	2. DATA 06 de maio de 2019	3. REGISTRO N° DCTA/ITA/TD-009/2019	4. N° DE PÁGINAS 119
5. TÍTULO E SUBTÍTULO: Effects of a fuel-rich gliding arc discharge in plasma-assisted fuel-lean combustion			
6. AUTOR(ES): Armando José Pinto			
7. INSTITUIÇÃO(ÕES)/ÓRGÃO(S) INTERNO(S)/DIVISÃO(ÕES): Instituto Tecnológico de Aeronáutica – ITA			
8. PALAVRAS-CHAVE SUGERIDAS PELO AUTOR: 1. Plasma-assisted combustion. 2. Gliding arc discharge. 3. Combustion.			
9. PALAVRAS-CHAVE RESULTANTES DE INDEXAÇÃO: Combustão; Descargas elétricas a arco; Física de plasmas; Controle de poluição; Física.			
10. APRESENTAÇÃO: (X) Nacional () Internacional ITA, São José dos Campos. Curso de Doutorado. Programa de Pós-Graduação em Física. Área de Física de Plasmas. Orientador: Prof. Dr. Pedro Teixeira Lacava. Coorientador: Dr. Julio César Sagás. Defesa em 29/04/2019. Publicada em 2019.			
11. RESUMO: Combustion processes have been an important factor in human progress. However, the exhaust gases can contain high-risk species, either by its toxicity to living beings or for contributing to environmental degradation. Among different techniques used for combustion pollutant control, it can be highlighted the use of non-equilibrium plasmas. This kind of plasma is a source of chemically active species such as radicals, ionized and metastable species, and also free electrons which promote the ionization and dissociation of the background gas molecules. In this study, a gliding arc discharge generated in a fuel-rich premixed mixture was applied to a swirl global fuel-lean flame, both of them generated in a mixture of air and natural gas. The discharge electrical diagnostic was performed to verify the influence of the gas flow rate and the mixture composition on the discharge repetition frequency. Both the increase of the total gas mass flow rate and of the fuel amount in the mixture increase the discharge repetition frequency. The chemical analysis of the plasma-assisted combustion exhaust gas showed that the discharge acts as a source of oxygen and hydrogen species (O, H, H ₂ , OH). It accelerates the hydrocarbon oxidation and lowers the levels of carbon monoxide, improving the combustion process.			
12. GRAU DE SIGILO: (X) OSTENSIVO () RESERVADO () SECRETO			